# ENGINEERED OUTER MEMBRANE VESICLES DERIVED FROM PROBIOTIC *ESCHERICHIA COLI* NISSLE 1917 AS RECOBINANT SUBUNIT ANTIGEN CARREIRS FOR THE DEVELOPMENT OF PATHOGEN-MIMETIC VACCINES

A Dissertation

Presented to the Faculty of the Graduate School

of Cornell University

in Partial Fulfillment of the Requirements for the Degree of

Doctor of Philosophy

by

Joseph A. Rosenthal

May 2014

**ENGINEERED OUTER MEMBRANE VESICLES DERIVED FROM PROBIOTIC *ESCHERICHIA COLI* NISSLE 1917 AS RECOBINANT SUBUNIT ANTIGEN CARREIRS FOR THE DEVELOPMENT OF PATHOGEN-MIMETIC VACCINES**

Joseph A. Rosenthal, Ph.D.

Cornell University 2014

The greatest strides in vaccine delivery over the last decade have come primarily from a new class of nanoparticulate antigen carrier that focuses on reverse-engineering the pathogen-immune cell interaction on the molecular level. Such "pathogen-like particles", or PLPs, take an elegant approach to biomimicry, attempting to artificially isolate or recreate a pathogen's natural ability to stimulate a targeted immune response. In this work, we focused on the transformation of the probiotic *E. coli* strain Nissle 1917 into an outer membrane vesicle (OMV) platform for $T_H1$-biasing delivery of a variety of recombinant antigens. We hypothesize that by harnessing the natural immunomodulation of the Nissle 1917 (EcN) bacterium, and pairing this immunomodulation with appropriate vaccine targets that require potent $T_H1$-biasing vaccine responses, we can engineer a recombinant antigen delivery platform that uniquely enhances antigen-specific immunity through pathogen-mimetic vaccination. As bionanoparticulate PLPs often suffer from requiring multiple boosts and external adjuvants to achieve pathogen-mimetic memory responses, we further enhanced our EcN OMV platform with controlled release delivery using injectable polymeric microspheres as a transient OMV depot.

From the immunological characterization of free and encapsulated EcN OMVs' vaccine capability, two vaccine targets were chosen to demonstrate the efficacy of the OMVs as a PLP platform for vaccine delivery. To test the capacity of the OMVs to functionally display and vaccinate against a heterologous antigen of viral origin, OMVs expressing a subunit of H1N1 hemagglutinin were produced and tested on BALB/c mice. Not only did the resulting immunological assays for vaccine response show great promise for a protective response, generating a 2.6-fold increase in IgG2a:IgG1 titers and a 8.1-

fold increase in IFN-γ:IL-4 T-cell secretion versus a gold-standard control, but further analysis using hemagglutination-inhibition assays demonstrated >50-fold enhancement in cross-strain protection against H3N2. Secondly, to test EcN OMVs' capacity to direct unique immunomodulation to less standard vaccine targets, OMVs expressing the peanut allergen Arah2 were produced as both a prophylactic vaccine (for preventing peanut allergy) and an immunotherapy (for treating extent peanut allergy). Using a BALB/c mouse model for peanut allergy sensitization, a free EcN OMV vaccine dose was administered prior to sensitization, which following anaphylactic challenge post-sensitization resulted in protective survival of 100% of vaccinated mice. Encapsulated controlled release of lower doses of the Arah2-displaying EcN OMVs administered following sensitization were also successful at protecting >50% of mice from some level of anaphylaxis post-challenge while minimizing side-effects relative to traditional sublingual immunotherapy.

The engineering and *in vitro/in vivo* testing of EcN OMVs as vaccine antigen carriers demonstrated promising efficacy as a pathogen-mimetic platform for protective immunomodulation. Successful testing with a variety of recombinant antigens provides the foundation upon which further development of the EcN OMV platform can lead to a promising host of PLP vaccines.

## BIOGRAPHICAL SKETCH

Joseph A. Rosenthal was born February 18, 1988, in Houston, Texas. He received his Bachelor of Science in Bioengineering from Rice University in 2010. During his time at Rice, Joseph conducted research on viral nanoparticle engineering under the tutelage of Dr. Junghae Suh. His projects at the time primarily focused on using molecular engineering to repurpose adeno-associated virus serotype 2 (AAV2) into novel nanotherapeutic modalities. While at Rice, Joseph's scholarship was recognized via several notable awards, including a Goldwater Scholarship, the Samuel T. Sikes, Jr. Scholarship in Engineering (Brown School of Engineering), and the W.L. Moody, Jr. Scholarship (Rice University). Following graduation, Joseph started his PhD work in the Department of Biomedical Engineering at Cornell University under the guidance of Dr. David Putnam. His research has been supported by a coordinated Hertz Foundation Graduate Fellowship and National Science Foundation Graduate Research Fellowship.

To my wife, Melisa.

**ACKNOWLEDGEMENTS**

My gratitude to my advisor, Dr. David Putnam, cannot be overstated. As a graduate student, I constantly came to Dr. Putnam with requests to go my own direction, pursue my own interests, and challenge my own results – even when side projects and rapidly multiplying lines of inquiry were not the most straightforward path to graduation. Dr. Putnam always responded with patience and clarity in guidance, coupled with the most important gift an advisor can give a student: trust in independence. It was as both a student and a colleague that my work under Dr. Putnam allowed me to grow as a scientist and a professional academic. I also owe much thanks to my committee members, Dr. Michael Shuler, Dr. Matthew DeLisa, and Dr. Yung-Fu Chang, for their insight and support in completing this body of work. I was also blessed to have had many other advisors and collaborators during my thesis work, including Dr. Susana Mendez, Dr. Cynthia Leifer, and Dr. Gary Whittaker, whose collective expertise in their subfields of immunology helped elevate an immunological quandary into preclinical application.

This work would not be possible without the support of the Hertz Foundation and the National Science Foundation, whose fellowships permitted and encouraged the aforementioned independence. I would like to especially thank Jay Davis and Dr. Tom Weaver of the Hertz Foundation, for their guidance and direction throughout the winding path of graduate study. None of this work would be possible without the support of Cornell University and its various facilities either, and I extended specific thanks to John Grazul and John Hunt of the Cornell Center for Materials Research, the Cornell School of Veterinary Medicine, and the Cornell Animal Health Diagnostic Center, for the use of their facilities and expertise.

Team Putnam is, hands down, the most extraordinary group of researchers I have ever had the privilege to work with. I would be remiss not to thank all of those who supported me in so many ways: Bailey, Lindsey, Nicole, Mingchee, Jose, Hannah, Jen, Jeisa, Cassie, and of course Anne, without whom I

likely would never have begun work on this project. The DeLisa lab was also instrumental in this work, and I would like to thank Jack, Chenny, and Jenny for their continued help and support.

I was blessed beyond measure to work with four of the most talented undergraduate researchers at Cornell, without whom I would be almost completely useless. The work presented in this dissertation is as much a testament to their skill and determination as it is to my own. Tiffany, Kaho, Pam, and Nicole: you have my eternal thanks for all your long hours and outstanding insight.

Finally, my family has been an outstanding motivator throughout the completion of this work, and I owe them my deepest gratitude. My parents, David and Debbie; my sister, Sarah; and all my family back in Texas (both Rosenthal and Pferdehirt): thank you for your love and confidence. Last but never, ever least, I thank my wife, Melisa, for helping in a thousand and one ways to support the hopeless case that is the engineering graduate student with love, understanding, and a remarkable confidence that someday I might actually finish this dissertation and graduate.

**TABLE OF CONTENTS**


BIOGRAPHICAL SKETCH v
DEDICATION vi
ACKNOWLEDGEMENTS vii
**1. CHAPTER 1: INTRODUCTION 1**
1.1 Vaccine immunology 1
1.2 Recombinant subunit vaccines and the adjuvant fallacy 2
1.3 Pathogen-like particle vaccines 5
1.4 Bacterial outer membrane vesicles (OMVs) 8
**2. CHAPTER 2: PRODUCTION AND CHARACTERIZATION OF *E. COLI* NISSLE 1917 OMVS AS REOMBINANT ANTIGNE VACCINE CARRIERS 14**
2.1 Introduction 14
2.2 Materials and methods 18
2.2.1 Design of Nissle *nlpI*-mutant JH1 and *lpxM* mutant JH1-*LpxM* 18
2.2.2 Mouse immunizations 18
2.2.3 Assessing OMV vaccine immune response 19
2.2.4 In vitro analysis of immune cell stimulation by EcN OMVs 19
2.3 Results and discussion 20
2.3.1 Vaccination using green fluorescent protein (GFP) as a model antigen 20
2.3.2 Biomolecular and immunological characterization of EcN OMVs 29
2.3.3 Additional exploration of EcN OMV vaccine response dependence on dose and antigen presentation 50
2.4 Conclusions 58
**3. CHAPTER 3: ENHANCEMENT OF ECN OMV VACCINES WITH SELF-BOOSTING CAPACITY GENERATED BY CONTROLLED RELEASE FROM INJECTABLE POLYMERIC MICROSPHERES 59**
3.1 Introduction 59
3.2 Materials and methods 62
3.2.1 PLGA microsphere synthesis
3.2.2 OMV stability studies 63
3.2.3 In vitro release studies of microspheres-encapsulated OMVs 63
3.2.4 Mouse immunization 63
3.2.5 Assessing OMV vaccine immune response 64
3.2.6 In vitro analysis of immune cell stimulation by EcN OMVs 65
3.2.7 ELISA for serum antibody response 65
3.2.8 Splenocyte analyses 66
3.3 Results and discussion 66
3.3.1 Assessing OMV stability under physiological conditions relevant to polymeric controlled release 66
3.3.2 Initial confirmation of PLGA microparticle encapsulation of model fluorescent OMVs 68
3.3.3 In vitro controlled release studies of PLGA microsphere-encapculated OMVs 68

3.3.4 Characterization of *in vivo* immunological enhancement of EcN OMV vaccine carriers via controlled release 73
3.4 Conclusions 78
**4. CHAPTER 4: ADAPTATION OF THE ECN OMW VACCINE PLATFORM FOR CREATION OF AN INFLUENZA VACCINE CAPABLE OF CROSS-STRAIN PROTECTION 79**
4.1 Introduction 79
4.2 Materials and methods 81
4.2.1 Preparation of OMVs 81
4.2.2 Protein analyses 81
4.2.3 Mouse immunizations 82
4.2.4 Assessing OMV vaccine immune response 82
4.2.5 In vitro analysis of immune cell stimulation by EcN OMVs 83
4.2.6 ELISA 83
4.2.7 Hemagglutination inhibition assays 84
4.2.8 T-cell activation analyses 84
4.3 Results and discussion 85
4.4 Conclusions 90
**5. CHAPTER 5: ADAPTATION OF THE ECN OMV VACCINE PLATFORM FOR THE TREATMENT OF PEANUT ALLERGIER: GENERATION OF A PROPHYLACTIC PEANUT ALLERGY VACCINE AND CONTROLLED RELEASE OMV-MEDIATED IMMUNOTHERAPY 91**
5.1 Introduction 91
5.2 Materials and methods 93
5.2.1 Mouse immunizations 93
5.2.2 Adaptive immunity analysis 93
5.2.3 Peanut protein sensitization and peanut allergy challenge of mice with corresponding analysis of serum and T-cells 93
5.2.4 OMV encapsulation in PLGA microspheres 94
5.2.5 Sublingual immunotherapy dosing 94
5.2.6 ELISA for serum antibody response 95
5.2.7 Cytokine secretion analyses 95
5.2.8 Peanut allergy challenge 95
5.3 Results 96
5.3.1 EcN OMVs direct $T_H1$-biased immunity against Arah2 allergens in BALB/c mice 96
5.3.2 Prophylactic vaccination with EcN OMVs protects against anaphylactic challenge in sensitized BALB/c mice 99
5.3.3 Immunotherapy for peanut allergy possible via controlled release of EcN OMV vaccine carriers 106
5.4 Conclusions 109
**6. CONCLUSIONS AND RECOMMENDATIONS 113**
**APPENDIX I: ADDITIONAL AND EXPANDED MATERIALS AND METHODS 118**
**APPENDIX II: APPLICATION OF THE ECN OMV PLATFORM TO HETEROLOGOUS BACTERIAL ANTIGEN DELIVERY, A TEST CASE: *MYCOBACTERIUM AVIUM SUBSPECIES PARATUBERCULOSIS* 124**
**APPENDIX III: MODELING INTACT PATHOGEN IMMUNE CELL PRESENTATION AND POLYREACTIVE ANTIBODY GENERATION (USING HIV AS A MODEL) 130**
**REFRENCES 145**

# CHAPTER 1

# INTRODUCTION

## 1.1 Vaccine Immunology

While a full review of human immunology is not required to understand the basic principles of vaccine engineering as it pertains to this project, a simple review of the basic cells and factors involved will be useful. Indeed, for the purpose of this work, the classical understanding of the development of a simple response to a bacterial pathogen, which ultimately is the exact response a traditional vaccine aims to replicate[1–3], will suffice. Upon introduction of a foreign material, the injection site becomes inflamed, either due to tissue damage and/ or stress (facilitated by many common chemical additives, or adjuvants, used in vaccines today) or innate pathogen recognition by tissue-resident immune cells such as mast cells or macrophages (leading to the secretion of pro-inflammatory cytokines)[1]. This facilitates recruitment of additional phagocytes, such as monocytes and neutrophils, which in the case of infection would help clear up the site but in the case of vaccines primarily serve simply to sustain the inflammation[3,4]. The immediate responders to and mediators of this inflammatory response comprise *innate immunity*[1]. This inflammation in turn promotes the activation of dendritic cells, which pick up antigens from the infecting agent and deliver them to lymphoid tissue[3,5]. In the lymph nodes, dendritic cells present their antigens to naïve CD4 T-cells, which respond if they have T-cell receptors specific to the antigens. These antigen-specific CD4 T-cells then go on to activate antigen-specific B-cells, which results in the secretion of antibodies specific to the pathogenic antigen. Depending on a variety of factors that occur within the lymphoid tissue during this process, CD4 T-cells may also go on to activate antigen-specific cytotoxic CD8 T-cells (which help control intracellular pathogens) and facilitate the transformation of B- and T-cells into memory cells[3,6]. This secondary response, comprising *adaptive*

*immunity*[1], effectively assures a pathogen-clearing response while additionally, and more importantly for vaccination, ensuring that subsequent exposure to the same pathogen will not require the comparatively lengthy process of "educating" adaptive immune cells[3].

For the purpose of the following discussion, the most important takeaway is as follows. During a successful immune response to a classical pathogen infection, a variety of innate and adaptive immune cells have to 1) be stimulated, 2) interact with an antigen, and 3) develop lasting antigen-specific memory. Simply put, an effective vaccine directly or indirectly interacts with the immune cells described above to achieve a similar response.

### 1.2 Recombinant Subunit Vaccines and the Adjuvant Fallacy

Vaccine design has, in principle, come a long way from Edward Jenner's work[3] over two centuries ago, where a vaccine was the simple concept of exposing the immune system to a pathogen that 1) facilitated an improved immune response when later challenged naturally by an infection of that same or related pathogen, and 2) did not cause a similar or worse infection of its own. Vaccines now, at their most rudimentary level, attempt to balance two crucial factors that were key in even Jenner's original smallpox vaccine: pathogenic identity and immune stimulation. The search for stronger adjuvants that can direct immune responses down specifically biased paths represents the field's advances and goals concerning the latter[6–8]. The recombinant subunit approach to vaccines, on the other hand, best represents advances made concerning the former[9].

The principle of recombinant subunit vaccines is simple to grasp but often difficult to apply to complicated pathogens. On a molecular level, immune responses do not target pathogens as a whole but instead develop incredibly refined affinity for specific pathogen-related molecular targets. The innate immune system has a range of targets it's evolved to recognize without any additional "training",

and they mostly come in the form of what are called pathogen-associated molecular patters, or PAMPs[1,10]. Toll-like receptor (TLR) agonists such as bacterial lipopolysaccharide (LPS) are the most prevalent examples[11,12]. The adaptive immune system, on the other hand, has a far more elegant and, appropriately, adaptive capacity for molecular target identification. Foreign bodies deemed to be non-host are probed against a potential-target space whose diversity has been estimated to exceed $10^{11}$ possible targets for B-cells and up to $10^{18}$ targets for T-cells[3]. Exquisitely organized directed evolution that plays out within lymph node follicles during infection (or vaccination) directs selection of immune cells that recognize prominent and specific subunits of pathogen-associated molecules, or antigens, and directs an adaptive immune response against the pathogen in question by seeking out those antigens. Recombinant subunit vaccines therefore follow a simple strategy: if one can isolate the best antigens from a pathogen, then attempting to formulate a medicinal product out of a complicated, mostly-intact organism can be replaced by a simple mixture of several recombinant protein products.

While there have been notable successes in taking recombinant subunit vaccines beyond the lab and into clinical applications, especially as related to conjugate vaccines for applications ranging from meningitis to *Haemophilus influenzae*[13,14], the significant challenge facing the field revolves around the crucial trade-off in attempting to dramatically simplify the development of antigen-specific immune responses. Indeed, the recombinant subunit antigens are almost always very poorly immunogenic, requiring some additional adjuvanting material to be added to direct the immune system to take notice of the vaccine antigen[9]. Unfortunately, both classic adjuvants such as aluminum hydroxide compounds and more cutting-edge squalene-based adjuvants such as Novartis' MF59[7,15] are inadequate attempts at fully engaging the immune system in a meaningful way. The reason is simple: adjuvanting materials primarily work by generally aggravating injection-site tissue to recruit immune cells, rather than mimicking pathogenic infection and engaging the highly-evolved antigen-selection machinery described above via directed immunostimulatory antigen presentation to adaptive immune cells[6,8,16]. The result is

often an immune response typified by poor memory, only partially-evolved antibody selection and hypermutation, and minimal cellular immunity induction.

This problem is further compounded by a need to direct the immune system in more subtle ways for certain pathogens. Not all immune responses are created equal, and stimulating the "wrong" immune response in a vaccine can render it essentially useless[2,3]. While modern immunology tries to avoid gross simplifications concerning "branches" of the immune system specific to pathogen types, the simple fact is that certain pathogens require certain tailored immune responses to be effectively suppressed and cleared. As an example, the adjuvant aluminum hydroxide[7,17] stimulates a balanced immunological interplay between responses dominated by the $T_H1$ and $T_H2$ subtypes of T-cells, which is ideal for many pathogens such as poliovirus and meningococcal meningitis. Successful immune responses against many other pathogens, however, requires the generation of a more biased immune response, such as $T_H1$ bias for combatting tuberculosis or malaria[18,19]. While dozens of excellent antigen targets for tuberculosis and malaria vaccines have been identified over the past several decades, the inability to tie appropriately biased immune responses to their recombinant subunit forms is essentially the largest barrier to making progress in vaccine development. Indeed, unless more advanced means of tying specifically tailored immune responses to recombinant subunit antigens can be discovered, the technology itself can expect to continue to only produce incremental advances rather than breakthrough preventative therapies[4,6,9].

### 1.3 Pathogen-like Particle Vaccines

Targeted vaccine delivery is a viable alternative to adjuvanting materials, focusing on the cellular- and nanoscale-level presentation/exposure of the recombinant subunit antigens to the immune system. This may take the form of liposomal or polymeric particles laden with antigen targeted to lymph nodes to facilitate controlled antigen release there, or alternatively might seek to use nanoparticles to deliver small recombinant pathogen peptides or even DNA intracellularly to immune cells[4,20–23]. Design considerations become very similar to that of more classical controlled release and drug delivery problems, including biocompatibility, accuracy of targeting, and pharmaceutical delivery kinetics. Such considerations must in turn be appropriately balance with the previously discussed goals of a recombinant subunit vaccine in general, such as biased immunity stimulation and immune memory induction.

A subset of this approach is the pathogen-like particle (PLP), which also focuses on targeted antigen delivery while simultaneously seeking to replicate the interaction between pathogen and immune cell. PLPs usually have several key goals: 1) delivery of recombinant pathogen antigens directly to immune cells in a way that mimics what the pathogen itself would do, 2) use of a variety of molecular cues to stimulate the immune system without additional adjuvant, and 3) direct stimulation in a way that enhances immune system bias most effective in combatting the target pathogen. While few PLPs are currently in use or very close to clinical application[9,24], several are moving through clinical trials and all represent significant improvements to the current vaccine technology paradigm[4,22,25]. These PLPs use a variety of techniques to directly deliver and enhance immunostimulation to their antigen. A prototypical PLP is illustrated in **Figure 1.1** as an example. Antigenic moieties may be encapsulated or surface displayed in association with a synthetic or biologically-derived material, and are delivered in particulate form via various targeting moieties, such as antibodies to B-cell or T-cell receptors. Delivery is supplemented with the release of soluble factors that act as cues for the stimulation of appropriate

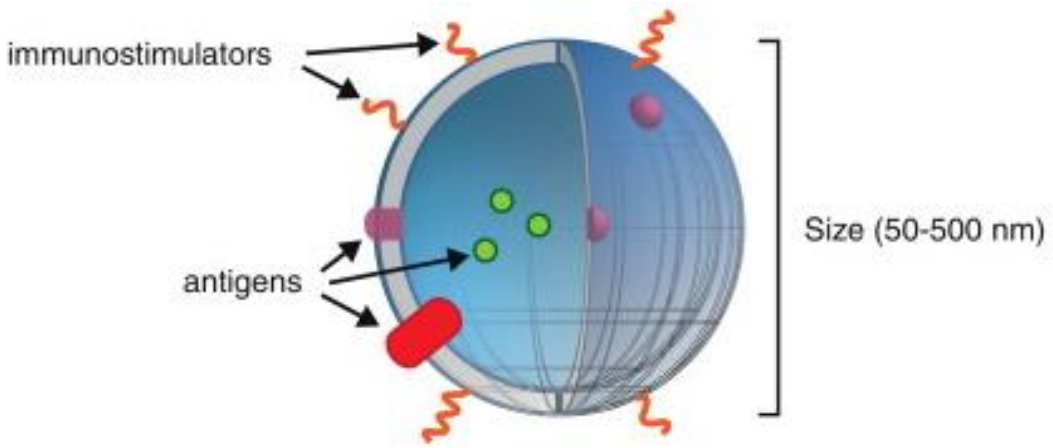


**Figure 1.1: Model pathogen-like particle (PLP).** A prototypical PLP seeks to break down a pathogen into its most basic factors, as "seen" by the immune system, packaging soluble antigen and immunostimulatory co-factors into a simple synthetic particle , which can be recognizable by immune cells via additional surface-presented antigen and/or other moieties that target the PLP to certain immune cell surface markers. Adapted from artwork by Linxiao Chen.

immune responses; for example, to facilitate a cellular immunity through T-cell stimulation and $T_H1$ bias, the PLP might be designed to co-encapsulate and release IL-2 and IFN-γ.

Disadvantages of PLPs, much like their design parameters, closely mirror those of current advances in drug delivery technology. As complexity and multimodality of the particle platform increases, thus improving its ability to behave like a pathogen, cost and complexity of synthesis increase as well. Additionally, singular targeting modalities and co-factors come very short of harnessing the true complexity of biological organisms they seek to replace. The most advanced PLPs being developed today rarely use more than two or three pathogen-like moieties; a simple pathogenic organism such as a bacteria, as a point of contrast, displays hundreds of different protein and lipopolysaccharide modalities, many of which have some interaction with the immune system at least in minimal capacity. Thus in their current form, most PLPs will likely be limited to tailored applications where cost, complexity, and scalability are less of an issue.

It is important to note that much of the preceding discussion is tailored around the concept of a PLP being exclusively or at least partially synthetic. In reality, the most successful PLPs to date are actually entirely biologically-derived. Virus-like particles such as those used in Gardasil® (for human papilloma virus)[24] and Mosquirix® (for malaria)[18] have achieved impressive results by simply attaching antigens to the surface of self-assembling viral capsid proteins, which function as mildly immunostimulative and naturally-targeted antigen carriers when injected as a vaccine. While production cost, extent of target pathogen applicability, and sufficient efficacy remain very real hurdles for such formulations as well, their success makes a compelling case for seeking a middle ground that can effectively harness some component of the inherent biological complexity involved in the host-pathogen response while still refining the concept of vaccine delivery through antigen carriers into a feasible application.

### 1.4 Bacterial Outer Membrane Vesicles (OMVs)

Bacterial outer membrane vesicles, or OMVs, are biological phenomena that occur in gram-negative bacteria and have potential applications to vaccine engineering as naturally immunoactive carrier particles[10,26–28]. Under certain conditions – sufficient bacterial culture density to facilitate the advantages of quorum sensing and communication, biofilm formation, competition with different prokaryotes for resources, interactions with a hostile host environment – bacteria have been shown to spontaneously bud off proteoliposomal vesicles from their outer membrane. The formation of these vesicles can involve a fairly dramatic reorganization of the inner and outer membrane to facilitate periplasmic leakage and surface component organization, respectively. The end result is a bionanoparticle whose surface is often representative of the biomolecular complexity of its bacterial source, and whose interior is filled with soluble components from the periplasmic space. Naturally produced OMVs have been hypothesized to be evolved for the delivery of both signaling agents and cytotoxic products, essentially acting as a remote extension of the bacteria itself capable of spreading its influence over larger, less localized length scales[26,27].

The immunology of OMVs is of special interest, as it has been found to be surprisingly complex. Recent data demonstrates that OMVs are highly immunogenic despite being entirely non-infectious and non-replicative. The simplest source of such immunogenicity is their exterior composition. Bacterial outer membranes are comprised of a variety of innately stimulatory TLR agonists and, more generally, PAMP-rich biomolecules, and such composition is directly reflected in a particular bacteria strain's OMVs[10]. Additionally, OMVs seem to be selectively enriched in particularly potent TLR agonists such as LPS (acting on TLR 2 and 4), BLP (TLR 2 and 1/2), and flagellin (TLR 5). Further analysis also reveals the internal inclusion of various "vita-PAMPS", periplasmic components such as dsDNA and ribosomal subcomponents that if released intracellularly can induce immunological reactions reflective of intracellular infection (by acting through TLRs such as TLR 9 and TLR 13)[29]. These moieties are made

more relevant when considering studies have shown that OMVs can interact with immune and non-immune cells alike to deliver such agents by interacting with extracellular receptors via surface contact, being internalized via phagocytosis and additional clathrin independent pathways and thus releasing factors intracellularly, and even partially fusing to cell membranes[10,27]. These delivery routes in turn trigger a variety of immunological cascades that have been shown to not only lead to downstream engagement of immune reactions, but tend to mirror activation traditionally reserved for active intracellular infections. Such capacity has been pursued as a means to use OMVs as a vaccine against their pathogenic source, with an OMV vaccine against meningococcal meningitis currently on the market in several countries outside the United States[13,30–33].

Previous work by our group[34,35] and others[36] has focused on harnessing this self-adjuvancy potential as a potent recombinant vaccine antigen carrier. The general strategy is fairly simple (**Fig. 1.2**): 1) deregulate vesiculation in a bacteria of interest through genetic mutation, thus turning the mutant into an OMV "factory"; 2) induce expression of a fusion protein involving an exogenous antigen of choice and some moiety that facilitates transport to the outer membrane; and 3) harvest resulting OMVs through simple centrifugation. While we've investigated several potential routes of antigen delivery from expression in the cytoplasm, the route detailed in this project utilizes the bacterial enterotoxin ClyA as its means to transport an antigenic protein subunit to the outer membrane[37,38]. As we've previously reported[34], ClyA has the unique capacity to not only facilitate exportation through the periplasmic space, but can additionally insert itself in the outer membrane in a fashion that externalizes any polypeptide sequence linked via its C-terminus.

Published work demonstrates that such approaches to incorporating recombinantly expressed antigens into OMVs can result in immunostimulatory[35] and even protective[36] vaccines. In this respect in particular, recent studies by a variety of groups are both illustrative of the promise of engineered OMV

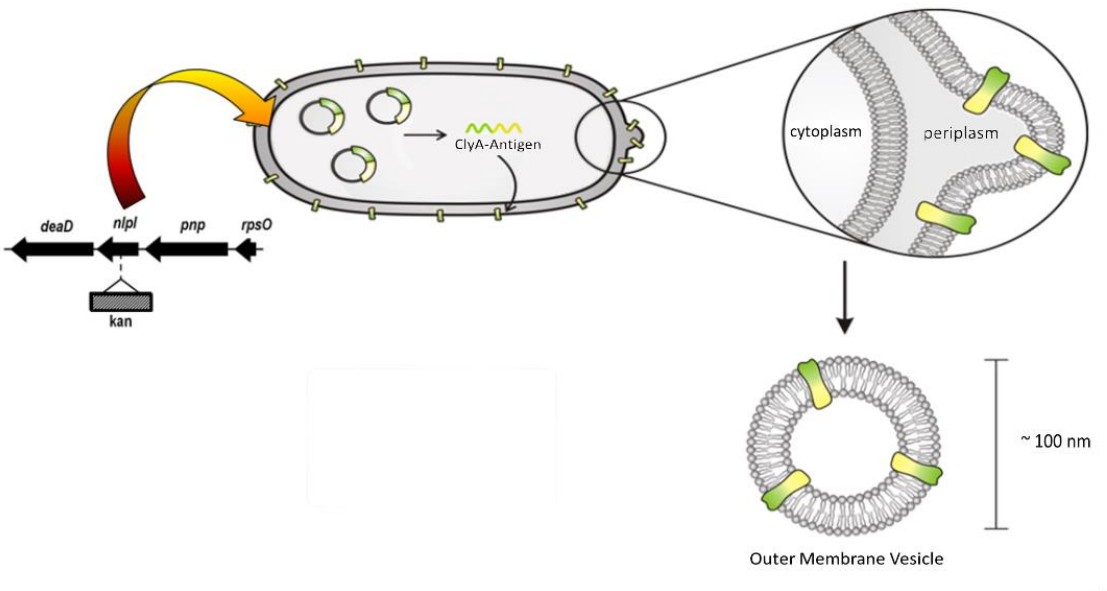


**Figure 1.2: Generating engineered OMVs from *E. coli* that surface display exogenous antigens.** *E. coli* genetically modified to overproduce OMVs (such as via *nlpI* mutation used in this proposal) are transformed with a plasmid encoding the appropriate ClyA-antigen fusion, in this case ClyA-GFP. Once transcribed, ClyA co-localizes the chimera to the *E. coli* outer membrane. As the bacteria continuously bud off OMVs, and the plasmids are designed to be under a high-copy-number promoter, the average OMV generated through the induced hypervesiculation will have a substantial number of recombinant ClyA-antigen fusions included in its membrane. Adapted from artwork by Dr. David Chen.

vaccines as well as useful in guiding identification of an optimal path forward to rationally harness their potential. Unsurprisingly, some of the most instructive studies of OMV vaccine immunology have come from recent attempts to better understand the protective effect of the *N. meningitides* vaccine, particularly the vaccine against serogroup B[30,39–42]. This vaccine of particular interest to the vaccine community as standard recombinant approaches to vaccinating against serogroup B are largely ineffective. Specifically, molecular deconstruction and immunological analysis of the available OMV vaccine (Novartis' Bexsero®) has yielded two useful insights. First, the efficacy of the vaccine stems from an impressive capacity to capture the natural (and naturally immunostimulative) biomolecular complexity of the bacterium it is derived from. Like many lethal pathogens of interest as vaccine targets, *N. meningitides* presents a complex array of hundreds of immunologically active protein and lipid moieties to the immune system during infection, and a myriad of studies have demonstrated that while recombinant multivalent antigen presentation does indeed enhance immunological protection, the reliance of serogroup B in particular on diverse glycosylated residues ties efficacy of the OMV vaccine very strongly to both the content and manner of PAMP presentation. Specifically, an OMV is capable of multivalent presentation of membrane antigens and immunostimulatory TLR-ligands directly to APCs in a biomimetic fashion that both naturally enhances vaccine adjuvancy and intrinsically links diverse epitope libraries through cross-presentation. Indeed, detailed molecular analysis of Bexsero vaccine components has revealed evidence of strong concentrations of TLR2, 4, and 5 ligands, which potently stimulate immune cells even independent of additional adjuvant[11,41–44]. This leads into the second major insight of these studies: unlike many recombinant formulations, Bexsero and other OMV vaccine formulations seem to be capable under the right circumstances of triggering $T_H1$-biased responses. This has been demonstrated in challenge models as well as cellular studies, and while no study has yet directly linked this capacity to the inherent superiority of this vaccine formulation to relative to other standard recombinant vaccine competitors, it stands to reason that given the reliance

of the immune system on a TLR4-driven $T_H1$-biased response to combat acute meningococcal meningitis, this is a non-trivial discovery.

To summarize, the unique protection of Bexsero® is illustrative of an OMV vaccine harnessing a diverse, immunostimulatory array of bacterial biomolecules to direct a certain type of protective immune response, likely one with a $T_H1$-biasing component. It is important to note that for this particular instance, such a finding is more serendipitous than intentional; however, a broadened assessment of recent approaches to use OMV vaccines in a more rationally engineered fashion continues to highlight similar themes. Various recent works[41,45,46] suggest OMV-derived protection via $T_H1$ bias can at least be regularly achieved against a variety of pathogens using appropriate source-strain bacteria. Furthermore, expanded molecular analysis of OMVs shows divergent composition for divergent bacterial sources – that is, the source matters when searching for the right bacterial biomolecules to get the right stimulation. For the purpose of engineering OMVs not merely as vaccines against their source-strain, but against a variety of displayed exogenous antigens, the selection of bacterium needs to be driven less by the pathogenesis of the organism and more by the contribution of certain TLR agonists to a $T_H1$ bias.

Such observations by the field are the first step towards engineering an OMV platform biotechnology for recombinant vaccine delivery, which ultimately is the goal of this work. While questions persist about safely regulating and normalizing the endotoxin content of such formulations[27], host tolerance as a whole has been positive in many animal models[10,35,36,47] and a variety of regulatory agencies have given the platform their preliminary blessing[30]. Perhaps the greatest unknown concerning OMVs as vaccine carriers, therefore, is the immunological “black box” they still represent. Given what is known about OMVs as immunostimulatory agents, there is obvious motivation to simplistically optimize their potential for directing immune responses without having to attempt to re-engineer them on a molecule-by-molecule basis. Current efforts are more often than not focused on adaptations of

bacterial strains already commonly used in microbiology and biological engineering laboratories, as they are after all both well-understood experimental entities and already proven to be economical as sources of recombinant vaccines and a variety of other therapeutics. However, one could alternatively argue that given the available insight into the importance of the link between the right assembly of bacterial immunogens and the right direction of an immune response, it would make better sense to thoroughly investigate less mainstream targets for OMV production based on what their OMVs can rationally be expected to produce in a self-directed, self-adjuvanted immune response. Stated another way, if one is no longer limited by making vaccines derived from the pathogen vaccine target itself, what then would the ideal OMV source look like?

## CHAPTER 2

## PRODUCTION AND CHARACTERIZATION OF *E. COLI* NISSLE 1917 OMVS AS RECOMBINANT ANTIGEN VACCINE CARRIERS[¥]

### 2.1 Introduction

*E. coli* strain Nissle 1917 is a probiotic bacteria getting increasing attention from clinicians and microbiologists alike[48–53]. Probiotic organisms, almost exclusively bacteria, are organisms that, when introduced into the native gut flora, have regulatory properties that can be palliative for variety digestive problems[54]. Establishment of probiotic colonies in the gut have been shown to rebalance other native gut fluora populations, act as a competitive barrier to foreign and opportunistic pathogens in the intestines, and stimulate upregulation of suppressive factors that can inhibit autoimmunity and allergy. The later phenomenon is one where EcN uniquely excels, and has gained the interest of many clinicians who are pursuing it as a dietary supplement capable of treating general irritable bowel disease, Crohn's disease, and even more globalized allergic responses such as food allergy and asthma. Indeed, EcN seems to have an intrinsic ability to facilitate a probiotic effect through direct, local immunomodulation that can have a host-wide impact[48,50,52].

This ability has in turn piqued the interest of microbiologists, who have investigated the bacteria in vitro and in vivo to ascertain what allows it to so potently modulate a host's immune system. While the picture remains somewhat incomplete, EcN seem to derive their probiotic abilities from targeted disruptive interactions with adaptive immune cells (**Fig. 2.1a**), primarily T-cells but also gut-resident dendritic cells and macrophages[48,51,55–58]. Several well-known biomolecular factors have their expression

---

[¥]Reproduced in part with permission from Rosenthal JA et. al, *NanoLIFE* **2013**, 3(3). 

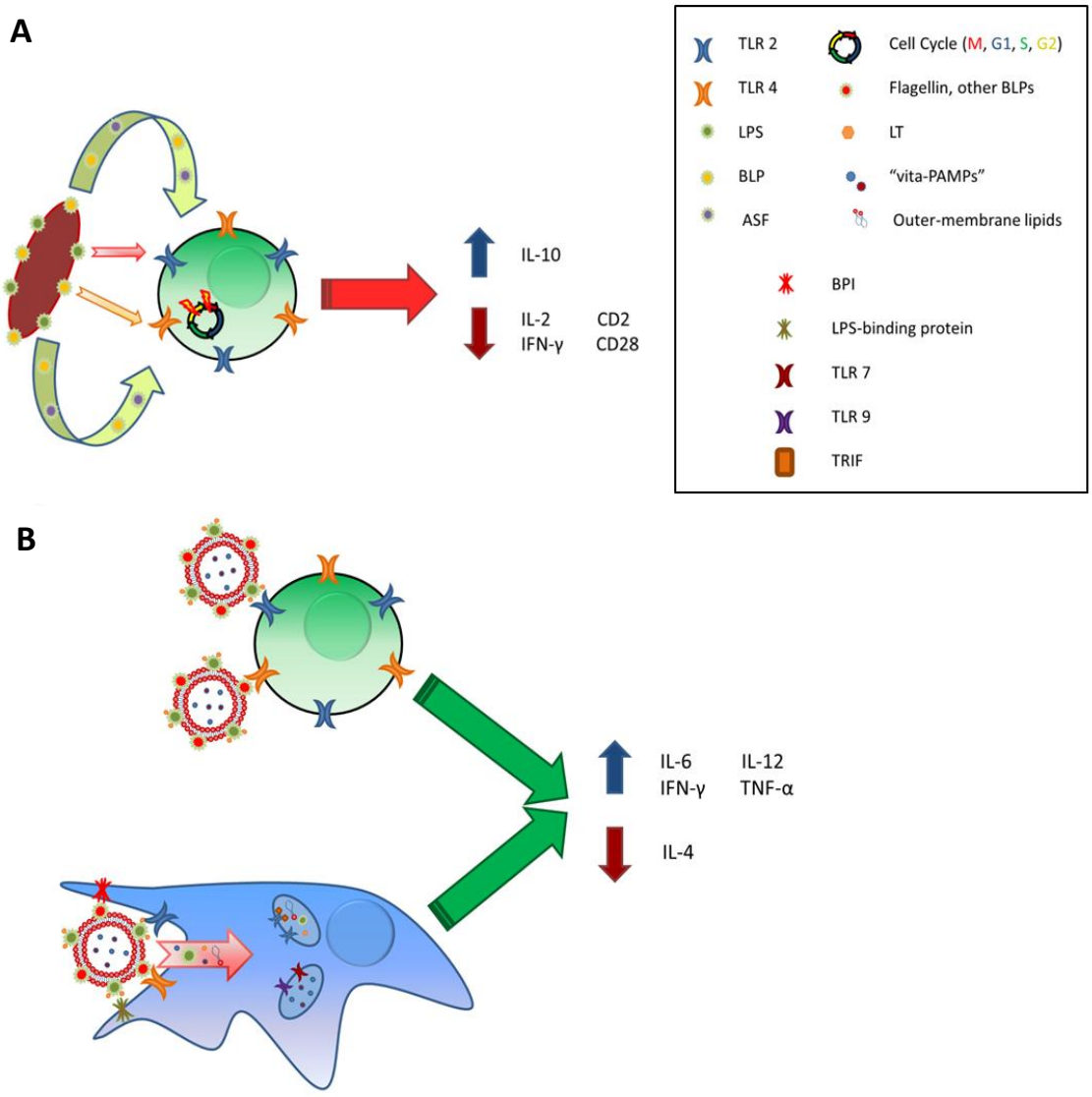


**Figure 2.1: Isolation of Nissle 1917 (EcN) immunostimulatory factors from immunosuppressive mechanisms via OMV engineering.** (**A**) EcN membranous and soluble TLR agonists work together to stimulate, overwhelm, and disrupt adaptive immune cell functions, inducing pseudo-anergy and tolerance. (**B**) By isolating the membrane-bound targeting/stimulating components of EcN's unique adaptive immunity modulation from its secreted factors, and using them to generate bionanoparticles that can target immune cells for extracellular and intracellular delivery of immunostimulatory factors, EcN's natural capacity for immunosuppression can be re-engineered to have a potent adjuvanting effect.

substantially upregulated in EcN, whose closest relatives within the *E. coli* species are, interestingly, functionally divergent and highly pathogenic strains[59,60]. Specifically, membranous, strain-specifically glycosylated LPS, flagellin, and mannose-rich BLPs, as well as secreted BLPs and other bacterial assorted secreted factors (ASFs), target immune cells and transduce modulatory signals primarily through TLRs 2, 4, and 5[48,55]. These signals cause a variety of immunosuppressive effects that directly target the immune cells themselves, especially T-cells, such as decreased propensity to enter G2 or M phases and attenuated immunostimulatory and inflammatory activity through decreased secretion of cytokines (IL-2 and IFN-γ) and costimulatory molecules (CD2 and CD28)[55,57]. Additionally, direct immunosuppressive function is induced by upregulated IL-10 expression and secretion following interaction with EcN. The general resulting mechanism of action theory holds that TLR agonists selectively target EcN to gut-associated immune cells and induce strong immunogenic responses, which are followed by large-scale secretions of soluble immunostimulatory factors. This combination essentially overwhelms the immune cell and induces pseudo-anergy and immunosuppressive pathway activation, which in turn leads to the observed immunosuppressive effect.

In this project, we seek to exploit the immunostimulatory potential of EcN's primarily membranous biomolecular mechanisms while isolating it from the immunosuppressive secretory machinery that drives its clinical activity. EcN has evolved its niche role in gut ecology to be capable of strong targeting and induction of immune cells[48–62] – while easily overshadowed by its immunosuppressive capacity, this uniquely tailored capacity makes it an ideal candidate for an OMV source. **Figure 2.1b** details mechanistically why this would be the case. EcN OMVs, due to the membrane material they are derived from, can take advantage of strongly transducing a variety of TLRs in a specific combination that apparently can strongly activate T-cells. Additionally, even ignoring the advantages that specific multivalent combinations of TLR agonists seem to have in selectively targeting certain immune cells, the presence of such TLRs in addition to bactericidal/permeability-increasing

protein (BPI) and LPS-binding protein on the surface of macrophages should additionally facilitate strong phagocytic interactions with the EcN OMVs. Of specific interest is predicting the more exact immune response generated by such cellular interactions. Considering the potential for linking antigen delivery with strong T-cell targeting and stimulation, in addition to their capacity for robust antigen-presenting cell (APC) stimulation and intracellular delivery of bacterial PAMP-rich agonists, a compelling argument could be made for likely $T_H1$ bias in an antigen-specific response leading to strong cellular immunity and memory[3]. As such a response, combined with the scalable and economic production source of *E. coli*, fulfills key elements of an ideal vaccine carrier for stimulating effective responses to a variety of current vaccine targets[4–6], EcN OMVs warrant investigation as promising candidates for recombinant subunit antigen delivery.

Herein we report the biomolecular and immunological characterization of EcN OMVs as a recombinant vaccine carrier utilizing the model antigen green fluorescent protein (GFP). Importantly, this data will be presented relative to OMVs derived from a standard laboratory K12 *E. coli* strain, JC8031 (EcJ), to highlight the advantages of using EcN as an OMV source strain. A standard 8-week prime-boost vaccination regimen in BALB/c mice resulted in substantial $T_H1$-biased anti-GFP immunity characterized by a robust humoral and cellular response. Further biomolecular analysis revealed that this favorable response was at least partly enhanced by enrichment in TLR agonists such as flagellin and mannose, which upon further *in vitro* and *in vivo* assessment resulted in enhanced inflammation, innate and adaptive immune cell recruitment and stimulation, and broad-spectrum TLR activation. We additionally report several other characteristics of the EcN OMV vaccine platform, including the capacity to achieve potent anti-antigen immune responses at low doses of antigen and the apparent dependence of this immunity on pathogen-mimetic surface display of said recombinant antigens.

## 2.2 Materials and Methods

**2.2.1: Design of Nissle *nlpI*-mutant JH1 and *lpxM* mutant JH1-*LpxM*.** *nlpI* and *lpxM* mutations were generated using P1 transduction of the *nlpI*::kan and *lpxM*::kan alleles, creating strains JH1 (Δ*nlpI*) and JH1-*LpxM* (Δ*nlpI*Δ*lpxM*), from the Keio collection[63]. Briefly, *E. coli* Nissle 1917 bacteria were grown overnight and incubated with P1 lysates from appropriate Keio single mutants, as described elsewhere[64]. Transduction was performed using 50 mM $CaCl_2$ for 20 min at 37 °C and 1 M Na-citrate for 40 min at room temp, and selective plating was done using medium containing 20 mM Na-citrate. Visual characterization was done using a LEO 1550 FESEM, a FEI Tecnai F20 TEM, and an Olympus BX41 for SEM, TEM, and fluorescent microscopy, respectively. Further protein characterization was done using BCA assay and Western blot, while LPS was analyzed using a KDO colorimetric assay and proteomics were done using the isobaric tag for relative and absolute quantitation, or iTRAQ, method.

**2.2.2: Mouse Immunizations.** Ten groups of ten 8-week old BALB/c mice (Charles River Laboratories) each were immunized s.c. with 100 µL of PBS containing purified protein or OMV preparations as described. The ten treatment groups were immunized with, respectively: PBS, 2.5 µg GFP/H1N1 HA, 2.5 µg ClyA, 2.5 µg GFP and ClyA mixture, 2.5 µg ClyA-GFP/H1N1 HA fusion, 2.5 µg alum and ClyA-GFP/H1N1 HA mixture (Alyhydrogel®, 1.3% aluminum hydroxide [mass:volume]), and recombinant fluorescent equivalents of EcJ+ClyA-GFP/H1N1 HA, EcJ (empty), EcN+ClyA-GFP/H1N1 HA, and EcN (empty). Two doses of vaccine (priming dose and boosting dose) were administered 4 weeks apart. Blood was collected from the mandibular sinus immediately before and 2 weeks after the first immunization, immediately before the boosting dose, and at 2 and 4 weeks after the boosting dose. Terminal splenectomies were performed on half (n=5) of all ten groups immediately before administration of the boosting dose and on the other half (n=5) following the final blood collection. The protocol for the

animal studies was approved by the Institutional Animal Care and Use Committee at Cornell University (protocol number 2009-0096).

**2.2.3: Assessing OMV vaccine immune response.** Standard microtiter ELISA was performed on collected serum samples from vaccinated mice in 96-well plates. Wells were incubated with purified GFP overnight, followed by serial dilution incubation with serum. Secondary antibodies for IgG, IgM, IgG1, and IgG2 were subsequently incubated and detected using HRP. Hemaggluniation inhibition assays were run using serum incubations with formalin-neutralized PR8 and X31 virus, and were detected via visual inspection of hemagglunination patterns. ELISA was also used to quantify antigen-specific T-cell response. Purified splenic T-cells were cultured for 7 days in complete RPMI, then seeded into wells and incubated in triplicate with GFP for 48 h. Anti-IFN-$\gamma$, IL-4, and IL-10 antibodies were then used to detect the presence of stimulated cytokine release. Further proliferation analysis on T-cells was also done on similarly cultured T-cells. Cultured T-cells were trypsinized, centrifuged at 1000 rpm, and diluted to $1X10^6$ cells/mL in complete RPMI, then labeled with CFSE (Invitrogen). $2X10^5$ cells were seeded into 96-well plates, incubated with 30 $\mu$L 100 $\mu$g/mL GFP, and allowed to proliferate at 37 °C for 4 days. FACS was used to assess loss of CFSE in proliferating cells. Additional *in vivo* inflammation response analysis was done using subdermal injections in BALB/c mice ears (n=4), on which histopathology was conducted 30 h post-injection of the OMV samples.

**2.2.4: In vitro analysis of immune cell stimulation by EcN OMVs.** Bone marrow-derived macrophages were harvested from BALB/c femur bone marrow, column purified, and cultured in complete RPMI for 7 days. Following this, they were plated in 6-well plates, incubated with ClyA-GFP(+) OMVs, and assessed for phagocytosis-induced fluorescence and IL-12/4/10 expression via FACS analysis. T-cell activation via OMV-pulsed dendritic cells was assessed using DCs incubated for 2 days with OMVs; coculture was conducted with CFSE-labeled T-cells in 24-well plates and proliferative analysis was done 7 days following initial seeding. CFSE-labeled B-cells were assessed identically to antigen-restimulated T-cells,

as described previously. Knock-out macrophages were acquired as generous gifts from Dr. Cynthia Leifer, and were stimulated with OMVs for 3 hours prior to media analysis of TNF-α.

**NOTE: Additional Materials and Methods can be found in Appendix I.**

## 2.3 Results and Discussion

### 2.3.1: Vaccination using green fluorescent protein (GFP) as a model antigen

Previously, we reported the successful expression and functional folding of a variety of recombinant antigens on the surface of K12 *E. coli* OMVs by inducing expression of a chimera consisting of the antigen fused to the C-terminus of enterobacterial cytotoxin ClyA[34], as illustrated previously in **Figure 1.2**. For the present study, green fluorescent protein (GFP) was selected as the primary model antigen for two reasons. First, GFP's natural fluorescence allowed simple quantitation of antigen content in all vaccine preparations, owing to the ClyA-antigen chimera's capacity to retain proper antigen folding upon outer membrane insertion[35]. GFP's second advantage was its poor immunogenicity in mice, which allowed for maximal demonstration of the vaccine carrier's immunostimualtory potential. OMV overproduction was induced in EcN via genetic knockout of *nlpI*[28,34] to produce the antigen delivery platform (**Fig. 2.2a**). OMVs released by the hypervesiculating EcN mutants expressing ClyA-GFP exhibited uniform size and shape while retaining characteristic bilipid membrane structure (**Fig. 2.2b**) and carried fluorescent membrane-bound, surface displayed GFP (**Fig. 2.2c**). To demonstrate the effect of probiotic strain-selection on the immune response, similar GFP-containing OMVs were produced as a control using non-probiotic K12 *E. coli* strain JC8031 (EcJ)[34,35]. Western blot analysis confirmed comparable ClyA-GFP content in both OMV preparations (**Fig. 2.2d**), allowing for meaningful comparisons between the two strains' abilities to trigger an immune response against the model antigen.

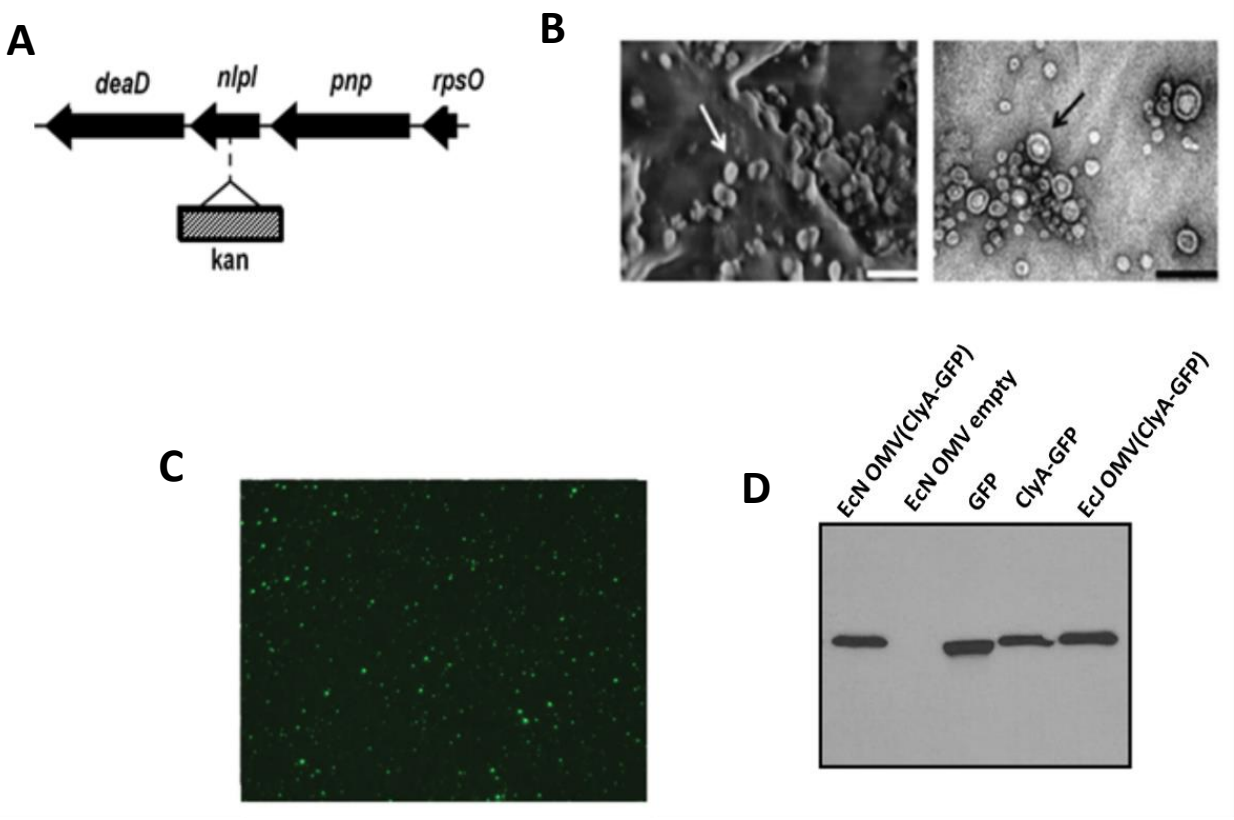


**Figure 2.2: EcN *nlpI* mutant strain produces functional OMVs for recombinant subunit vaccine applications. (A)** OMV over-production was achieved in EcN via a marked deletion of *nlpI* as illustrated here on a genetic map of the *E. coli* genoma, 71.0-71.1 min. **(B)** FE-SEM micrographs (left panel) demonstrate predominantly uniform size and shape of EcN OMVs, while TEM micrographs (right panel) highlight characteristic bilipid membrane. Scale bars = 200 nm. **(C)** Fluorescent micrograph of ultracentrifugation-purified OMVs from EcN cultures transformed with ClyA-GFP-contating plasmid. **(D)** Western blot with anti-GFP antibodies of OMV suspensions from EcN and EcJ cultures transformed with ClyA-GFP-containing plasmid.

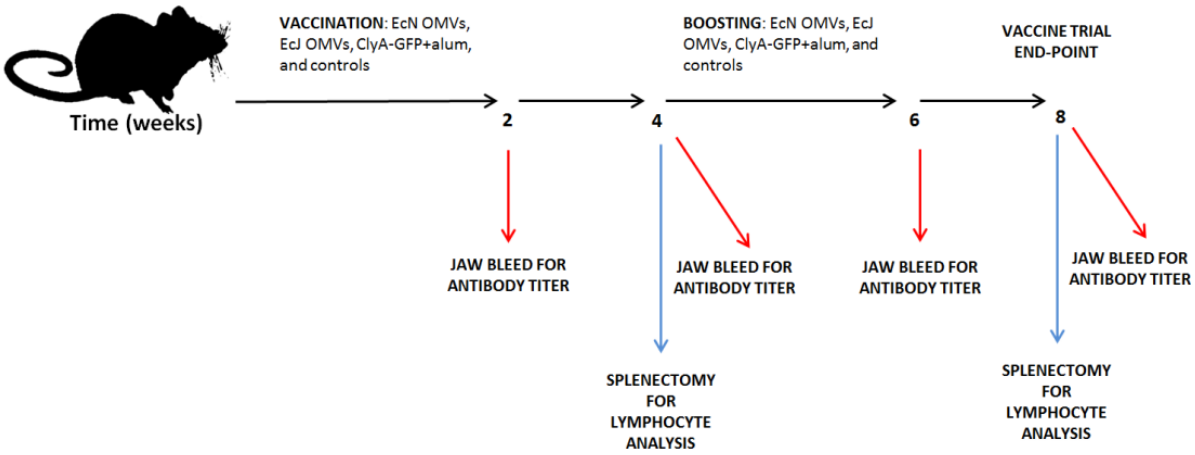


**Figure 2.3: Schematic of vaccination regimen for murine model immunization**. At time of initial vaccination, n=10 mice were vaccinated; at t=4 wk, n=5 mice were sacrificed for splenectomy, leaving n=5 mice to continue the experiment to its conclusion at t=8 wk. t=0 wk is referred to as the "Pre prime" period, 0<t<4 wk is referred to as the "Post prime" period, t=4 wk is referred to as the "Pre boost" period, and 4<t≤8 wk is referred to as the "Post boost" period.

To test the ability of EcN OMVs to generate a strong adaptive response to GFP, we immunized BALB/c mice via subcutaneous injection with formulations of OMVs containing ClyA-GFP and free of additional adjuvant (**Fig. 2.3**). To ensure the meaningful experimentation relative to a substantially competitive positive control, we separately injected vesicle-free ClyA-GFP adsorbed onto an enhanced aluminum hydroxide adjuvant delivery system, Alhydrogel®. IgG titers assayed four weeks after the final boost indicated induction of a strong humoral response by both EcN and EcJ OMVs comparable to the gold standard of alum (**Fig. 2.4a**), consistent with previous work[35] and reflective of progressive generation of a robust response (**2.5**). However, IgM titers showed some divergence in the humoral responses (**Fig. 2.4b**), with lower IgM levels generated by EcN OMVs indicating either early class-switching or a discrepancy in B-leukocyte stimulation by membranous endotoxins. Further divergence could be seen in IgG1 versus IgG2 titers. The EcN OMVs elicited an IgG2-dominant humoral response (**Fig. 2.4c** and **2.6**), which taken together with the relative decrease in final IgM titer suggests induction of a $T_H1$-facilitated immune response consistent with heightened cellular immunity stimulation[65]. In contrast, EcJ OMVs mirrored the alum-positive control with a larger IgG1 fraction, suggesting a less remarkable response more in line with standard adjuvants. As a result, these data not only indicate that the EcN OMVs can function as an effective antigen carrier for stimulating humoral immunity, but additionally suggest a strain-dependent advantage conferred by EcN in stimulating a more favorable $T_H1$ response.

Further analysis of the mice's OMV-induced adaptive immunity revealed a favorable T-cell response reflective of the EcN OMVs' divergent humoral response. Specifically, spleen-derived T-cells from mice vaccinated with ClyA-GFP EcN OMVs had proliferation responses to antigen restimulation comparable to the alum-positive ClyA-GFP control and significantly greater than that triggered by EcJ OMVs (**Fig. 2.7a**). This result is generally indicative of a superior immunostimulatory effect on naïve T-cell populations, and is in direct agreement with the driving hypothesis that the EcN membrane may be

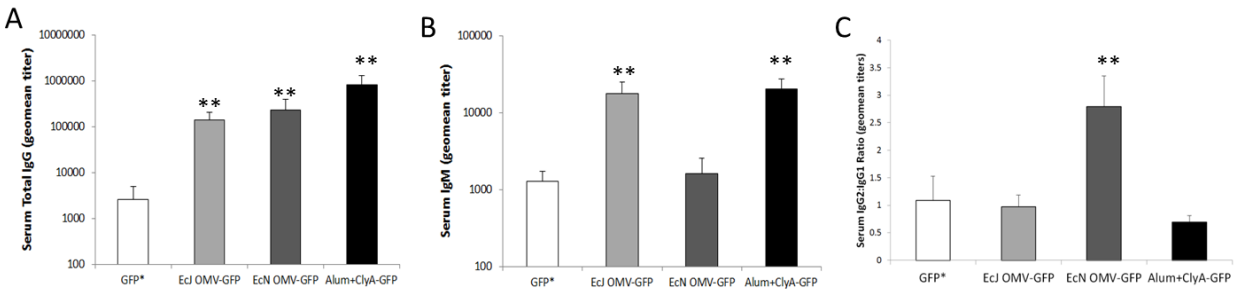


**Figure 2.4: EcN OMV platform generates robust humoral immune response in mouse model.** (**A-C**) Terminal data points from BALB/c mice vaccinated and boosted once with antigen-normalized (or protein normalized, as appropriate) doses of purified GFP, ClyA, ClyA+GFP, ClyA-GFP(+) and (-) EcJ OMVs, ClyA-GFP(+) and (-) EcN OMVs, ClyA-GFP+Alum, and PBS (n=5). (**A-B**) Class-specific anti-GFP antibody serum titers. (**C**) Ratio of serum titers of IgG1 to IgG2. (**A-C**) GFP***** data are representative of ClyA, ClyA+GFP, ClyA-GFP (-) ECJ and EcN OMVs, and PBS control subjects. Alum = Alhydrogel®. ******P<0.001. All values are given as mean + s.d.

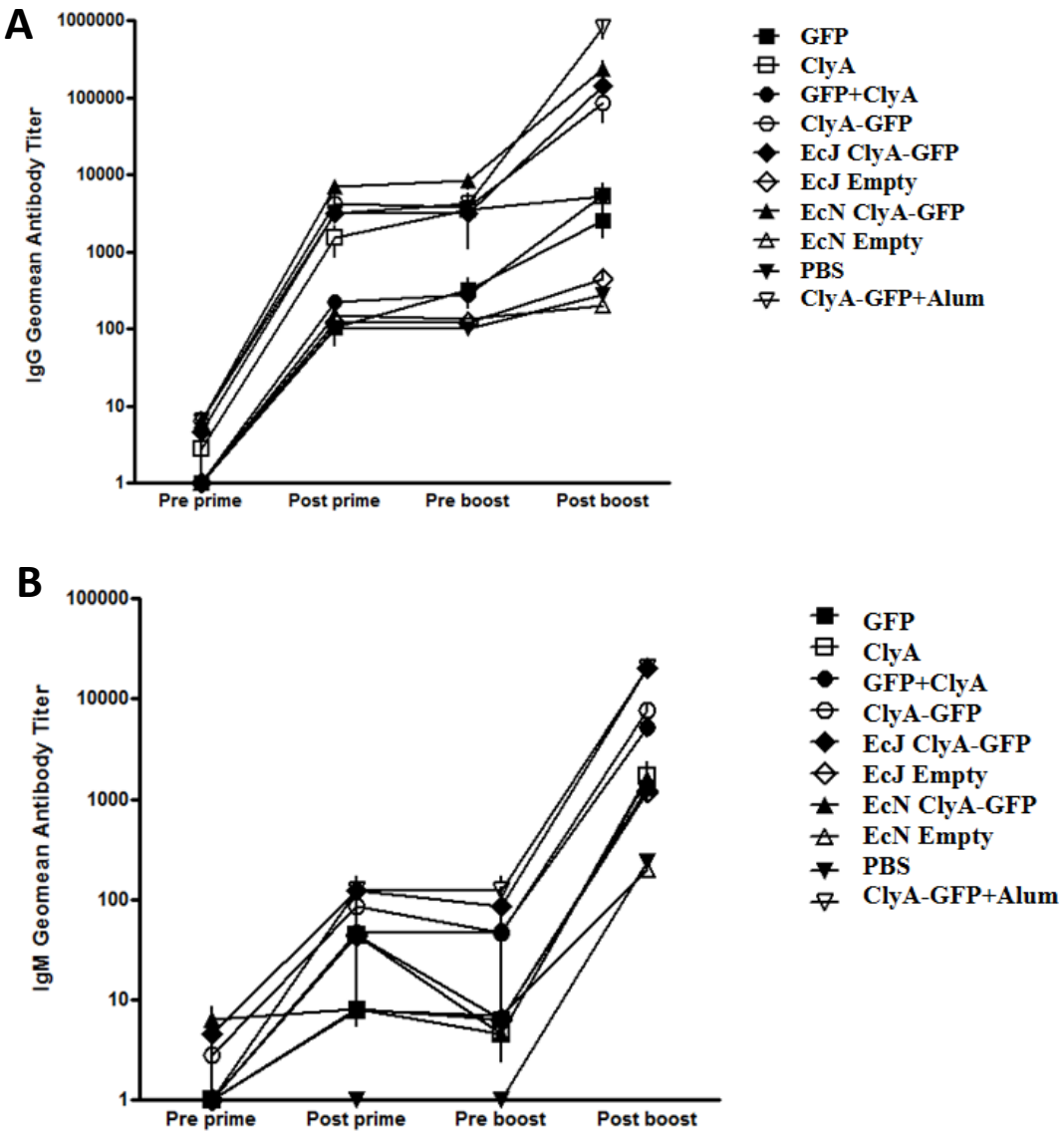


**Figure 2.5: Progressive generation of humoral immunity by EcN and EcJ OMV vaccines. (A-B)** Serum samples from jaw bleeds of all mice participating in the experiment were assayed for GFP-specific **(A)** IgG and **(B)** IgM at four time points: immediately prior to injection with priming vaccination dose (t=0 wk), following the priming vaccination (t=2 wk), immediately prior to injection with boosting vaccination dose (t=4 wk), and at the termination of the experiment (t=8 wk). Titers were determined by ELISA. All values are given as mean +/- s.d.

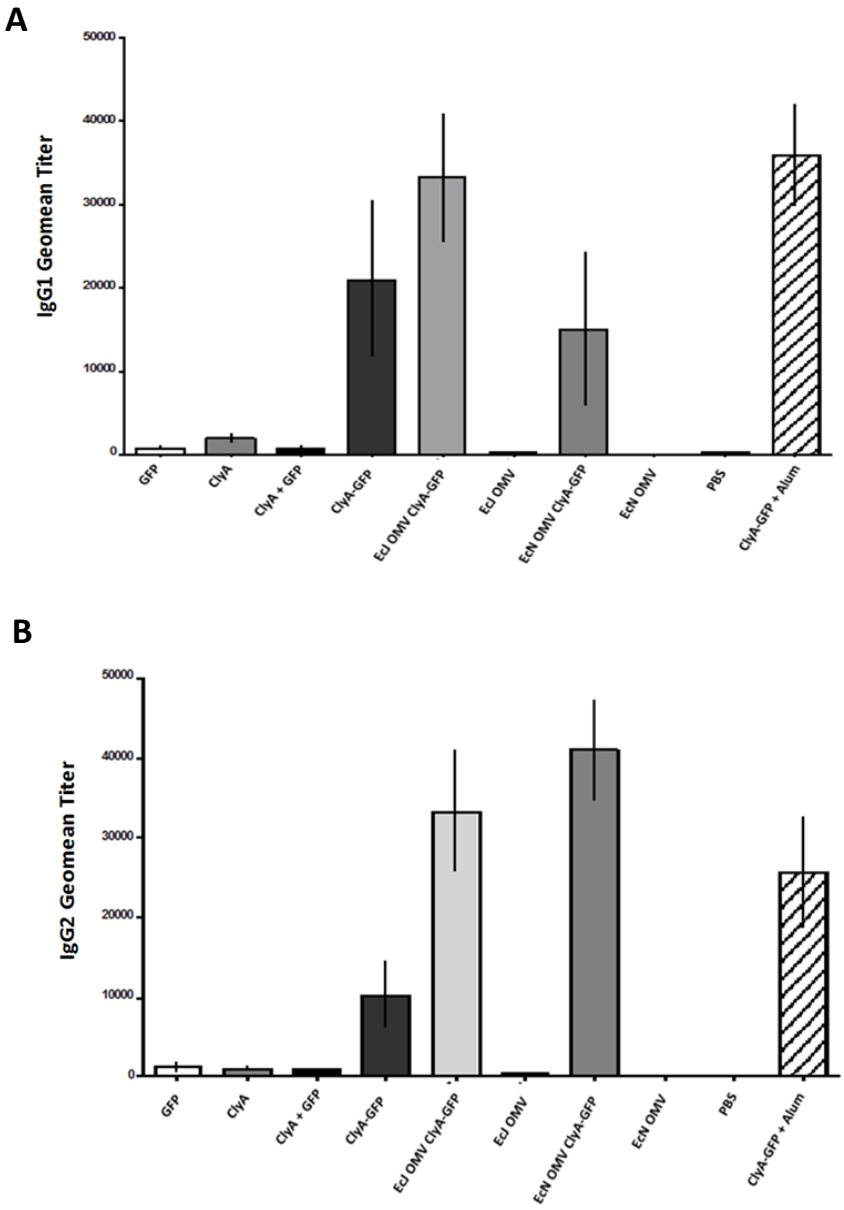


**Figure 2.6: Anti-GFP IgG1 and IgG2 serum titers from immunized and boosted mice**. **(A-B)** Serum samples from all mice (n=5) at conclusion of experiment (t=8 wk) were assayed for anti-GFP **(A)** IgG1 and **(B)** IgG2 titers. Titers were determined by ELISA. All values are given as mean +/- s.d.

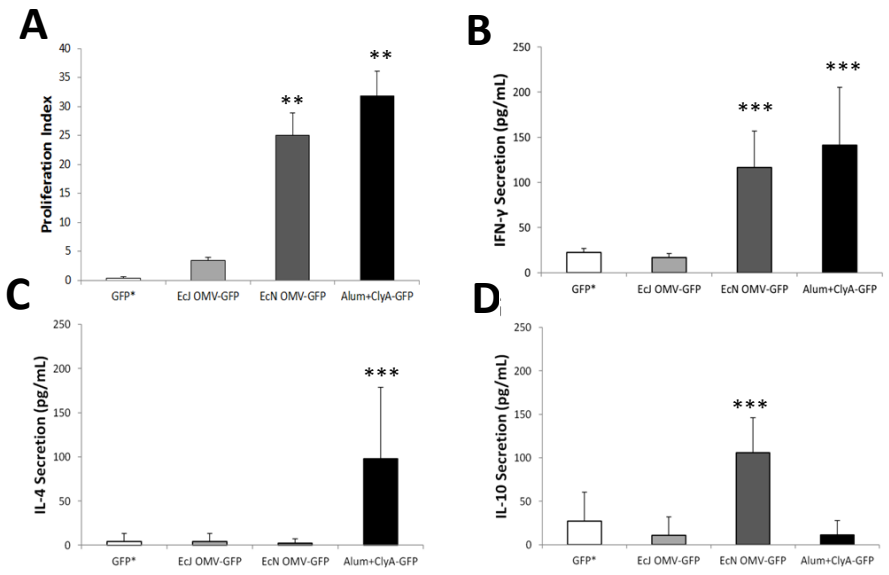


**Figure 2.7: EcN OMV platform generates robust cellular immune response in mouse model.** (**A-D** ) Terminal data points from BALB/c mice vaccina ted and boosted once with antigen-normalized (or protein normalized, as appropriate) doses of purified GFP, ClyA, ClyA+GFP, ClyA-GFP(+) and (-) EcJ OMVs, ClyA-GFP(+) and (-) EcN OMVs, ClyA-GFP+Alu m, and PBS (n=5). (**A**) Proliferation index of GFP-restimulated spleen-derived T-cells harvested from end-point subjects, measured via CFSE stain. (**B-D**) Cytokine secretion levels from cultured, GFP-restimulated spleen-derived T-cells harvested from end-point subjects. (**A-D**) GFP***** data are representative of ClyA, ClyA+GFP, ClyA-GFP (-) ECJ and EcN OMVs, and PBS control subjects. Alum = Alhydrogel®. ******P<0.001, *******P<0.05 determined by Tukey's HSD post-hoc test. All values are given as mean + s.d.

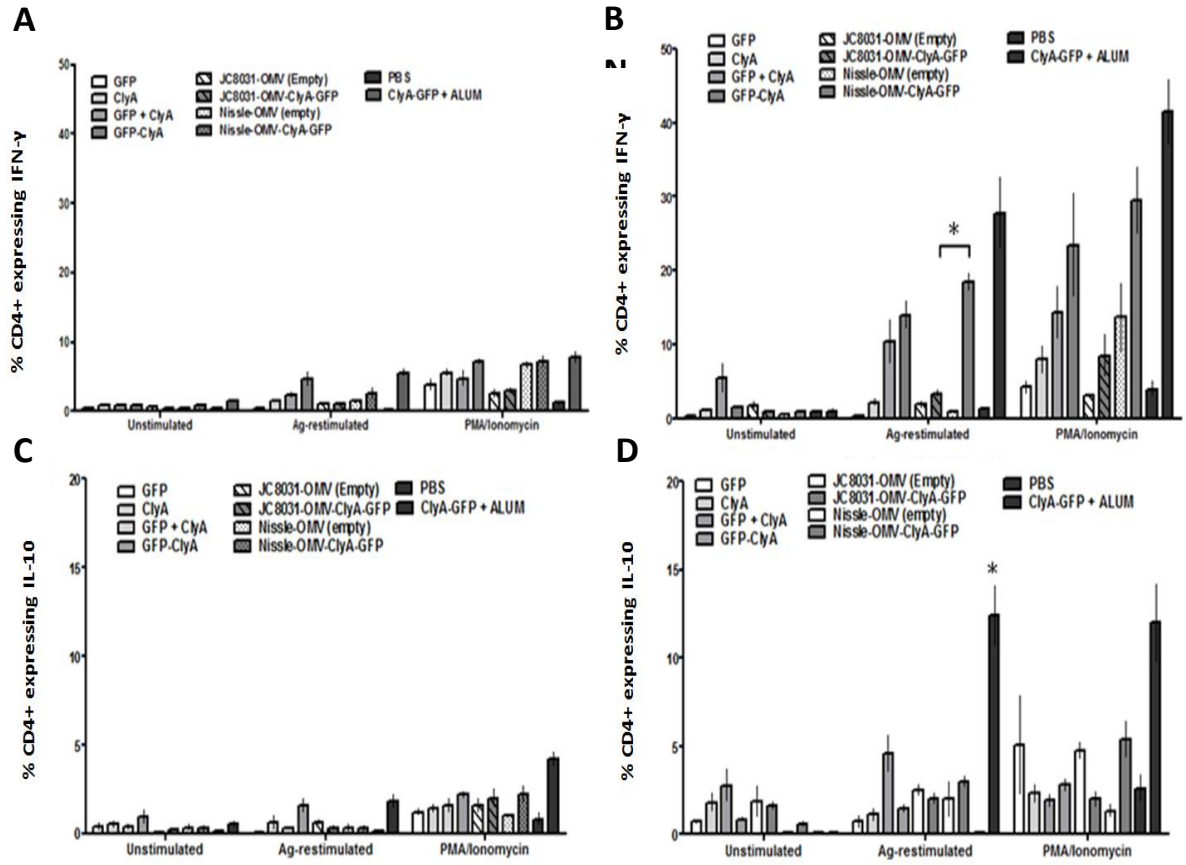


**Figure 2.8: Divergent induction of cytokine expression in spleen-derived, restimulated mouse T-cells by EcN and EcJ OMV vaccines indicates superior cellular immunity potential for EcN OMVs. (A-D)** Mouse spleens were harvested (n=5) pre-boost (t=4 wk; **A** and **C**) and at the conclusion of the experiment post-boost (t=8 wk, **B** and **D**), from which T lymphocytes were isolated, restimulated, tagged for either IFN-γ (**A-B**) or IL-10 (**C-D**) expression, and analysed via FACS. PMA/Ionomycin was used as a positive-stimulation enhancing control. *P<0.001 determined by Tukey's HSD post-hoc test. All values are given as mean +/- s.d.

privileged as an adjuvant material in its ability to actively target T cells. Moreover, EcN but not EcJ OMVs promoted a similarly dramatic increase in antigen-restimulated T-cell IFN-γ secretion (**Fig. 2.7b**) and expression levels (**2.8a-b**). Taken together, these results highlight the ability of EcN OMVs to induce a strong cellular immune response, which correlates well with the $T_H1$ response suggested by the IgG2:IgG1 ratio. Depressed IL-4 (**Fig. 2.7c**) and IL-10 (**Fig. 2.7d**, **2.8c-d**) levels relative to IFN-γ further support the induction of a favorable $T_H1$-biased response by EcN OMVs. To date, this level of $T_H1$-indicative IFN- γ/IL-4 discrepancy has rarely been reported in the literature for adjuvant-free vaccine carriers, and never for OMV-based systems. Importantly, this also sets it aside from standard adjuvants such as alum, which produce a mixed $T_H1$/ $T_H2$ response that is often insufficient at leveraging the advantage of $T_H1$ immunity against certain intracellular pathogens. Also of note was the observation that IL-10 secretory activity from EcN OMV restimulation was elevated relative to EcJ OMVs and the alum-positive control. Considering the successful induction of elevated T-cell IFN-γ levels, this suggests a unique use of IL-10 in a supplementary and indirectly beneficial role in generating a favorable yet non-detrimental T-cell response, such as influencing a shift in the $T_H1$/$T_H2$ balance while controlling potential runaway inflammation[66]. Taken together, the model antigen-specific humoral and cellular immunity induced by the EcN OMV carriers are indicative both of a protective vaccine response[67] and, more importantly, a response tuned to be useful in targeting pathogens that are most effectively neutralized by the more elusive $T_H1$-biased response[68].

**2.3.2: Biomolecular and immunological characterization of EcN OMVs**

While superior immunostimulation relative to the non-probiotic K12 *E. coli* OMVs was in line with our central hypothesis concerning EcN OMVs' derived potential for $T_H1$ bias, we were interested in seeing whether more detailed analysis of inherent discrepancies between the two strains' OMVs could further corroborate and add clarity to the initial mouse study's findings. We started by attempting to characterize the biomolecular composition of the two OMVs. We began by doing full quantitative

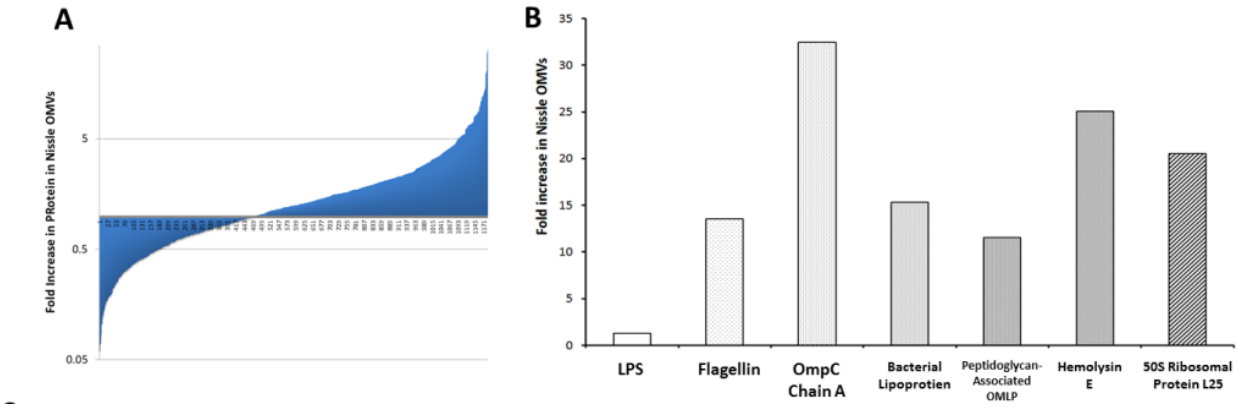


**Figure 2.9: Proteomic analysis of EcN and EcJ OMVs reveals discrepancies in biomolecular content.** Total proteomic composition, totaling 756 individual protein residue hits cross-referenced between three *E. coli* proteome databases, is fairly similar between both EcJ and EcN OMVs as a whole (**A**), with divergent outliers being classified as those enriched greater than 5-fold in one OMV relative to the other. (**B**) PAMP-rich TLR agonists significantly enriched in EcN OMVs relative to EcJ OMVs and relative to EcN:EcJ LPS discrepancy (LPS assayed separately).

proteomic analysis using protein gel mass spectrometry and isobaric tag for relative and absolute quantitation, or iTRAQ. The results were primarily as expected: the majority of proteins were similarly present and in roughly equal quantities within both strains' OMVs, with several more dramatic differences revealed at either end of the spectrum (**Fig. 9a**). Of interest, however, was the specific enrichment of a variety of well-known PAMP-rich proteins and recognized TLR agonists within the EcN OMVs relative to the EcJ OMVs. The most significantly elevated of the group (**Fig. 2.9b**) range from TLR2 agonists BLP and OmpC, to TLR4 agonist OMLP, to TLR5 agonist flagellin. Intrigued, we additionally investigated the most well-known bacterial TLR agonist, LPS, via KDO colorimetric assay. Surprisingly, LPS content was primarily conserved between the two OMVs. While this makes the proteomic analysis more meaningful (as large LPS discrepancies would have left room for argument as to whether any other PAMP-related factor could really have made a difference), it also leaves questions concerning contributions of differential glycosylation to the divergent immune responses. In other words, could differential levels of glycosylation make up for similar quantities of glycosylated residues? Glycosyl composition analysis using combined gas chromatography/mass spectrometry (GC/MS) readily revealed a potential answer (**Fig. 2.10a-b**). While KDO remained similar, as did a variety of other glycosyl residues, significant differences in heptose:mannose ratio between the two OMVs stood out. While heptose is a primarily immunologically uninteresting sugar often commonly associated with LPS, mannose is a primary target of innate immune recognition via macrophages and even complement activation, which given the likely density of mannose on the EcN OMV surface could actually facilitate interactions with the mannose-binding lectin pathway. While glycosyl linkage analysis unsurprisingly painted a more complicated picture (for which further analysis is currently ongoing), on the surface it reinforces the heptose/mannose dichotomy while bringing up additional questions concerning ribose and glucose discrepancies. Regardless, the integrated picture of proteomic and gycosyl analysis helps remove a significant component of the "black box" problem of the EcN OMV, pointing at a host of

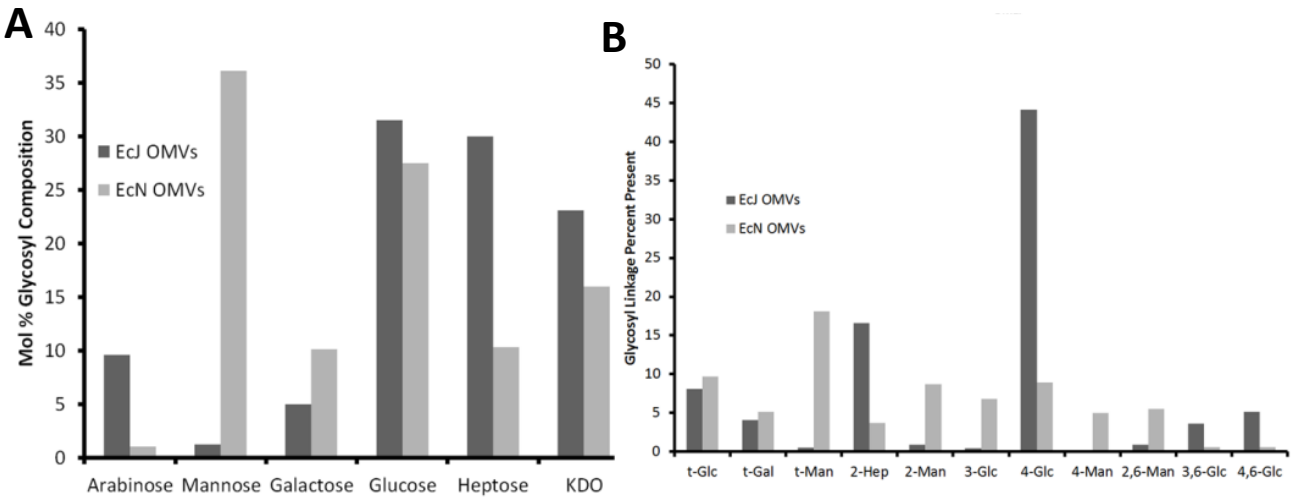


**Figure 2.10: Glycosyl composition analysis of EcN and EcJ OMVs reveals additional, immunologically relevant discrepancies in biomolecular content.** Glycosyl analysis revealed that both sugar composition (**C**) and linkage (**D**) was in certain cases equivalently divergent relative to protein composition between the two OMVs.

immunologically relevant biomolecules whose enrichment likely play a role in the observed immunogenicity of the resulting antigen carrier.

As the most obvious link between the biomolecular analysis results and the immune system itself were potential interactions between TLRs and mannose-binding moieties and their respective OMV surface ligands, we began experimental observation of the EcN OMV/immune cell interface with the innate immune system. Before refining our analysis to controlled in vitro cell culture, we began with immunopatholgy studies. While on a macroscopic level OMV vaccine inflammation was observed to be similar to that of the alum control in duration and recovery time (**Fig. 2.11**), such observations are not necessarily reflective of an adjuvant's capacity for local immune cell engagement and recruitment. Hence, we further explored the capacity of EcN OMV self-adjuvancy to robustly induce an innate response via initial dermal inflammation. Using a subdermal injection model in a BALB/c mouse ear and subsequent histological analysis, we assessed the acute inflammation response generated by both EcN and EcJ OMVs. The resulting immunopathology revealed a surprisingly marked difference. At 30 h post-injection, EcN OMVs demonstrated the ability to dramatically remodel the dermal tissue, cause local vasculature swelling, and recruit dense populations of leukocytes (**Fig. 2.12c**) relative to a blank PBS control (**Fig. 2.12a**). Such a reaction is an established sign of an adjuvanting material capable of stimulating the required innate immunity activation for a good vaccine response[4,7]. EcJ OMVs, on the other hand, stimulated a much less dramatic inflammatory response with an equivalent OMV dosage (**Fig. 2.12b**). Taken together, these data imply that the probiotic strain-dependent nature of EcN OMVs' unique immune response is in part dependent on a strong stimulation of innate immunity, a result well in line with biomolecular analysis detailed above.

Importantly, the strain-variable innate immune stimulation resulted from equivalent doses of OMV-bound LPS, generally considered to be the most important innate bacterial immunomodulator[10]. This implies that the immunostimulatory mechanism for the EcN OMVs is not fully dependent on the

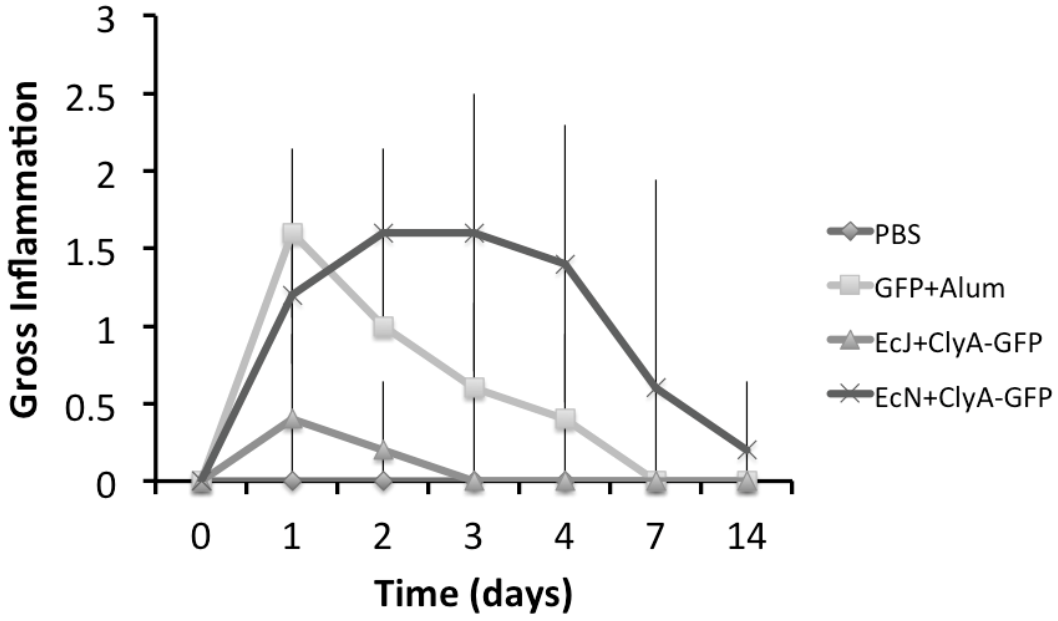


**Figure 2.11: Inflammation in vaccinated mice is similar between adjuvancy sources Alhydrogel®, EcJ OMVs, and EcN OMVS.** Gross inflammation (n=5) was graded 0-3, with 0 being equal to no apparent inflammation, 1 being mild redness causing no visible irritation, 2 being moderate redness causing no visible irritation, and 3 being moderate-to-severe redness resulting in substantial dryness and scabbing as well as evident irritation. All values are given as mean +/- s.d.

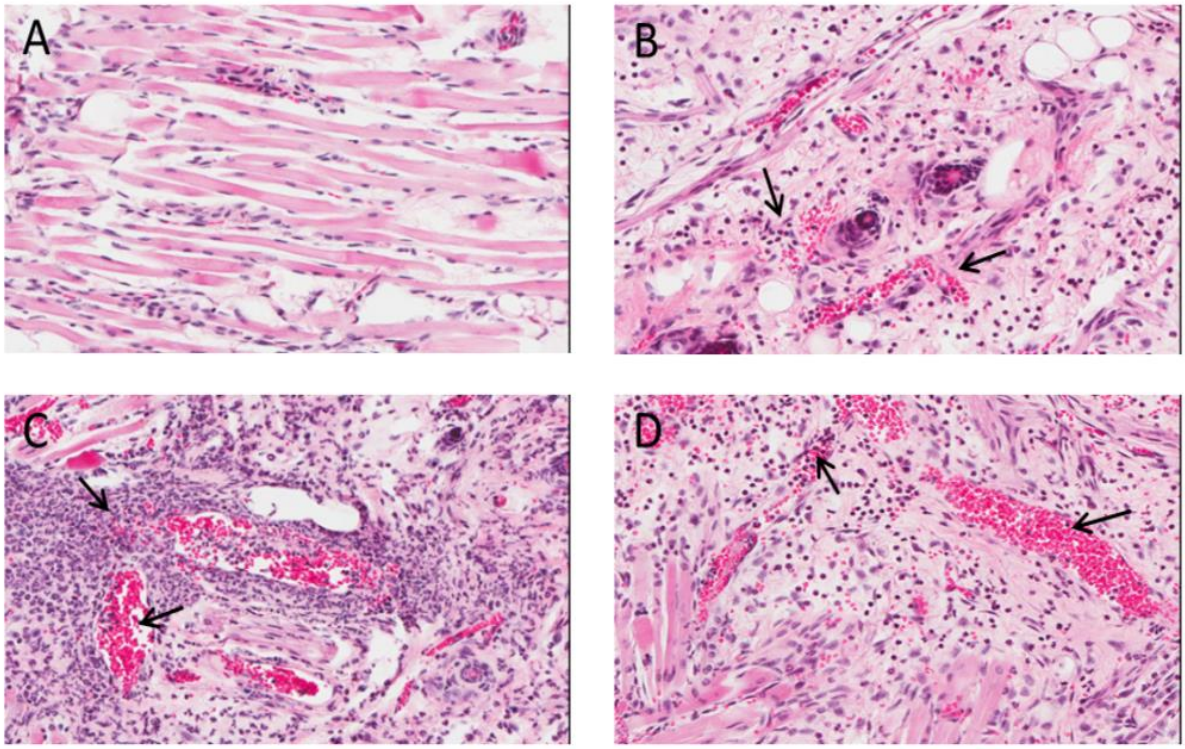


**Figure 2.12: EcN OMVs induce robust innate immunity stimulation via inflammation enhancement**. (**A-D**) Histological sections from BALB/c mice ears injected sub-dermally with equivalent doses of: (**A**) PBS; (**B**) EcJ OMVs; (**C**) EcN OMVs; **(D)** *LpxM* EcN OMVs. Mice were sacrificed after 30h. Increased tissue remodeling, vasculature congestion, and leukocyte recruitment (as indicated by arrows) can be seen in **(B)** relative to (**A**), are significantly enhanced in **(C)**, and are attenuated but not removed in (**D**).

fairly toxic bacterial moiety. Therefore, we next investigated whether or not direct reduction of LPS-induced endotoxicity would substantially attenuate the enhanced innate response observed with EcN OMVs. A genetic knockout of the *lpxM* gene in *E. coli* inactivates the MsbB lipid A acyltransferase and is known to minimize LPS-based endotoxicity[69]; therefore, *lpxM* was knocked out in the EcN *nlpI* mutant to generate mutant EcN OMVs (**Fig. 2.13**) and allow investigation of the influence of LPS on the activation of the innate response. Following identical subdermal mouse ear injections, the previously observed immunopathology was partially attenuated but ultimately still reflective of an appreciable inflammatory response (**Fig. 2.12d** and **Fig. 2.14**). Thus, a non-endotoxicity-dependent, probiotic strain-dependent advantage in innate immunity stimulation is clearly conferred by EcN as an OMV source, likely due to the presence of other highly active immunostimulatory membranous PAMPs[47] and TLR agonists as suggested by the proteomic and glycosyl analysis.

Analysis of EcN OMV macrophage stimulation, an important cellular component of innate immunity, provided additional support for an enhanced probiotic strain-dependent mechanism of innate immunity stimulation. When bone marrow-derived mouse macrophages (BMMs) were incubated with equivalent amounts of ClyA-GFP-containing EcN and EcJ OMVs, they internalized a significantly greater number of the former (**Fig. 2.15a** and **Fig. 2.16**). These results suggest that the EcN outer membrane is a more potent activator of macrophage phagocytosis. Further analysis of BMM cytokine expression profiles following OMV incubation additionally revealed a significant discrepancy in IL-12 and IL-4 expression induced by EcN and EcJ OMVs (**Fig. 2.15b**). Specifically, EcN OMVs stimulated elevated IL-12 but not IL-4 expression relative to EcJ OMVs, indicating a propensity for EcN OMVs to facilitate $T_H1$ dominance during the adaptive immunity transition. This may highlight a synergistic coupling of enhanced targeting via superior PAMP-dependent TLR crosslinking and subsequent intracellular delivery of membranous and soluble bacterial factors[10]. The opposite expression levels induced by EcJ OMVs in turn suggests facilitation of a mechanism more in line with $T_H2$ bias[70]. These results corroborate

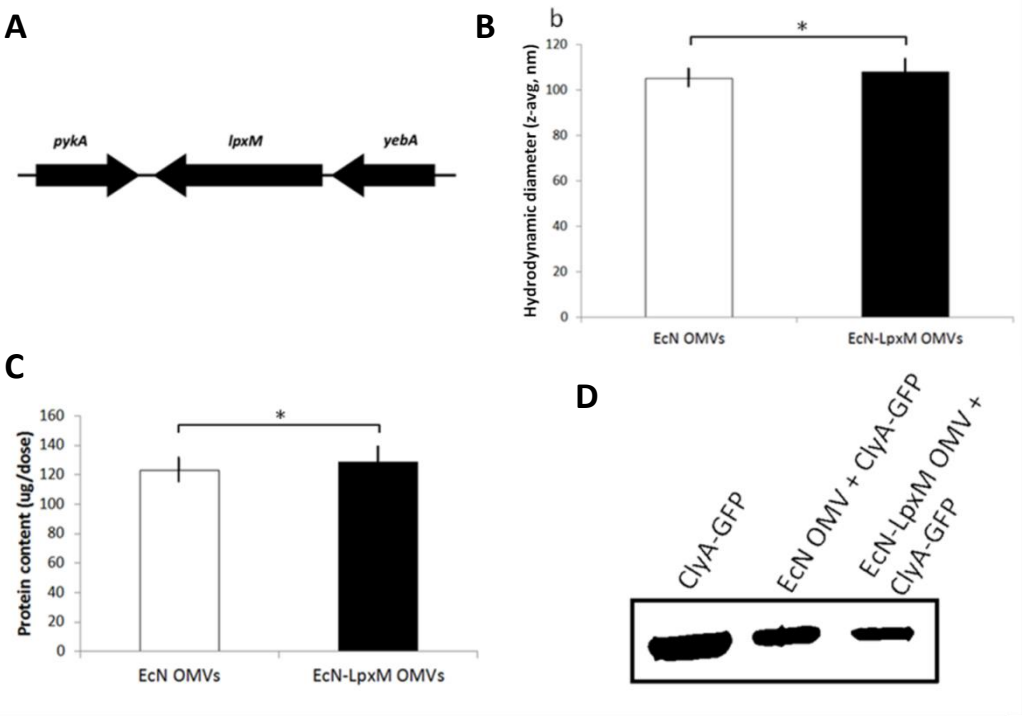


**Figure 2.13: *LpxM*-mutant EcN OMV generation does not appreciably alter OMVs. (A)** Location of *lpxM* mutation site in the *E. coli* genome, located at 41.75 min. **(B)** Dynamic light scattering hydrodynamic z-avg particle sizes of both OMVs. Formulations assessed in PBS. **(C)** GFP fluorescence-standardized ClyA-GFP(+) vaccine doses of EcJ and EcN OMVs assayed for total protein content via BCA assay. **(D)** Western blot with anti-GFP antibodies of OMV suspensions from EcN cultures transformed with ClyA-GFP-containing plasmid. Background coloration altered to improve contrast. **(B-C)** *no statistically significant difference. All values are given as mean +/- s.d.

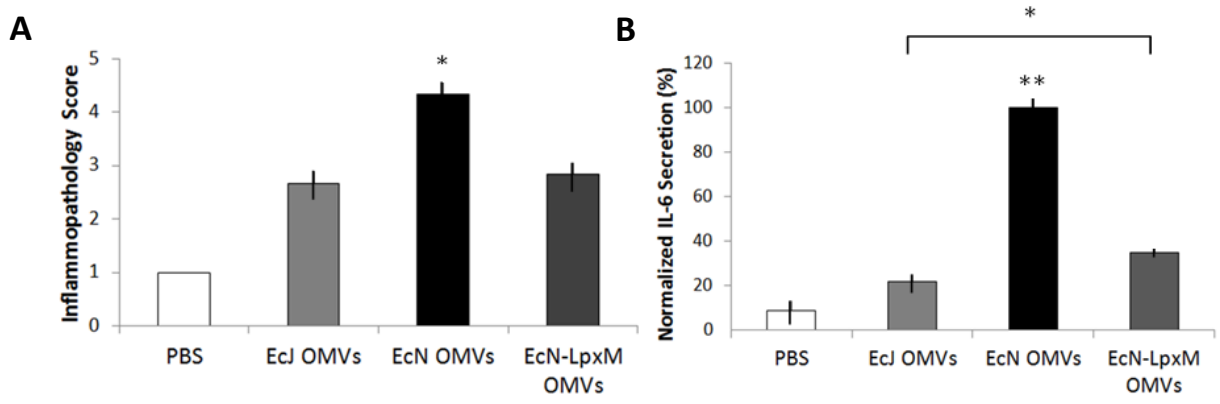


**Figure 2.14: *LpxM* mutation confers quantifiable reduction, but not ablation, of proinflammatory OMV response. (A)** BALB/c mice were injected subdermally on each ear with 10 µL of OMV solution. After 30h, the mice were sacrificed and their ears were immediately resected and placed in 10% buffered formalin. Immunopathology was rated on a scale of 1-5, 5 representing the greatest extent of effacement of normal tissue architecture by the inflammatory response. Each data point represents a representative frame taken from one ear section (n=6). **(B)** J774.1 murine macrophage culture was incubated for 12h with protein content-standardized OMV doses, following which the culture media was collected and analyzed via ELISA for IL-6 content. **(A-B)** *P<0.005, **P<0.0001 determined by Tukey's HSD post-hoc test. All values are given as mean + s.d.

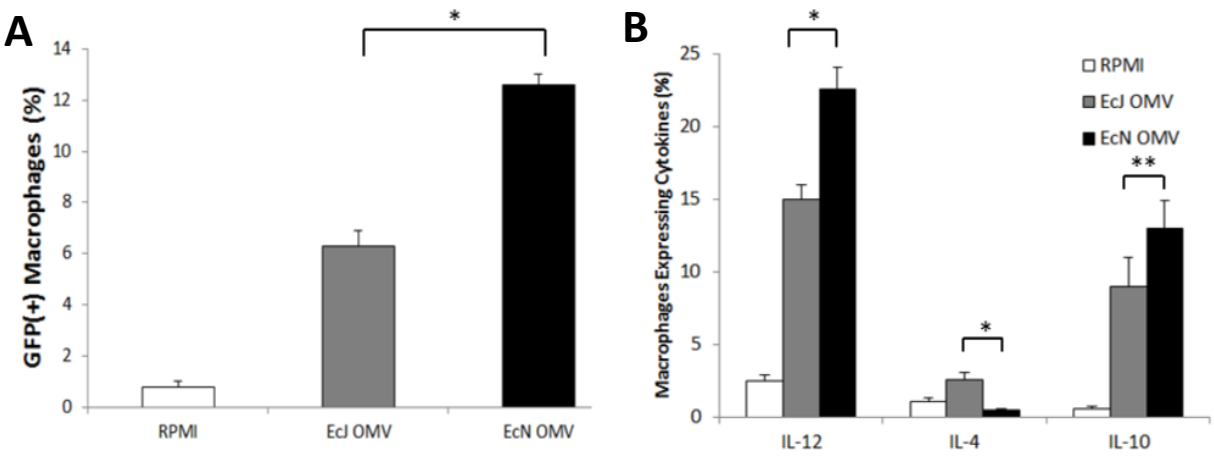


**Figure 2.15: EcN OMVs induce robust stimulation in macrophages.** (**A**) Percentage of primary mouse bone marrow-derived macrophages (BMMs) positive for GFP after 12h incubation with ClyA-GFP(+) OMVs. (**B**) Percentage of BMMs expressing cytokines IL-12, IL-4, and IL-10 after 12h incubation with OMVs.

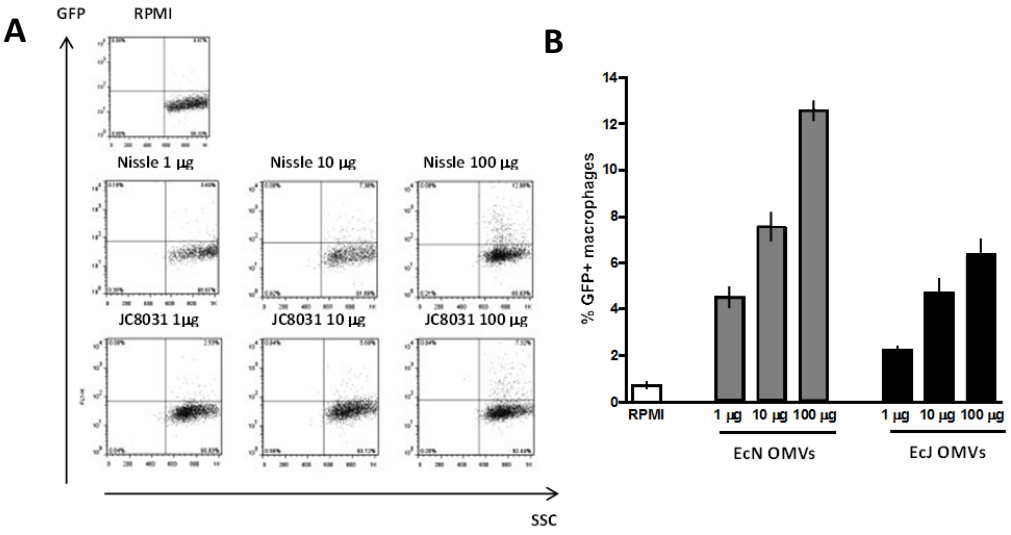


**Figure 2.16: EcN OMVs stimulate stronger phagocytic responses in macrophages. (A-B)** Primary macrophages cultured from BALB/c mouse bone marrow were incubated with variable quantities of ClyA-GFP(+) EcN or EcJ OMVs and assayed for fluorescence levels via FACS. **(A)** FACS analysis; **(B)** summarizing graph. Masses given represent amount of OMVs added as determined by total protein content. All values are given as mean +/- s.d.

previous observations of a $T_H1$-$T_H2$ discrepancy being crucial to the mechanistic benefits conferred by using the EcN OMVs.

Wanting to more specifically clarify the relationship between potential TLR agonists and macrophage activation, we ran additional in vitro studies using TLR and TLR-related pathway knockout macrophages. First, to establish the importance of TLR transduction via OMVs, EcN and EcJ OMVs were incubated with MyD88 knockout and wild type mouse macrophages. The results of a subsequent TNF-α assay clearly indicated the importance of the MyD88 pathway for OMV-induced macrophage activation (**Fig. 2.17**). To begin to parse apart the potential ramifications of the divergent biomolecular analysis, we began by noting that both EcN and EcJ OMVs contained the potent TLR4 ligand LPS, while EcN was enriched with a variety of non-TLR4 TLR agonists. Therefore, a simple subsequent test to determine whether EcN's non-TLR4 TLR agonists could make a significant impact on macrophage activation was to repeat the assay using TLR4-knockout macrophages. This time, while both EcJ and EcN OMVs remained capable of attenuate macrophage activation, EcN OMVs retained a significantly highly stimulatory potential (**Fig. 2.17**), reinforcing the importance of the noted discrepancies in biomolecular content. From there, we expanded our assessment to probe a wider range of TLR knockouts by using macrophages where all except one of the TLRs had been knocked out. As expected, TLR pathway activation-dependent luciferase expression revealed that EcJ OMVs seem to activate both mouse and human macrophages through TLR2- and TLR4-dependent pathways (**Fig. 2.18**), though the preceding experiment implies a slightly larger discrepancy in the importance of TLR4 for macrophage activation itself. While the results for the EcN OMVs revealed a dramatically different story involving substantial activation of a range of TLRs, the magnitude of that activation needs to be tempered by the likely bleed-over of some TLR5 activation, which is a problem with the particular assay selected. Regardless, the results can be confidently summarized as follows: 1) while EcJ OMVs rely primarily on the TLR4 pathway for stimulating macrophages, EcN OMVs supplement TLR4 activation with additional, non-TLR4 MyD88

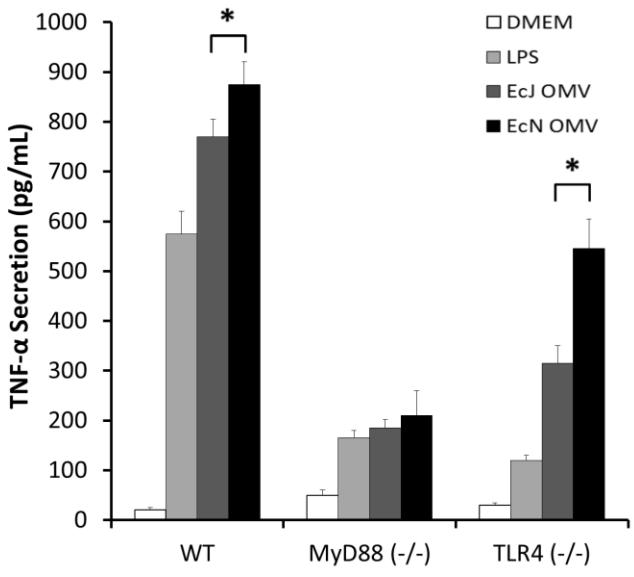


**Figure 2.17: EcN OMVs stimulate macrophages via a MyD88-dependent, TLR4-dependent/independent pathway.** Macrophage TNF-α secretion stimulated by OMV incubation in wild type (WT), MyD88 deficient, and TLR4 knockout cell lines. LPS (0.1 ug) used as a positive control. *P<0.005 determined by Tukey's HSD post-hoc test. All values given as mean + s.d.

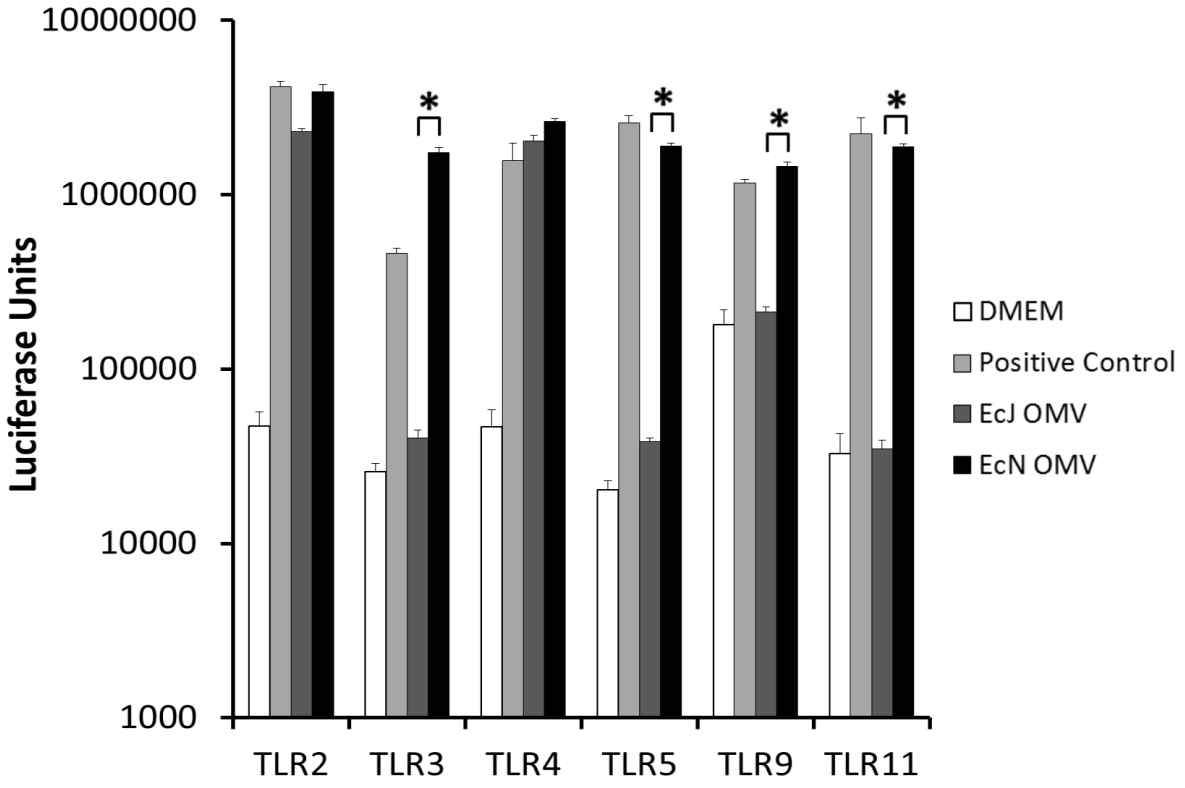


**Figure 2.18: EcN OMVs stimulate macrophages via expanded interactions with diverse TLRs.**
Luciferase expression in TLR knockout macrophages (expression correlates with individual TLR activation) incubated with OMVs. *P<0.005 determined by Tukey's HSD post-hoc test. All values given as mean + s.d.

activation; 2) EcN OMVs are potent TLR5 activators, likely owing to their enriched flagellin content; and 3) EcN OMVs likely stimulate a variety of other TLRs in mice as well as human macrophages, though the exact strength and relevance of such activation is unknown at this time.

Returning to our interest in assessing the nature of the $T_H1$-$T_H2$ discrepancy noted in the initial vaccine trial, we noted that an important link between a heightened inflammatory response, likely mediated by strong macrophage activation, and the development of a strong adaptive T-cell response are antigen-loaded dendritic cells (DCs) that migrate from the site of inflammation to local lymph nodes[2]. To determine if DC-dependent T-cell activation could benefit from the strain-dependent immunomodulation induced by EcN OMVs, we assessed the ability of bone marrow-derived mouse DCs (BMDCs) incubated with EcN and EcJ OMVs to induce proliferation in spleen-derived mouse T-cells. The pronounced increase in naïve T-cell activation by BMDCs primed with EcN OMVs (**Fig. 2.19a**) relative to those primed with EcJ OMVs suggests that the selection of EcN as the OMV source improved the ability of the OMVs to effectively interface with and stimulate antigen-presenting cells (APCs). Additionally, the ability of the EcJ OMV control to also stimulate T-cells through BMDC-dependent activation, albeit to a lesser extent than EcN OMVs, helps rule out the possibility that they caused a DC-dependent T-cell suppression[48], which would have made conclusions concerning a strain-dependent $T_H1/T_H2$-bias discrepancy difficult. Finally, recalling our initial interest in direct OMV/T-cell interactions, we incubated the mouse T-cells with the two OMVs in absence of any DC co-stimulation and probed for MyD88 activation as a simple measure of hypothesized TLR activation. A Western blot run on T-cell lysate post-incubation highlights the expected discrepancy (**Fig. 2.19b**): EcN OMVs trigger enhanced MyD88 expression relative to EcJ OMVs, in line with the driving hypothesis concerning the EcN-derived mechanism of enhanced OMV immunostimulation.

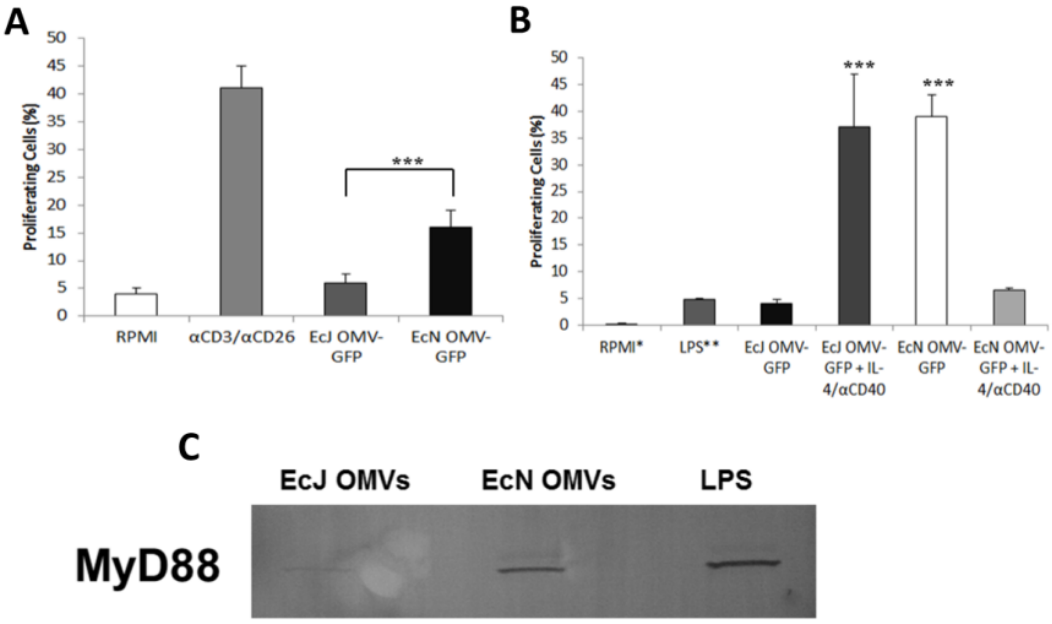


**Figure 2.19: EcN OMVs effectively stimulate adaptive immune cells.** (**A**) Proliferation of primary mouse spleen-derived T-cells following co-culture with mouse bone-marrow derived dendritic cells pre-incubated with equivalent amounts of EcJ and EcN OMVs. RPMI = negative control, αCD3/αCD26 = positive control. (**B**) Proliferation of primary mouse bone marrow-derived B-cells following incubation with OMVs, with or without additional T-cell helper factors. RPMI***** data are representative of additional controls αIgM, αCD40, and IL-4. LPS****** data are representative of additional controls αIgM/IL-4 and αCD40/IL-4. (**C**) Western blot using anti-MyD88 antibodies of T-cell lysates following in vitro incubation of primary mouse splenocytes with OMVs. LPS (10 ug) used as a positive control. (**A-B**) ***P<0.005 determined by Tukey's HSD post-hoc test. All values are given as mean + s.d.

Further assessment of crucial stimulation of DCs revealed additional insight into the unique mechanism being employed by the EcN OMVs to stimulated enhanced adaptive immunity. Two-photon microscopy of extracted lymph nodes was used to confirm that OMVs drained into lymph nodes following subcutaneous injection, where they spatially overlapped with adoptively transferred dendritic cells (DCs) (**Fig. 2.20a-c**). These results confirm that the OMV carriers and their delivered antigens are available to lymphoid-localized DCs, T-cells, and B-cells[3]. Subsequent *in vitro* stimulation of separately purified murine splenic DCs revealed that while both EcN and EcJ OMVs substantially upregulated CD86, EcN OMVs had a greater capacity to additionally upregulate CD80 as well (**Fig. 2.21**). This is promising, as CD80 has been implicated in modulating regulatory immunity in addition to traditional stimulatory cellular immunity[71].

Taken together, the enhanced stimulation of both macrophages and DCs by EcN OMVs builds a strong case for a PAMP-dependent mechanism for enhanced activation of professional APCs as a crucial component of the robust induction of adaptive immunity to a recombinant antigen. These data led us to consider that the EcN OMVs' immunomodulatory capability might take advantage of similarly improved interactions with the third major APC, namely B-cells. A capacity for direct B-cell stimulation, and thus direct surface-displayed antigen presentation, would also help explain the enhanced cross-strain protection observed when H1N1 HA was used as a secondary model antigen. Accordingly, we measured induced proliferation of splenic mouse B-cells via incubation with EcN and EcJ OMVs. This analysis revealed that EcN OMVs possessed significant potential for T-cell independent B-cell activation due to their ability to stimulate B-cell proliferation in the absence of T-cell helper factors (**Fig. 2.19c** and **Fig. 2.22**). Such activation is not uncommon in pathogen infection[72], and likely resulted from a combination of the presence of EcN PAMPs and OMV nanoscale avidity enhancement[21]. Interestingly, this phenomenon was in strong contrast to the EcJ OMV control's ability to activate B-cells, which was entirely dependent on the addition of T-cell helper factors IL-4 and anti-CD40. Such a strong

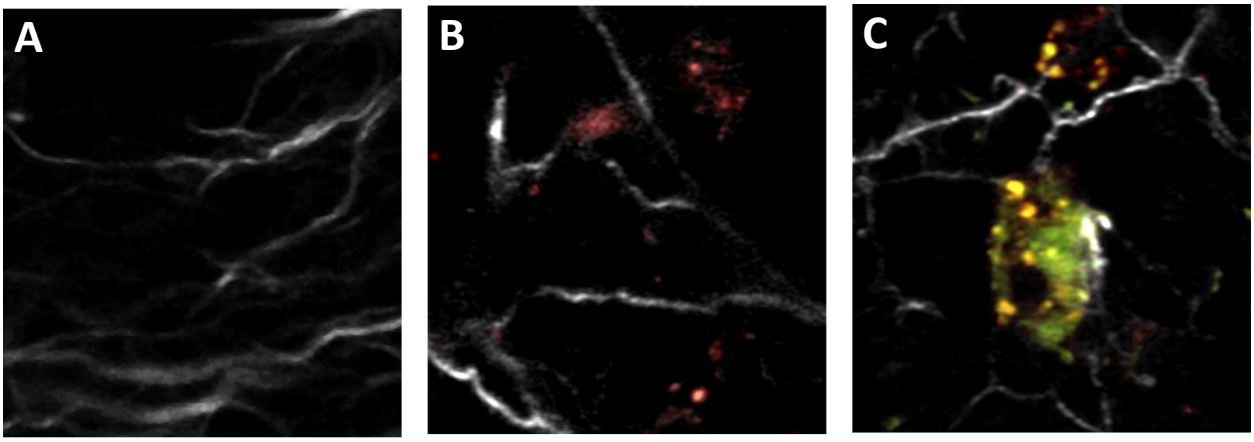


**Figure 2.20: EcN OMVs visualized through two-photon microscopy demonstrate intact drainage from injection site to lymph nodes.** Representative two-photon microscopy of draining lymph nodes from mice (n=3, all groups) injected with PBS (**a**), fluorescently stained EcN OMVs (**b**), and fluorescently stained EcN OMVs and splenic dendritic cells (DCs) (**c**). White = collagen, red = OMVs, green = DCs, and yellow = OMV/DC overlap. Arrows denote OMVs (**b**) or DCs (**c**). Scale bar = 15 µm.

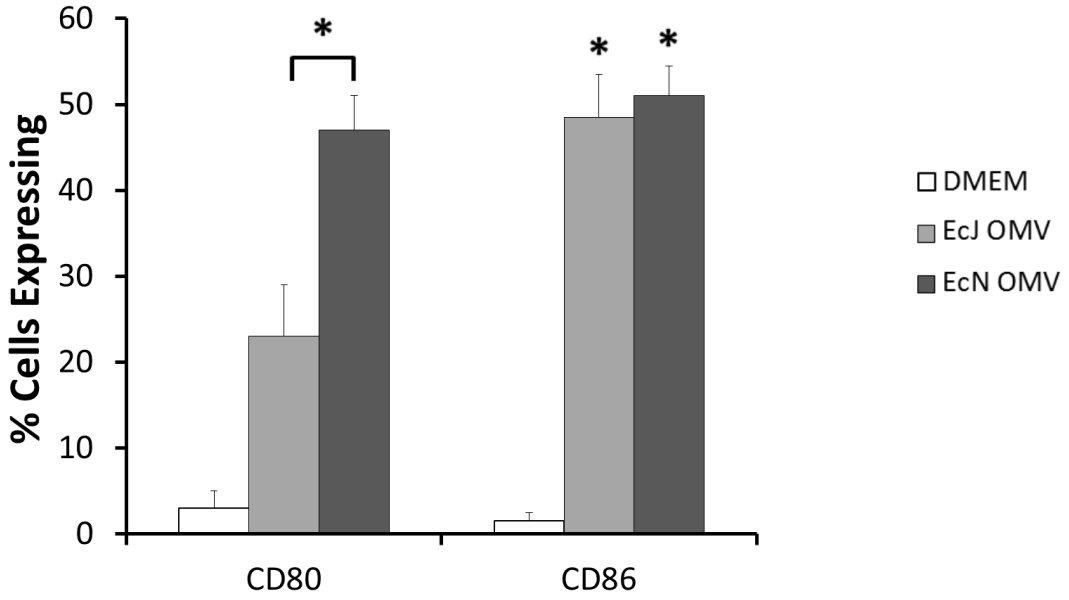


**Figure 2.21: EcN OMVs stimulate DCs more broadly than EcJ OMVs.** Flow cytometry analysis of primary mouse splenic DC stimulation by EcJ and EcN OMVs (n=3, all groups). *P<0.01. All values are given as mean + SD.

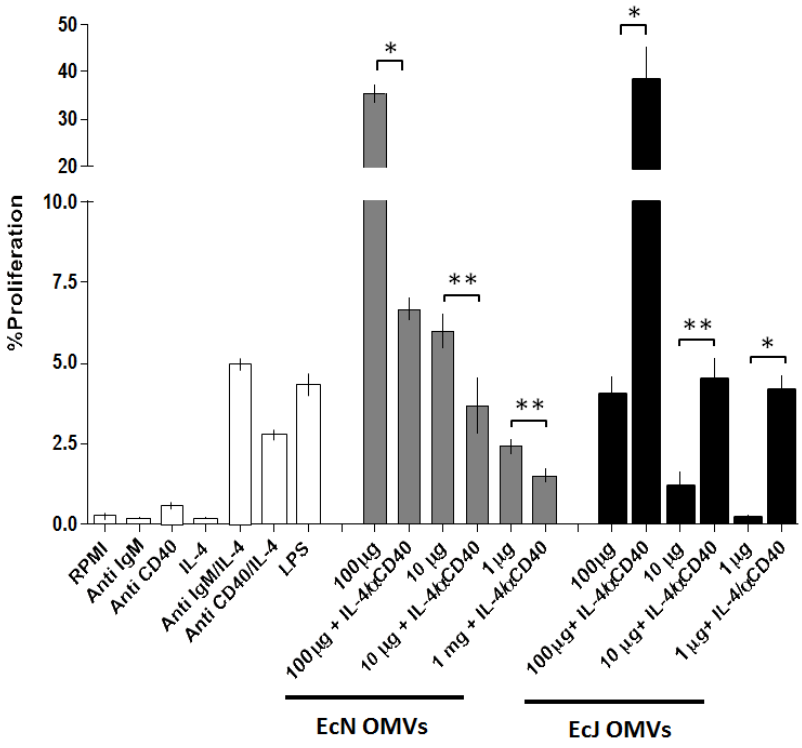


**Figure 2.22: B-cells are activated by EcN or EcJ OMVs via different mechanisms.** Primary bone marrow-derived BALB/c mouse B-cells were incubated with various quantities of EcN or EcJ OMVs either in the presence or absence of T-cell-derived proliferation induction helper factors IL-4 and anti-CD40. *P<0.001, **P<0.01 as determined by Tukey's HSD post-hoc test. Masses given represent amount of OMVs added as determined by total protein content. All values are given as mean +/- s.d.

discrepancy further highlights the important benefit EcN provides to *E. coli* OMV antigen carriers, providing robust humoral immunity through a supplemental T-cell independent mechanism that can work in parallel to, and perhaps even uniquely enhance, the establishment of a $T_H1$-dominated adaptive response.

### 2.3.3: Additional exploration of EcN OMV vaccine response dependence on dose and antigen presentation

The vaccination studies in **2.3.1** and resulting in-depth immunological analysis in **2.3.2** left two questions unanswered that we decided to probe with additional vaccination studies in BALB/c mice again using the ClyA-GFP construct as a model antigen. First, the results of the inflammation analysis left mild concerns related to the potential for detrimental, long-term injection-site side effects of EcN OMV vaccination. To determine whether the advantages of EcN OMV immune activation on the cellular-level could be sufficiently maintained while using decreased vaccine doses to attenuate enhanced inflammation, a dosing study was done while paying closer attention to the short-term and long-term injection-site immunopathology. Second, several converging observations supported the hypothesis that EcN OMVs, and perhaps OMVs in general, that surface display their recombinant exogenous antigens can take advantage of the presentation of intact, fully-folded antigen epitope space to enhance anti-antigen adaptive immunity. To test whether antigen externalization actually made a significant difference, we repeated the vaccination trial while comparing the results of ClyA-GFP OMVs to ssTorA-GFP OMVs, the latter of which uses a well-studied Tat signaling pathway[73] to transport attached peptides to the periplasmic side of the outer membrane while not enabling membrane externalization.

The results of the dosing study were straightforward and encouraging. By varying the dose down to two orders of magnitude of the original dose used in **2.3.1**, we found that up to a 10-fold reduction in vaccine dose could stimulate a similar humoral (**Fig. 2.23a-c**) and cellular response (**Fig. 2.24**

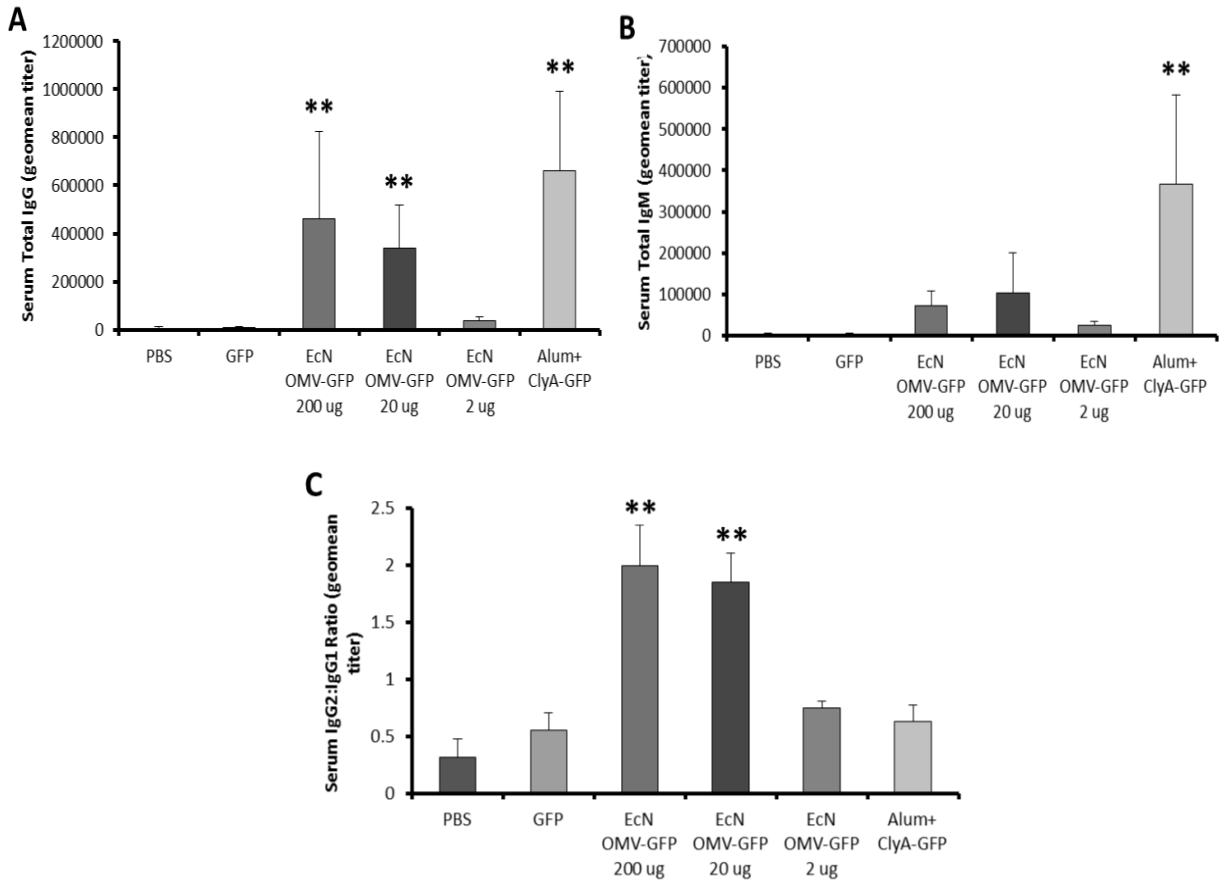


**Figure 2.23: EcN OMV carriers generate strong anti-antigen humoral immunity at more dilute vaccination doses.** (**A-C**) Terminal data points from BALB/c mice vaccinated and boosted once with antigen-normalized (or protein normalized, as appropriate) with EcN OMVs and controls (n=5). (**A-B**) Class-specific anti-GFP antibody serum titers. (**C**) Ratio of serum titers of IgG1 to IgG2. (**A-C**) Alum = Alhydrogel®. **P<0.05 determined by Tukey's HSD post-hoc test. All values are given as mean + s.d.

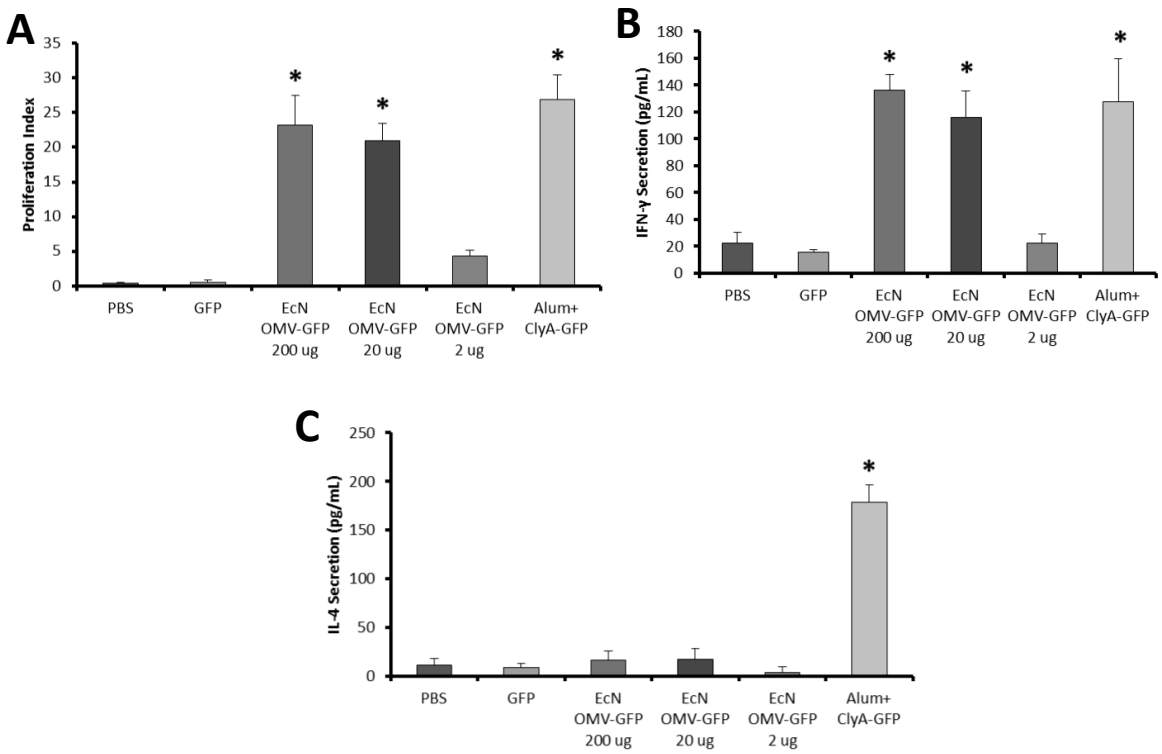


**Figure 2.24: EcN OMV carriers generate strong anti-antigen cellular immunity at more dilute vaccination doses.** (**A-C**) Terminal data points from BALB/c mice vaccinated and boosted once with antigen-normalized (or protein normalized, as appropriate) with EcN OMVs and controls (n=5). (**A**) Proliferation index of antigen-restimulated spleen-derived T-cells harvested from end-point subjects, measured via CFSE stain. (**B-C**) Cytokine secretion levels from cultured, antigen-restimulated spleen-derived T-cells harvested from end-point subjects. (**A-C**) Alum = Alhydrogel®. *****P<0.005 determined by Tukey's HSD post-hoc test. All values are given as mean + s.d.

**a-c**). Additionally, gross inflammation observation (**Fig. 2.25**) demonstrated that the 10-fold reduction was all that was required to almost entirely eliminate injection site redness that lingered beyond the first few days in the original trial. We decided to do histological analysis of the injection site as well (**Fig. 2.26**), to ensure that gross inflammation observation correlated with a decrease in lasting tissue-level effects. Specifically, we stained for fibrin deposition using Masson's trichrome, which clearly demonstrated that the 10-fold dose reduction maintained immune cell recruitment while attenuating fibrous deposition that could lead to undesirable scaring in a human subject. Given these results, it is safe to conclude that dose optimization, combined with more refined techniques such as LPS endotoxicity mutations as described in **2.3.2**, can likely overcome any substantial side effects generated by an EcN OMV vaccine.

For the second study focusing on ClyA versus ssTorA as an antigen transporter, a similar parallel could be drawn between the results of the humoral (**Fig. 2.27**) and cellular (**Fig. 2.28**) immune response analysis and those presented in **2.3.1**, with one significant difference. As expected, the EcJ and EcN OMVs containing ClyA-GFP performed similarly to their identical experimentation presented previously. Concerning EcJ ssTorA-GFP, there was no statistically significant change in humoral or cellular response, suggesting that antigen internalization versus externalization for the EcJ OMV is not a very important factor. The same could not be said for the EcN OMV. The general humoral and cellular response, reflected by total IgG and T-cell proliferation stimulation, was clearly attenuated as a whole, implying that surface antigen presentation is important for the antigen delivery mechanism used by the EcN OMV. Moreover, delivering the GFP to the EcN OMV using ssTorA resulted in the removal of the favorable IgG2:IgG1 and IFN-γ:IL-4 ratios, implying a reduction in both functional humoral immunity (reduced opsonizing/neutralizing antibodies) as well as a loss of $T_H1$ bias. Additional experimentation may be needed to better support the apparent conclusion, but the results of this experimentation reinforce two phenomena previously suggested by the studies in **2.3.1** and **2.3.2**: 1) EcJ and EcN, despite

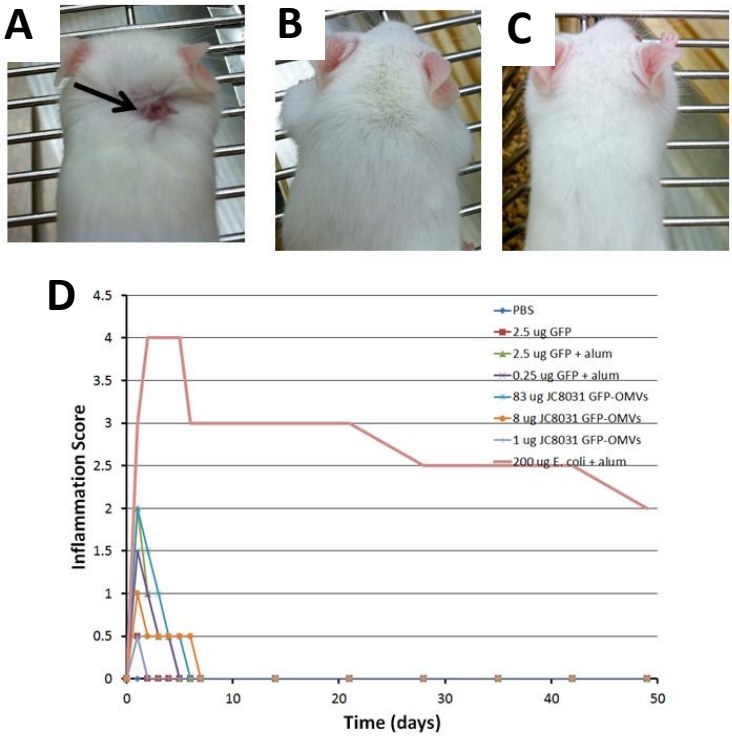


**Figure 2.25: Long-term inflammation study in mice demonstrates removal of injection-site side effects.** (**A-C**) End-point inflammation at the injection site of the vaccinated mice (n=5, all groups). Compared to an alum + killed E. coli positive control (**A**), low-dose OMVs remove potentially damaging bacterial factor-mediated inflammation (**B**) relative to an alum-antigen control (**C**). (**D**) Inflammation was tracked over a course of 90 days, and scored 0-5 (0 being completely normal, 3 being noticeably inflamed with evident hair loss, and 5 being permanently scarred with obvious fibrosis, complete hair loss, and clearly detrimental discomfort). All images are representative of experimental groups (n=5). Arrows note major marker of inflammation.

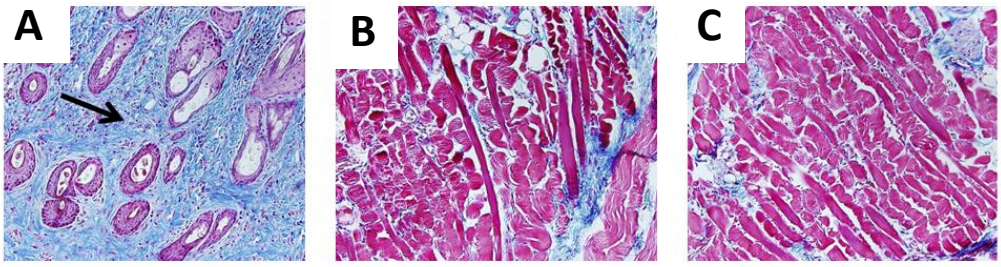


**Figure 2.26: Long-term immunopathology study in mice demonstrates removal of injection-site side effects.** ). (**A-C**) While the alum + killed E. coli control generated substantial fibrosis (blue) (**A**), low-dose OMVs eliminated mild fibrosis at the injection site (**B**) relative of the alum-antigen control (**C**) after 8 weeks following initial vaccination. (**A-C**): all images are representative of experimental groups (n=5). Arrows note major marker of inflammation.

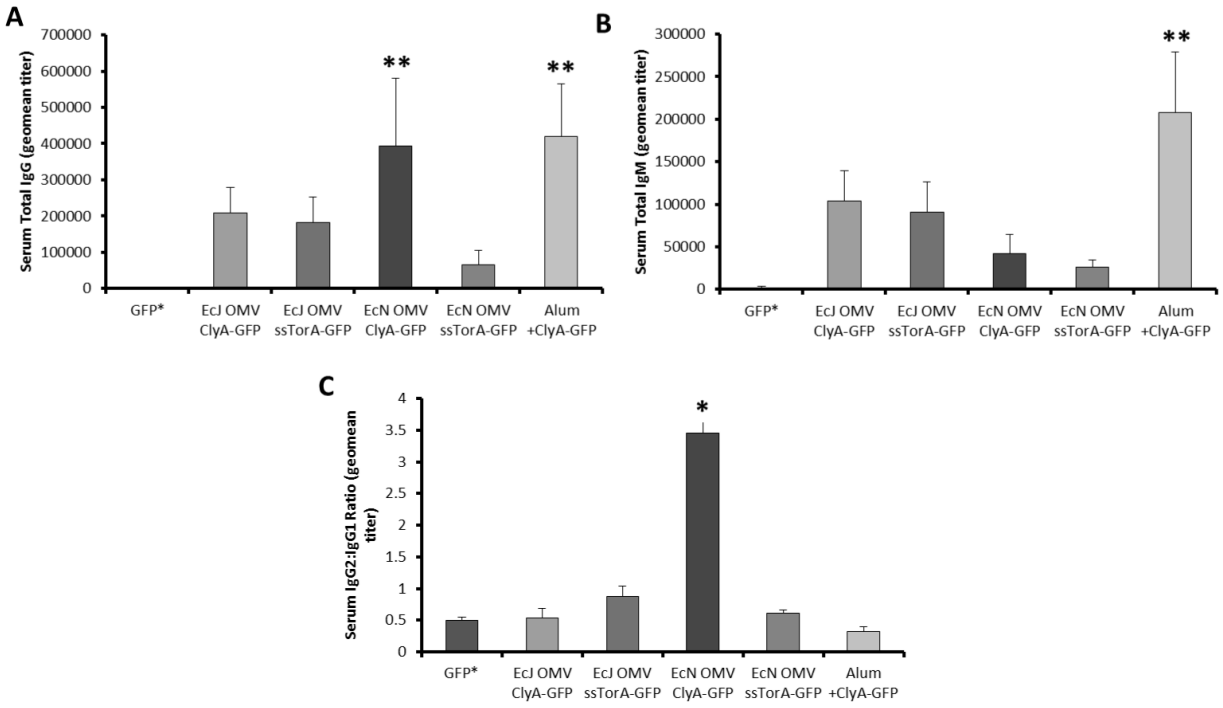


**Figure 2.27: EcN OMV carrier's enhanced anti-antigen humoral immunity is partially dependent on antigen surface presentation.** (**A-C**) Terminal data points from BALB/c mice vaccinated and boosted once with antigen-normalized (or protein normalized, as appropriate) with EcN OMVs and controls (n=5). (**A-B**) Class-specific anti-GFP antibody serum titers. (**C**) Ratio of serum titers of IgG1 to IgG2. (**A-C**) Alum = Alhydrogel®. ***P<0.005, ****P<0.05 determined by Tukey's HSD post-hoc test. All values are given as mean + s.d.

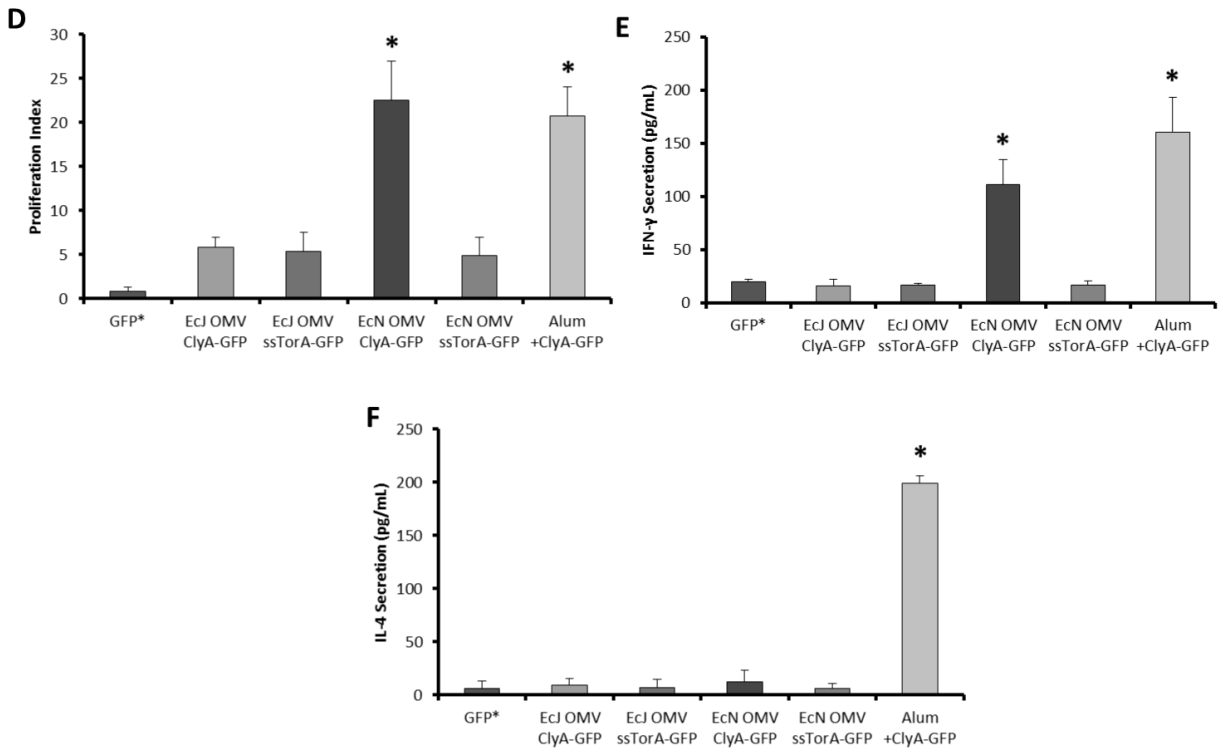


**Figure 2.28: EcN OMV carrier's enhanced anti-antigen cellular immunity is partially dependent on antigen surface presentation.** (**A-C**) Terminal data points from BALB/c mice vaccinated and boosted once with antigen-normalized (or protein normalized, as appropriate) with EcN OMVs and controls (n=5). (**A**) Proliferation index of antigen-restimulated spleen-derived T-cells harvested from end-point subjects, measured via CFSE stain. (**B-C**) Cytokine secretion levels from cultured, antigen-restimulated spleen-derived T-cells harvested from end-point subjects. (**A-C**) Alum = Alhydrogel®. *****P<0.005 determined by Tukey's HSD post-hoc test. All values are given as mean + s.d.

both being *E. coli*-derived OMVs, stimulate antigen-specific immunity through divergent pathways, and 2) antigen surface presentation is not only a potential advantage of our OMV antigen carrier platform in general, but may be intrinsically tied to the observed favorability of the EcN OMV vaccine response.

**2.4 Conclusions**

EcN OMVs demonstrated substantial promise as $T_H1$-biasing recombinant vaccine carriers. Initial testing using GFP as a model heterologous recombinant antigen demonstrated potent anti-antigen immunity, both humoral and cellular, that is indicative both of protective efficacy thorough bias resulting purely from self-adjuvancy; taken together, this provides ample evidence for investigation of applications in vaccine challenge models. Intriguingly, concerning the desire to create a pathogen-like particle that provides targeted self-adjuvancy with its delivery directly to innate and adaptive immune cells, the EcN OMVs benefited from a variety of molecularly-directed avenues of immune cells stimulation that appeared unique to the source strain EcN. This is meaningful in directing further OMV engineering: if molecular mechanisms of pathogenicity can be harnessed in OMVs to create pathogen-mimetic routes of similarly-biasing self-adjuvancy, then selection of OMV source strain may be an extremely significant selection.

# CHAPTER 3

# ENHANCEMENT OF ECN OMV VACCINES WITH SELF-BOOSTING CAPACITY GENERATED BY CONTROLLED RELEASE FROM INJECTABLE POLYMERIC MICROSPHERES

## 3.1 Introduction

So far, we've demonstrated the creation of a new type of PLP, the EcN OMV, for enhanced recombinant subunit antigen vaccine delivery. However, this vaccine carrier only improves on the capacity of our vaccine delivery to stimulate antigen-specific immunity on a one carrier-one immune cell level. Assuming that this is the only level on which a pathogenic infection drives an immune response neglects one of the more remarkable components of an immune response: its dynamic development through time evolution.

Even assuming ideal immunomodulatory capacity, the difference between the course of immune system exposure to a classical vaccine and that of an actual pathogen during infection are fairly dramatic (**Fig. 3.1a**)[1]. While there is no denying that almost every success story for vaccines relies on ignoring this discrepancy, it would be foolish to state that a real need in many vaccine targets is enhanced and broader immune memory without attempting to address the full, progressive immune response required under natural conditions to "train" the adaptive immune system. Put simply, if the problem is that adaptive immunity is not being sufficiently trained by a vaccine, perhaps the time course in which it is trained is the real problem.

Recalling that the goal of this project is to use the EcN OMV to create a holistic ***pathogen-mimetic vaccine***, it seems an obvious additional step to develop some way to engineer controlled release of the antigen carriers that can mimic how the immune system naturally learns to combat real pathogens. The concept of controlled release of recombinant subunits is not new, and has been attempted previously and currently by both human and veterinary medicine to enhance the potency

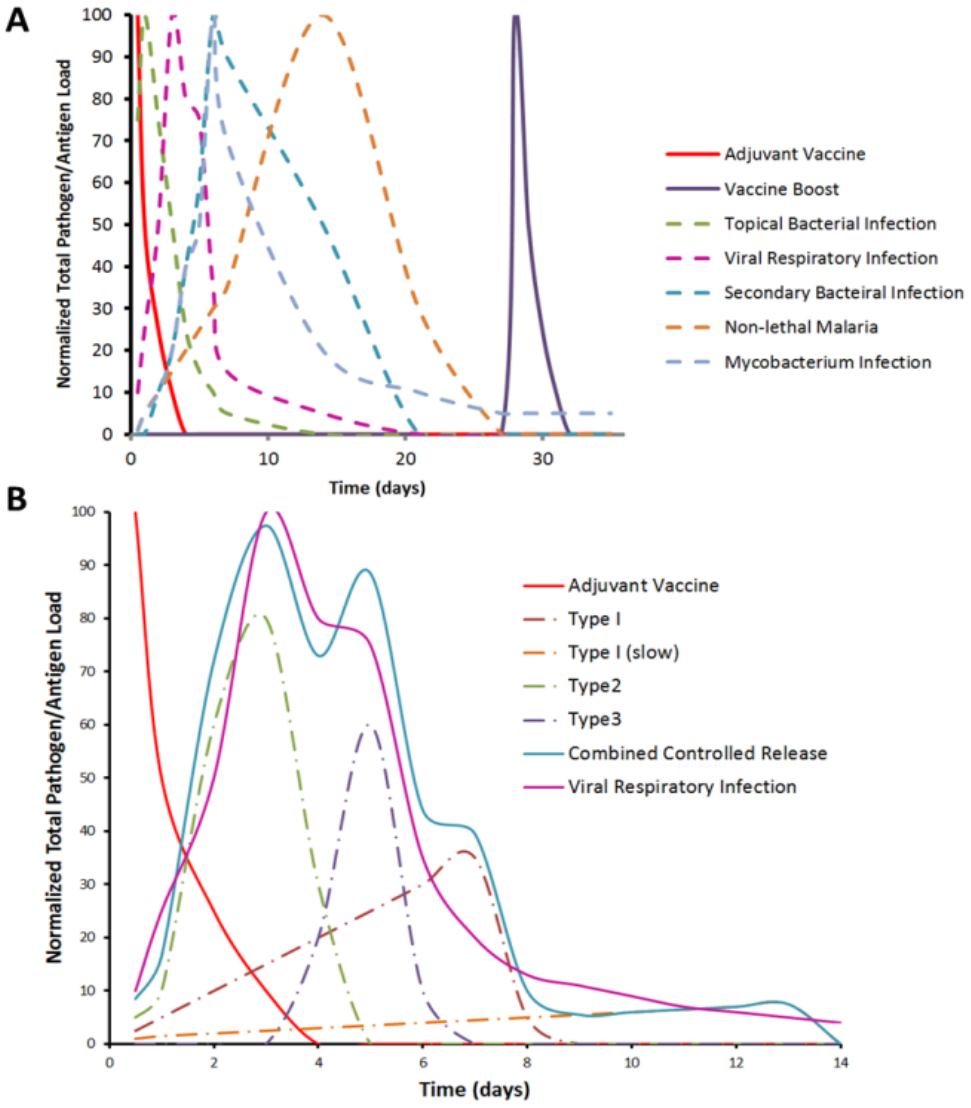


**Figure 3.1: Combinatorial controlled release can create pathogen-mimetic vaccines.** (**A**) Classical vaccination/boosting antigen delivery stands in stark contrast to the time period of pathogen antigen delivery by an actual pathogen infection. (**B**) By combining several different controlled release schemes, all present in an initial injection, a more complex antigen delivery timeline can be generated to much more closely mirror that of an actual infection.

and memory induction of simple vaccines. In contrast to such efforts, however, we propose the use of rationally designed kinetic release profiles that do not merely seek to prolong the exposure of the immune system to a pathogen, but specifically mimic ideal pathogen loads found to be successful in developing naturally potent immunity. To achieve this, we are interested in generating polymeric OMV-encapsulating microsphere libraries containing release kinetic "modules" that can be mixed and matched to achieve complex, pathogen-mimetic release profiles in single-dose injections.

The core concepts of our design should be simple and readily manipulated to model our desired release profiles. Ideally, we aim to create microspheres capable of the following release kinetics[74–76]:

**Type I:** Zero order: $Q_{t0} = Q_0 + K_0 t$
**Type II:** First order burst: $Q_{t1} = (Q_0 - K_1) + K_1 e^{K_2 t}$ ($K_1 > 0$ , $K_2 > 0$)
**Type III:** First order delayed burst: $Q_{t1} = (Q_0 - K_1) + K_1 e^{K_2 t}$ ($K_1 < 0$ , $K_2 < 0$)

Where:

$Q_{t1}$, $Q_{t2}$ =cumulative amount of encapsulated OMVs released at time "t"
$Q_0$ = initial amount of OMVs
$K_0$, $K_1$, $K_2$ = release rate constants
t = time (in days)

These simple equations, which can be fit for individual microparticle formulations through appropriate in vitro release studies, can be combined to achieve complex global release profiles. One can imagine, therefore, where several homogenous batches of microsphere-encapsulated OMVs are mixed in variable ratios to produce controlled release vaccines custom-tailored to individual pathogens, an example of which is illustrated in **Figure 3.1b** using a governing balance equation:

$$Q_{body} = Q_t - Ct$$

Where:

$Q_{body}$ = total amount of OMVs in the body at time "t"
$Q_t = \Sigma Q_{t0} + \Sigma Q_{t1} + \Sigma Q_{t2}$
C = OMV clearance rate constant
t = time (in days)

To come as close as possible to this goal without requiring complex polymeric engineering approaches, we opted to manipulate well-characterized resomers of poly(lactic-co-glycolic acid), or PLGA. PLGA is an attractive material for our desired controlled release applications, as it is already FDA approved and its release kinetics are tunable through a variety of parameter modulations. Additionally, there is some precedent for using PLGA as microspheres to encapsulated nanoparticles for controlled release applications using double emulsion preparation methods[75-76].

Herein we report the production and immunological characterization of two controlled-release formulations of PLGA microsphere-encapsulated EcN OMVs. By varying the double emulsion conditions of 50:50 PLGA resomers, we were able to create both zero-order and step-wise release spectrums, thereby achieving constant and multi-boost delivery of OMVs *in vitro*. While only the first step in creating truly pathogen infection-mimetic delivery, we nonetheless assessed these release modalities in a BALB/c mouse model to see if controlled release of OMVs removed the requirement for multiple injections of priming and boosting to achieve a potent response, as well as whether or not these first steps at enhancing vaccine memory through pathogen-mimetic timescale control were successful. Ultimately we found that humoral immunity was increased over 100-fold and $T_H1$ biasing was maintained with a single dose of either controlled release injection, and that the two release schemes had variable effects on enhancing memory responses that were indicative of a favorable increase in vaccine viability, though further study is required to better elucidate the functional effects on post-vaccination immunity.

### 3.2: Materials and Methods

**3.2.1: PLGA microsphere synthesis.** OMVs were emulsified in a dichloromethane solution of poly(lactic-co-glycolic-acid) (PLGA), 50:50 (MW 24-38 kDa), for 10-120 seconds using a handheld homogenizer at 5000-18000 rpm (VWR Disperser VDI12, Dispersing Tool S12N-5S). Subsequently, this solution was

emulsified in 1%-10% polyvinyl alcohol (PVA) in aqueous solution, ultimately generating two populations of microspheres: 2-5 µm low-porosity and 15-30 µm high-porosity microspheres respectively. Particles were harvested via centrifugation (5000g, 5 min, 4°C) following evaporative stirring in 0.3% PVA for 3 hours. Microspheres were then washed with deionized water and lyophilized following resuspension in an aqueous glucose buffer.

**3.2.2: OMV stability studies.** EcN OMVs suspended in PBS were tested for stability at -20-37 °C, pH 5.4-9.4, and under 1000-10000 rpm of stress. Trials were conducted over a 60 day period with regular sampling using DLS measurements; signal counts within the 80-200 nm range were considered indicative of intact OMVs, while counts outside of this range were considered indicative of degraded OMVs.

**3.2.3: *In vitro* release studies of microsphere-encapsulated OMVs.** 0.1 mg microspheres were suspended in 1 mL PBS and gently rotated at 37 °C for 50 days. At daily intervals up to 21 days (and weekly following), 100 uL samples of supernatant were taken and assayed for 1) protein content using a BCA assay (Thermo Scientific), and 2) intact OMVs using TEM. These findings were correlated with SEM micrographs of degrading microspheres and *in vivo* assessment of microsphere degradation (using subcutaneous injection of DY-700 [Dyomics] dyed PLGA microspheres visualized under an OV100 fluorescence imager [Olumpus]). BALB/c mice were injected subcutaneously with 1 mg of particles for *in vivo* fluorescence correlation studies.

**3.2.4: Mouse Immunizations.** Five groups of five 8-week old BALB/c mice (Charles River Laboratories) each were immunized s.c. with 100 µL of PBS containing purified protein or OMV preparations as

described. The five treatment groups were immunized with, respectively: 2.5 μg GFP, 2.5 μg alum and ClyA-GFP mixture (Alyhydrogel®, 1.3% aluminum hydroxide [mass:volume]), and recombinant fluorescent equivalents of EcN OMVs displaying ClyA-GFP, either freely dispersed in PBS, encapsulated in zero-order microparticles, or encapsulate in multi-boost microparticles. Two doses of vaccine (priming dose and boosting dose) were administered 4 weeks apart for the free OMVs; encapsulated OMVs were injected only once at the beginning of the experiment. Blood was collected from the mandibular sinus immediately before and 2 weeks after the first immunization, immediately before the boosting dose, and at 2 and 4 weeks after the boosting dose. Terminal splenectomies were on all five groups immediately following the final blood collection. The protocol for the animal studies was approved by the Institutional Animal Care and Use Committee at Cornell University (protocol number 2009-0096).

**3.2.5: Assessing OMV vaccine immune response.** Standard microtiter ELISA was performed on collected serum samples from vaccinated mice in 96-well plates. Wells were incubated with purified GFP overnight, followed by serial dilution incubation with serum. Secondary antibodies for IgG, IgM, IgG1, and IgG2 were subsequently incubated and detected using HRP. Hemaggluniation inhibition assays were run using serum incubations with formalin-neutralized PR8 and X31 virus, and were detected via visual inspection of hemagglunination patterns. ELISA was also used to quantify antigen-specific T-cell response. Purified splenic T-cells were cultured for 7 days in complete RPMI, then seeded into wells and incubated in triplicate with GFP for 48 h. Anti-IFN-γ, IL-4, and IL-10 antibodies were then used to detect the presence of stimulated cytokine release. Further proliferation analysis on T-cells was also done on similarly cultured T-cells. Cultured T-cells were trypsinized, centrifuged at 1000 rpm, and diluted to $1X10^6$ cells/mL in complete RPMI, then labeled with CFSE (Invitrogen). $2X10^5$ cells were seeded into 96-well plates, incubated with 30 μL 100 μg/mL GFP, and allowed to proliferate at 37 °C for 4 days. FACS was used to assess loss of CFSE in proliferating cells. Additional *in vivo* inflammation

response analysis was done using subdermal injections in BALB/c mice ears (n=4), on which histopathology was conducted 30 h post-injection of the OMV samples.

**3.2.6: In vitro analysis of immune cell stimulation by EcN OMVs.** Bone marrow-derived macrophages were harvested from BALB/c femur bone marrow, column purified, and cultured in complete RPMI for 7 days. Following this, they were plated in 6-well plates, incubated with ClyA-GFP(+) OMVs, and assessed for phagocytosis-induced fluorescence and IL-12/4/10 expression via FACS analysis. T-cell activation via OMV-pulsed dendritic cells was assessed using DCs incubated for 2 days with OMVs; coculture was conducted with CFSE-labeled T-cells in 24-well plates and proliferative analysis was done 7 days following initial seeding. CFSE-labeled B-cells were assessed identically to antigen-restimulated T-cells, as described previously. Knock-out macrophages were acquired as generous gifts from Dr. Cynthia Leifer, and were stimulated with OMVs for 3 hours prior to media analysis of TNF-α.

**3.2.7: ELISA for serum antibody response.** Polystyrene microtiter 96-well plates (Maxisorp; Nunc Nalgene) were coated with GFP (5 μg/ml in carbonate buffer, pH 9.6) and incubated overnight at 4 °C. Plates were blocked with 3% BSA in PBS containing 0.05% Tween-20 (PBST). Samples were serially diluted 2-fold in blocking buffer in a range of 1:200-1:3,276,800, added to the wells, and incubated for 2 hours at 37 °C. Plates were washed six times with PBST, and biotinylated goat anti-mouse IgG, IgM (Sigma), or monoclonal IgG1 or IgG2 (BD Pharmingen) were added to the wells (1 μg/ml) for 1 hour at 37 °C. Avidin-HRP (1:1000; Sigma) was then added and incubation continued for 30 min at 37 °C. After six additional washes with PBST, 3,3',5,5' tetramethylbenzidine substrate (1-Step TMB; Pierce) was added, and the enzyme reaction proceeded for 20 min. The reaction was stopped with 2 M $H_2SO_4$. The absorbance was quantified in a microplate spectrophotometer at a wavelength of 450 nm. Serum

antibody titers were determined by measuring the last dilution that resulted in three standard deviations above background.

**3.2.8: Splenocyte analyses.** Splenic T-cells were resuspended at a concentration of $2\times10^6$ cells/well in medium RPMI 1640 (supplemented with FCS and antibiotics), seeded into 96-well plates and incubated for 48 h with 5 μg GFP or RPP. Cytokine levels of IFN-γ, IL-4, and IL-10 were measured in the supernatants using standard ELISA kits (eBioscience). Splenocytes were isolated as described above, incubated with anti-CD3, anti-CD4, anti-CD8, anti-CD44, and anti-CD25 according to manufacturer recommendations (eBioscience), then run on a BD Biosciences LSR II Flow Cytometer. All analyses were done in FlowJo®.

### 3.3: Results and Discussion

#### 3.3.1: Assessing OMV stability under physiological conditions relevant to polymeric controlled release

It should be noted that OMV controlled release from microspheres is only possible if the OMVs themselves can maintain integrity under appropriate conditions related to formulation (induced turbulence for emulsion preparation) and in vivo controlled release (pH, temperature) over relevant time periods. Therefore, prior to attempting to formulate microsphere-encapsulated OMV preparations, we thoroughly probed the stability of EcN OMVs under a variety of conditions. The results (**Fig. 3.2**), measured by dynamic light scattering analysis of OMV samples post-incubation, indicate that while OMVs are indeed sensitive to prolonged exposure to temperatures above 0 °C and more extreme pHs, they are overall stable enough to survive both microparticle formulation and controlled release within a vaccinated organism.

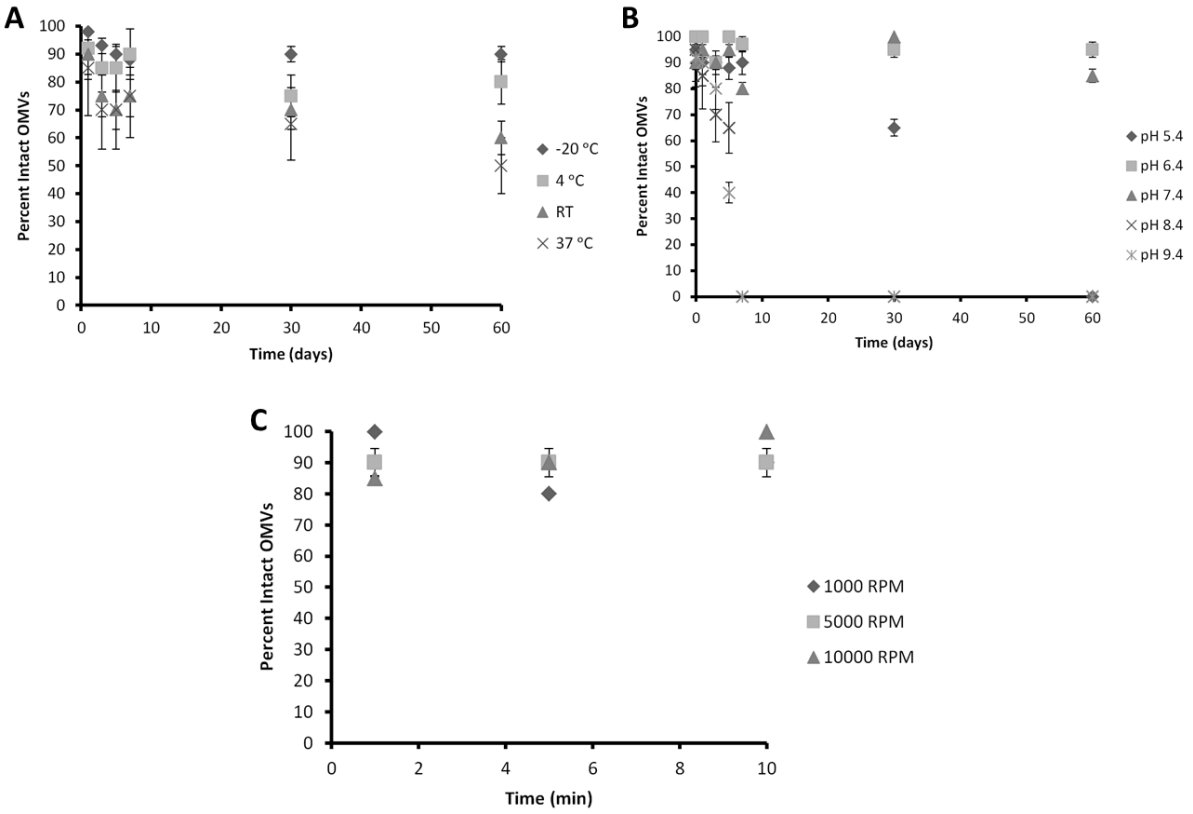


**Figure 3.2: Stability tests done on DLS-analyzed EcN OMV samples.** (**A**) EcN OMVs in PBS kept undisturbed at different temperatures. (**B**) EcN OMVs in PBS kept undisturbed at 4 °C with varied pHs. (**C**) EcN OMVs homogenized in 150 mL PBS at variable RPMs. (**A-C**) Percent intact OMVs represent analysis of peak intensities from dynamic light scattering measurements, where "intact" OMVs were only those comprising a peak that was not associated with degradation or aggregation. All data presented as mean +/- s.d. All time points representative of independent data (n=3).

### 3.3.2: Initial confirmation of PLGA microparticle encapsulation of model fluorescent EcN OMVs

In an initial proof-of-concept study, PLGA microparticles encapsulating EcN OMVs displaying ClyA-GFP were prepared in w/o/w emulsion using 50:50 PLGA (MW 24-38 kDa) and 1% poly(vinyl alcohol) (MW 17-25 kDa). The resulting particles demonstrated likely successful OMV encapsulation (**Fig. 3.3**), with selective microsphere sequestration of fluorescence within undried polymeric "droplets" visualized under light microscopy. While this particular initial study did not yield insight into the level of intact encapsulation of OMVs, nor their capacity to withhold OMVs meaningfully during controlled release, it was a useful check to confirm that OMVs could be successfully packaged under fairly vigorous double emulsion conditions.

### 3.3.3: *In vitro* controlled release studies of PLGA microsphere-encapsulated OMVs

Two controlled release profiles were created using PLGA microspheres: a zero-order and a step-wise release. The general reasoning behind the favorability and greater applicability of such release profiles was already discussed in a broader context, but within the narrow focus of applying singular release approaches to vaccination, these approaches parallel the two currently accepted methods of enhancing immune responses via vaccine administration over time: namely, continuous release or periodic re-administration. PLGA microparticles prepared in high surfactant conditions were observed to have decreased porosity, smaller size, and release in a fashion comparable to the former. Namely, release occurred at a fairly continuous rate over the course of 30 days *in vitro* (**Fig. 3.4**). Importantly, this was correlated using electron microscopy to the continued release of intact OMVs from gradually degrading PLGA microspheres. This correlation is non-trivial in a pre-animal model assessment, as the assumption that OMVs would remain intact during release, though supported by the data in **3.3.2**, required validation prior to further testing. Specifically, vesicles are not extremely stable bionanoparticles, and as a result some degradation is expected under controlled release conditions.

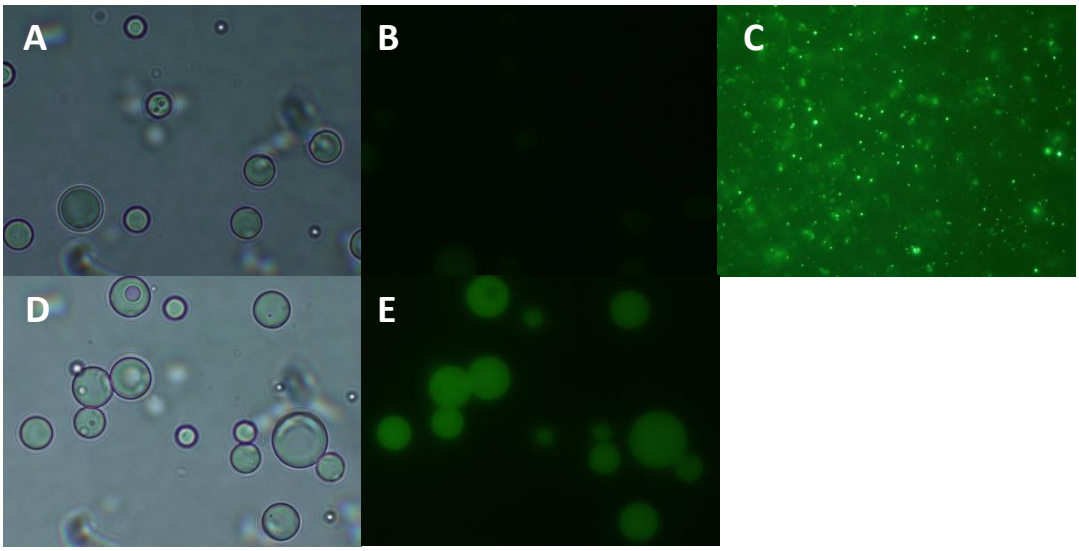


**Figure 3.3: OMVs encapsulated within aqueous core PLGA microparticles.** PLGA microparticles formed in a double emulsion with PBS have an aqueous core (**A**) and minimal autofluorescence (**B**). When concentrated OMVs laden with surface-displayed GFP (**C**) are mixed into the PBS for the double emulsion, the resulting microparticles (**D**) appear to successfully encapsulate the OMVs (**E**). All images taken at 100x immediately after completion of second emulsification in 1% PVA (**A-B**, **D-E**). Fluorescent images taken at 475 nm excitation (**B,C,E**).

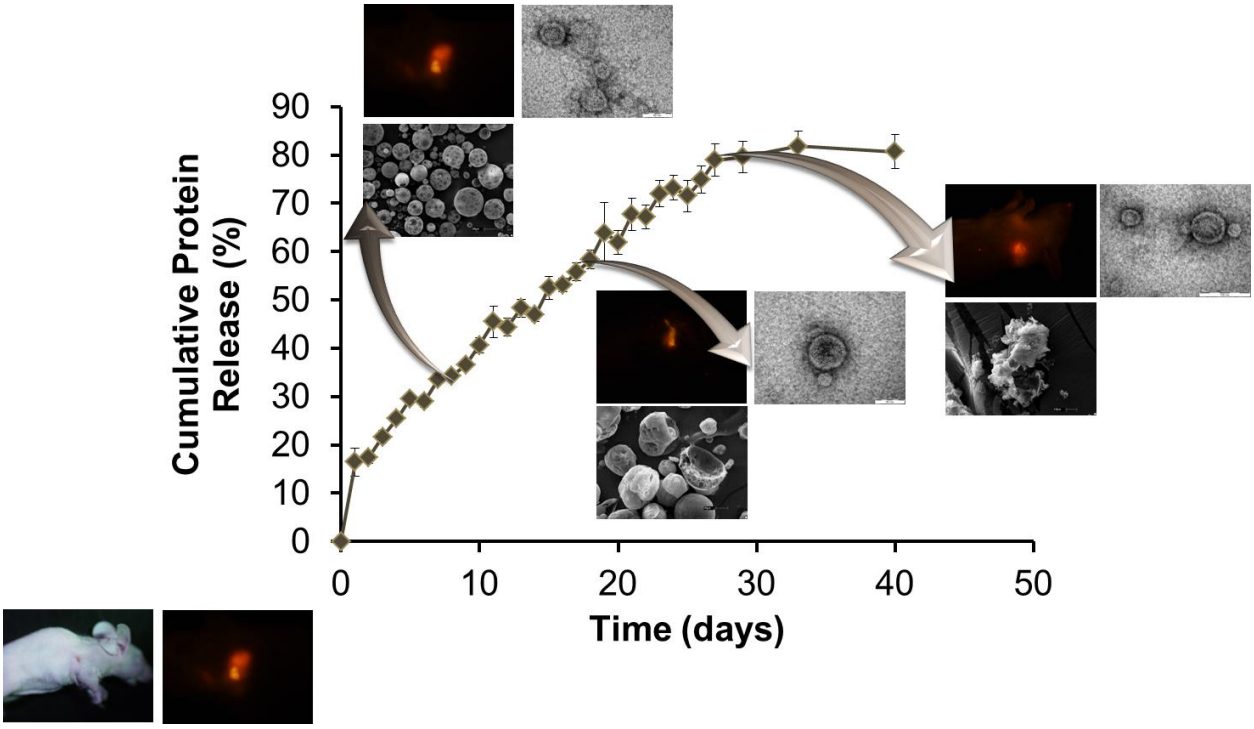


**Figure 3.4: Zero-order controlled release of OMVs from PLGA microspheres.** Microspheres formed under high PVA emulsion conditions (10%) resulted in 2-5 µm microparticles that released OMVs via zero-order linear mechanisms over a 25-30 day period in PBS at 37 °C. Release was quantified via BCA assay of supernatant samples. Insets at t = 10, 20, and 30 days show *in vivo* fluorescence tracking (top-left), TEM micrographs of supernatant OMVs (top-right), and SEM micrographs of degrading microspheres. Bottom left inset shows mouse positioning.

However, the integration of these studies makes it fairly clear that intact OMVs are being retained and released at a fairly constant rate from these smaller microspheres. Also of note is the correlation to gradual degradation *in vivo* as well, where whole-body fluorescent imaging of mice post subcutaneous injection with near-infrared dyed microspheres revealed similar degradation rates as observed more quantitatively *in vivo*.

While linear release has important implications both to simple enhancement of vaccine immunogenicity and more complex combinatorial applications given an expanded library, removing the reliance of the OMV platform on boosting doses inspired the further investigation of a "self-boosting" controlled release mechanism via further fine-tuning of particle synthesis. By destabilizing the regularity of microsphere formation through a lower surfactant content, the PLGA microspheres could be formed in a way that higher observed porosity was harnessed to achieve step-wise release over a prolonged period (**Fig. 3.5**). While this would be exceptionally challenging to achieve with small molecule delivery, the substantially smaller size differential between the hydrodynamic radius of an OMV (nanoscale) and a microparticle (microscale) allows for fairly straightforward manipulation of microsphere size and heterogeneity of composition to create step-wise release of encapsulated OMVs. Indeed, we observed that larger, composite microspheres (~30 μm in diameter) released OMVs in three roughly equal bursts: 0-7 days, 18-26 days, and 35-40 days following injection, respectively. While this is not a perfect mimic of the prime/boost regimen tested in **Chapter 2**, it remains mimetic of fairly standard three-dose boosting regimens for a variety of commercially available vaccines and thus was considered a likely candidate for testing single-dose self-boosting capacity of microsphere-delivered OMVs.

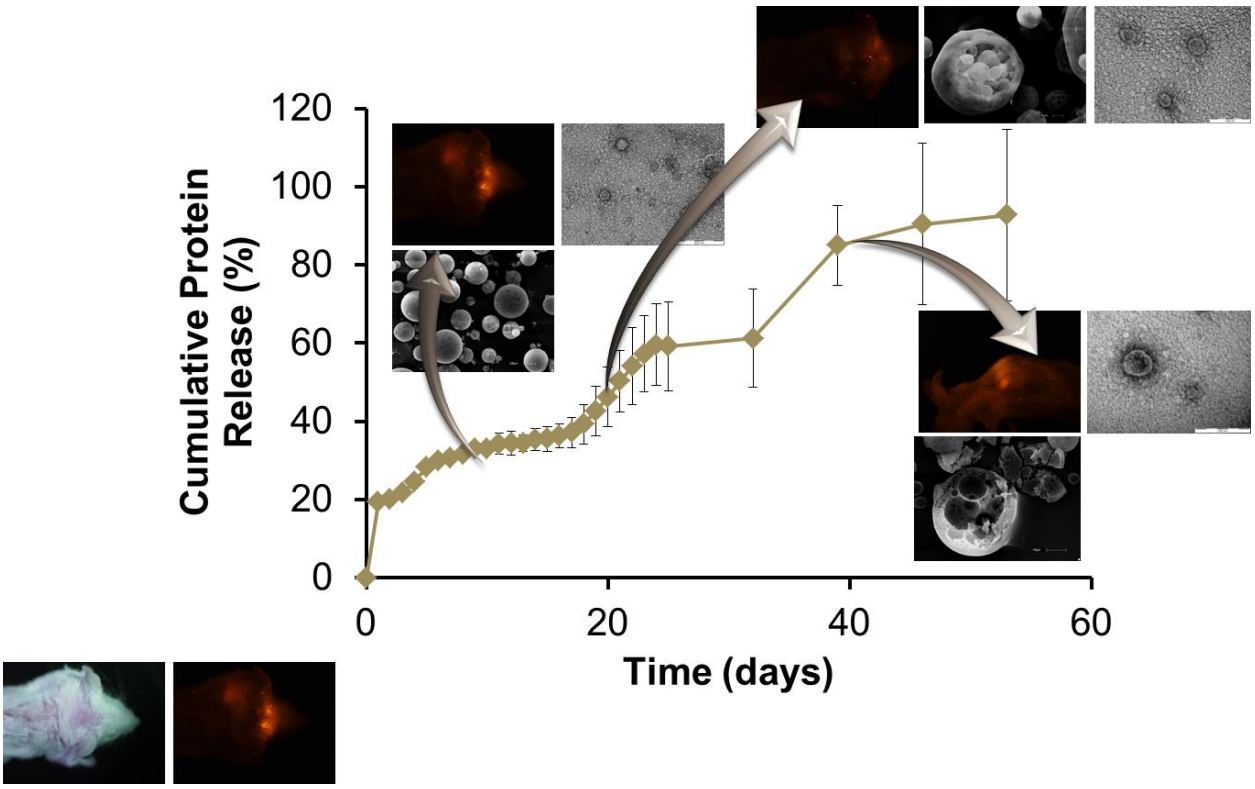


**Figure 3.5: Stepwise controlled release of OMVs from PLGA microspheres.** Microspheres formed under low PVA emulsion conditions (1%) resulted in multilayer 25-30 µm microparticles that released OMVs via multi-boost mechanisms over a 40-60 day period in PBS at 37 °C. Release was quantified via BCA assay of supernatant samples. Insets at t = 10, 20, and 30 days show *in vivo* fluorescence tracking (top-left), TEM micrographs of supernatant OMVs (top-right), and SEM micrographs of degrading microspheres. Bottom left inset shows mouse positioning.

### 3.3.4: Characterization of *in vivo* immunological enhancement of EcN OMV vaccine carriers via controlled release.

As first presented in **2.3.1**, humoral and cellular responses to EcN OMVs delivering a model antigen of GFP were assayed in a BALB/c mouse model. High anti-antigen IgG titers were maintained relative to free OMV injection (**Fig. 3.6**), further supporting the observation that OMVs released from microsphere encapsulation were intact and functional vaccine carriers. Intriguingly, both controlled release mechanisms resulted in 100-fold to 1000-fold increases in titers above negative control baseline substantially faster than the standard prime/boost administration of EcN OMVs, which is consistent with expected enhancement. Of substantial importance was the content of this humoral response as well – that is, the distribution of IgG2a vs. IgG1 titers within the total IgG population were once again indicative of $T_H1$ bias (**Fig. 3.7**). This demonstrates that not only are the OMVs released in this fashion still immunogenic, they retain the unique immunogenicity of the EcN OMVs. Cellular responses were also observed to be consistent with previously assayed EcN OMV responses: IFN-γ secretion post antigen restimulation *in vitro* substantially outpaced IL-4 secretion, again indicating a $T_H1$-bias (**Fig. 3.8**). Of particular interest, however, was the resulting IL-10 secretion. The gradual release of the EcN OMVs apparently caused an increase IL-10-secreting T-cells, which could be indicative of continual exposure to EcN OMVs leading to a more suppressive response than observed in previous administrations of OMVs.

To further explore a differential effect of continuous vs. multi-burst exposure to the EcN OMVs, we used flow cytometry to analyze splenic populations of T-cells in vaccinated mice (**Fig. 3.9**). Specifically, we looked at enhancement of antigen-responsive populations of isolated helper, cytotoxic, regulatory, and memory T-cells, respectively. For the former two, we observed a statistically significant shift in effector T-cell population towards cytotoxic T-cells in the multi-boost administration versus a shift toward helper T-cells in the continuous release administration, which may be indicative of the

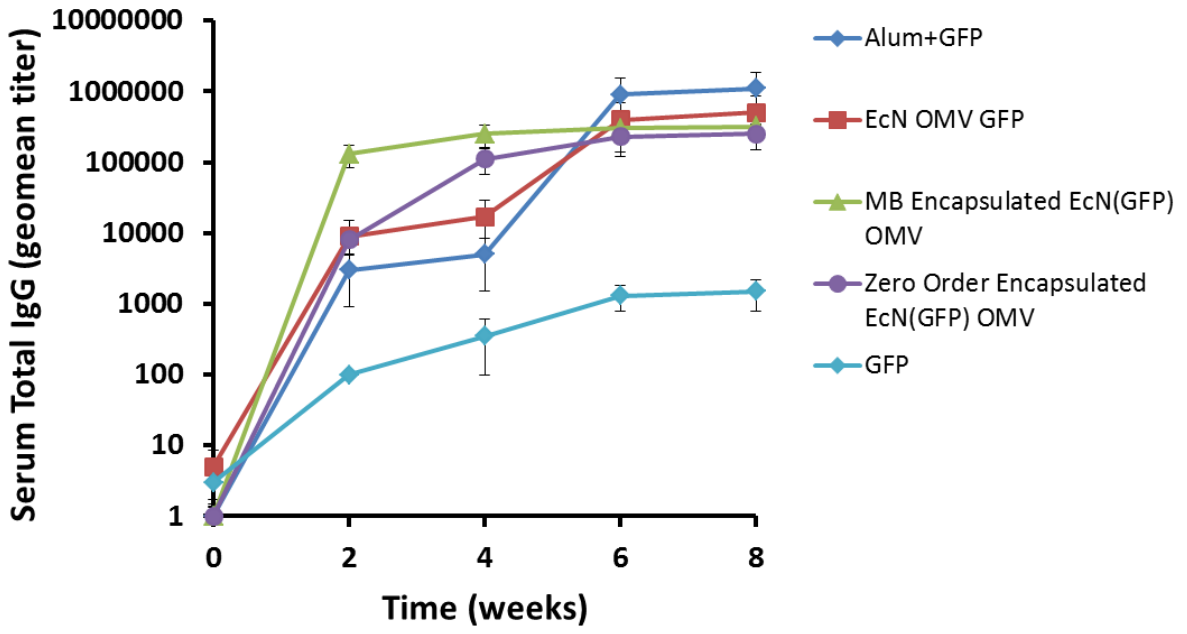


**Figure 3.6: Controlled release of OMVs via PLGA microspheres results in rapid protective levels of humoral immunity without additional boost.** BALB/b mice (n=5, all groups) were injected with 100 µL of purified model antigen GFP, aluminum hydroxide gel (alum) + GFP, and EcN OMVs displaying GFP twice over a course of 8 weeks; zero-order and multi-boost (MB) microparticles were injected once subcutaneously at t = 0 weeks. Given the terminal anti-GFP titer of 1000 for the negative control (GFP only), protective humoral immunity correlated to elevated titers was achieved at 100000. Titers were assayed via ELISA. All data given as mean +/- SD.

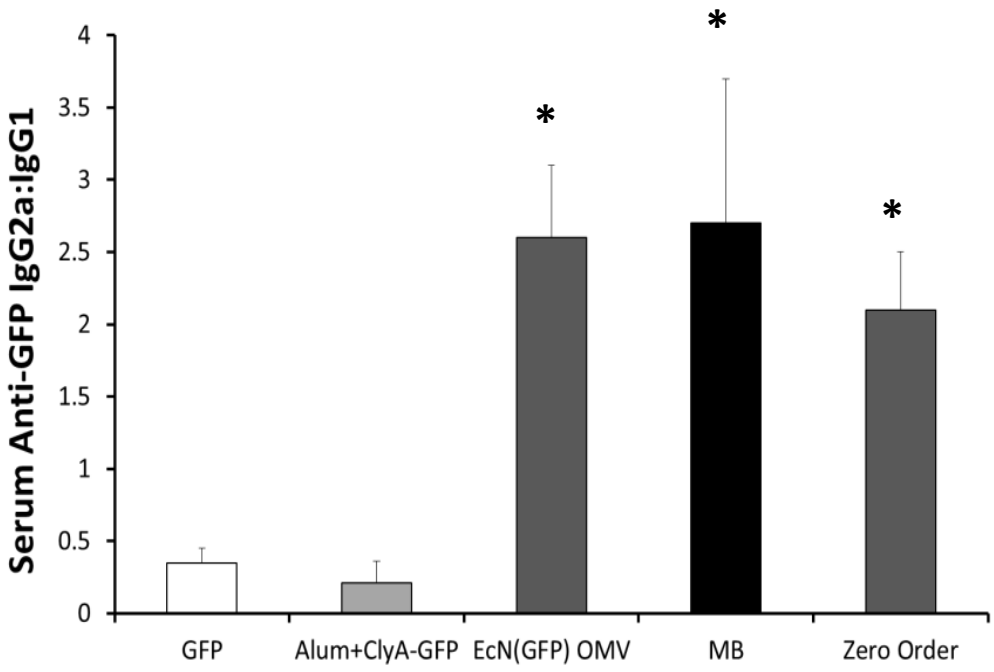


**Figure 3.7: Controlled release of PLGA microspheres retains $T_H$1-biased IgG2a:IgG1 titer ratios of free OMV prime/boost injections.** Titers were assayed via ELISA from terminal (t = 8 weeks) submandibular bleeds of vaccinated BALB/c mice (n=5, all groups). *P<0.05, as determined by Tukey's post-hoc test. All data given as mean + SD.

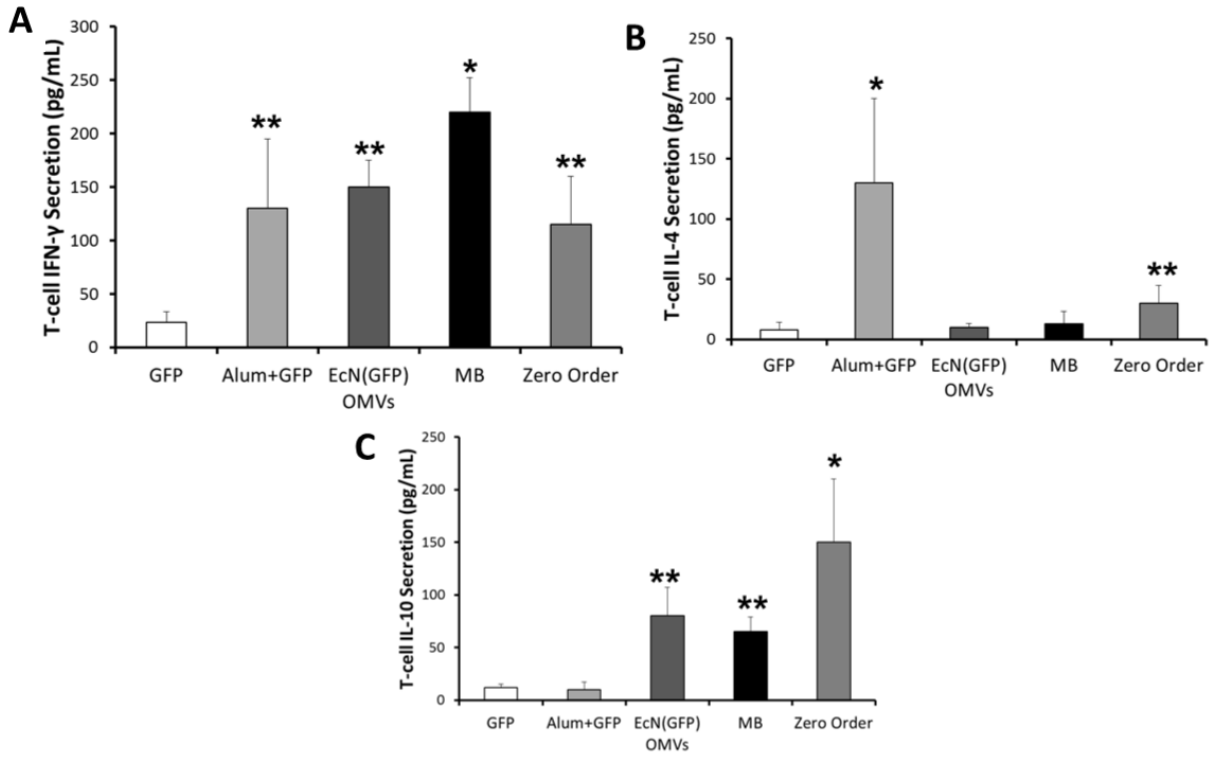


**Figure 3.8: EcN OMV vaccine retains robust, $T_H1$-biased cellular response in mouse model.** (**A-C**) Cytokine secretion levels from cultured, GFP-restimulated spleen-derived T-cells harvested from end-point subjects. Alum = Alhydrogel®. ***P<0.05, ****P<0.001 determined by Tukey's HSD post-hoc test. All values are given as mean + SD.

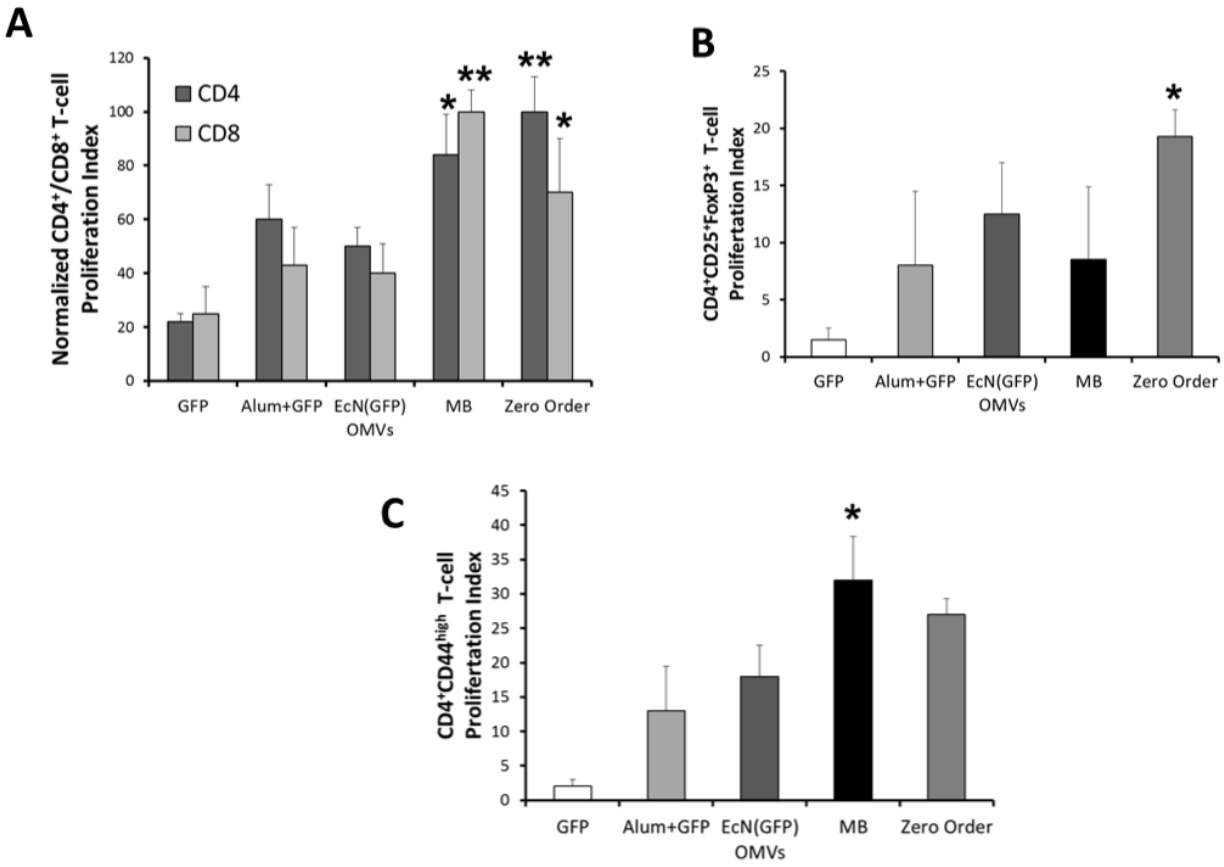


**Figure 3.9: Protection conferred by EcN OMV carrier vaccination resulted in splenic T-cell population shifts.** (**A-C)** Flow cytometry data of isolated primary splenocytes (n=5, all groups), normalized to the highest value in the data set, on pooled splenic T-cells isolated from mice in **c**, probing for CD4/CD8 T-cells (**A**), regulatory T-cells (**B**), and memory T-cells (**C**). ***P<0.05, ****P<0.001 determined by Tukey's HSD post-hoc test. All values are given as mean + SD.

former being better suited to applications targeting vaccination against intracellular pathogens. Assessment of regulatory T-cells further supported the previous observation that the continuous release of EcN OMVs by the smaller microspheres might be enhancing regulatory immunity. While this might be detrimental in certain classical vaccine applications, it opens doors to applications of EcN OMVs as immunotherapeutic vaccination for a variety of immunodysfunctions, which will be further explored in **Chapter 5**. Finally, an important motivation behind testing controlled release applications to OMV vaccination was the ability to enhance immunological memory. The multi-boost regimen in particular significantly enhanced antigen restimulation response in memory T-cells, indicating that controlled release spectrums (particularly ones that incorporate multiple boosts with periodic levels of slow release) can enhance OMV vaccination efficacy in ways primarily reserved for actively pathogenic vaccine formulations (such as attenuated viruses).

### 3.4: Conclusions

PLGA microspheres can be readily engineered to enhance the pathogen-mimetic capacity of EcN OMV PLP vaccine carriers, with both linear and "self-boosting" release profiles enhancing immunogenicity without compromising the capacity of an OMV as a nanoparticulate antigen delivery vector. Moreover, the specific release profile itself might present a new avenue for control over OMV immunostimulation. Specifically, discrepancies in cellular immunity discovered in BALB/c vaccination studies indicate that EcN OMVs can benefit from enhanced cellular memory and regulatory responses simply by varying the release profile of the encapsulating microsphere, broadening EcN OMV applicability as a vaccine carrier for both traditional and non-traditional vaccination applications.

# CHAPTER 4

# ADAPTATION OF THE ECN OMW VACCINE PLATFORM FOR CREATION OF AN INFLUENZA VACCINE CAPABLE OF CROSS-STRAIN PROTECTION

## 4.1 Introduction

Our interest in the OMVs as recombinant subunit antigen carriers extends beyond use simply for other bacterial pathogens. As proteins from eukaryotes can easily be expressed in a structurally and even functionally relevant fashion within bacteria, given appropriate codon optimization/harmonization and assuming proper glycosylation is not entirely essential, they can just as easily be incorporated into our OMV vaccine carrier platform. Moreover, as the robust, $T_H1$-biased antigen-specific immunity demonstrated by the EcN OMVs in Section **3.1** has important implications for vaccines against any intracellular pathogen[4,22,77] – bacterial, viral, or eukaryotic – it behooves us to investigate its applicability to a model, non-bacterial pathogen. In this study, we chose H1N1 influenza virus for several reasons. First and foremost, influenza is a very well-studied pathogen with a wide market for annual vaccination with room for improvement over the current state-of-the-art in terms of ready adaptability to seasonal variances in flu strain dominance[78]. Second, a vaccine that can achieve cross-protection between influenza strains with a single formulation is in high demand, and the fact that our platform combines $T_H1$-bias with the potential for total antigen epitopal space presentation (via functionally folded antigen surface display) gives it a good chance for achieving some amount of multi-strain protection. Finally, there is a simple in vitro assay for probing the efficacy of anti-hemagglutinin (a key influenza antigen and an obvious selection for our vaccine) antibodies by way of a red blood cell hemagglutination-inhibition[79]. This gives us the ability to challenge the functional efficacy of our EcN OMV-stimulated immunity in the same BALB/c model used previously without having to fully invest in an actual pathogen challenge model to get a sense of more than just antigen-specific immune response stimulation.

Influenza virus, the most common viruses of the Orthomyxovirus family, have been a focus of global health and vaccine development in particular for decades, both in the Western world and in the developing world. The virus is transmitted mucosally via contact with surface or aerosolized particles, and while not particularly stable, is particularly infectious nonetheless. Globally, influenza infection is characterized both by seasonal epidemics and infrequent pandemics, both of which pose unique challenges to vaccine design. The former is governed by yearly selection of dominant strains of the virus, which are characterized by the isoforms of its dominant antigens hemagglutinin and neuraminidase, while the latter is primarily driven by the evolution of new infectious strains that often occur when viral mutations result in animal influenza strains becoming infectious to humans. For the former, modern vaccines struggle with the mutagenicity of hemagglutinin and neuraminidase – specifically, vaccines traditionally have to be made to one form of each (i.e. H5N1, or avian flu) without being able to provide ample protection for other forms (i.e. H1N1, or swine flu). The latter is primarily crippled by the response time of current vaccine production technology, which is overly dependent on production methods that are dependent on inefficient incubation in hen eggs or recombinantly mutated virus production in mammalian cell culture. While an effective OMV vaccine might be seen by default to address the production complication – that is, bacterial production wherein the primary variable is simple transformation with an updated plasmid containing isolated antigens – the complication of strain diversity due to antigen mutagenicity is less simple. In general, the field focuses primarily on two potential solutions to this challenge: either the identification and vaccination of a non-mutagenic, universal antigen that is generally overlooked by the immune system when combating influenza, or vaccination using hemagglutinin and/or neuraminidase antigen subunits that results in cross-protection between influenza mutants due to presentation of conserved epitopes.

In this study, we present a novel approach to inducing cross-strain protection against influenza by vaccinating against a hemagglutinin subunit in a pathogen-mimetic fashion utilizing surface

presentation of antigen on the EcN OMV carrier. Specifically, an engineered hemagglutinin subunit from an emergent H1N1 strain was incorporated into an EcN OMV vaccine and tested in BALB/c mice for development of protective humoral and cellular immunity. Following demonstration of substantial $T_H1$-bias to a viral antigen, which is not typical of bacterially-derived recombinant vaccine system, we additionally assayed for cross-strain protection against mouse-adapted H3N2 virus. We found a significant enhancement of cross-strain neutralization in our platform relative to standardly adjuvanted recombinant vaccination, which is a promising start to further experimentation to quantify the capacity of OMV vaccines not just as a replacement technology for current influenza vaccines, but more importantly as a recombinant vaccine formulation capable of protecting against more than one strain of influenza at a time.

**4.2: Materials and Methods**

**4.2.1: Preparation of OMVs.** OMVs were purified in accordance with a previously established procedure (38) – please see Section **2.2.** Briefly, plasmid pBAD-ClyA-H1HA-His, containing an arabinose promoter, was transformed into *E. coli* Nissle 1917 vesicle-overproducing strain JH1. pBAD-ClyA-H1HA-His contained a bacterial codon-harmonized hemagglutinin N-terminal subunit fragment from emergent H1N1 influenza strain CA042009, amino acids 50-158. Protein expression was induced at this point by addition of L-arabinose to a final concentration of 0.2%.

**4.2.2: Protein Analyses.** Protein concentrations in OMV and purified recombinant protein preparations (used as controls in the vaccine study) were quantified by the bicinchoninic-acid assay (BCA Protein Assay; Pierce) using BSA as the protein standard. Fluorescence of GFP in protein and OMV samples was measured in a microplate spectrofluorometer (Gemini EM; Molecular Devices) using excitation and emission wavelengths of 481 nm and 507 nm, respectively (40). For SDS/PAGE, samples were prepared

in sample-loading buffer containing β-mercaptoethanol and heated at 90 °C for 10 min before electrophoresis on 10% polyacrylamide gels. Proteins were transferred to polyvinylidine difluoride membranes for Western blot analysis and probed with monoclonal mouse anti-his tag IgG (Invitrogen; 1:2000) primary antibody, and horseradish peroxidase conjugated goat anti-mouse IgG (Jackson Immunoresearch; 1:10000) secondary antibody. Membranes were developed by autoradiography with ECL detection reagents (GE Healthcare).

**4.2.3: Mouse Immunizations.** Ten groups of ten 8-week old BALB/c mice (Charles River Laboratories) each were immunized s.c. with 100 µL of PBS containing purified protein or OMV preparations as described. The ten treatment groups were immunized with, respectively: PBS, 2.5 µg H1N1 HA, 2.5 µg ClyA, 2.5 µg ClyA-H1N1 HA fusion, 2.5 µg alum and ClyA-H1N1 HA mixture (Alyhydrogel®, 1.3% aluminum hydroxide [mass:volume]), and recombinant fluorescent equivalents of EcJ+ClyA-H1N1 HA, EcJ (empty), EcN+ClyA-H1N1 HA, and EcN (empty). Two doses of vaccine (priming dose and boosting dose) were administered 4 weeks apart. Blood was collected from the mandibular sinus immediately before and 2 weeks after the first immunization, immediately before the boosting dose, and at 2 and 4 weeks after the boosting dose. Terminal splenectomies were performed on half (n=5) of all ten groups immediately before administration of the boosting dose and on the other half (n=5) following the final blood collection. The protocol for the animal studies was approved by the Institutional Animal Care and Use Committee at Cornell University (protocol number 2009-0096).

**4.2.4: Assessing OMV vaccine immune response.** Standard microtiter ELISA was performed on collected serum samples from vaccinated mice in 96-well plates. Wells were incubated with purified GFP overnight, followed by serial dilution incubation with serum. Secondary antibodies for IgG, IgM, IgG1, and IgG2 were subsequently incubated and detected using HRP. Hemaggluniation inhibition assays were run using serum incubations with formalin-neutralized PR8 and X31 virus, and were detected via visual inspection of hemagglunination patterns. ELISA was also used to quantify antigen-

specific T-cell response. Purified splenic T-cells were cultured for 7 days in complete RPMI, then seeded into wells and incubated in triplicate with GFP for 48 h. Anti-IFN-γ, IL-4, and IL-10 antibodies were then used to detect the presence of stimulated cytokine release. Further proliferation analysis on T-cells was also completed on similarly cultured T-cells. Cultured T-cells were trypsinized, centrifuged at 1000 rpm, and diluted to $1X10^6$ cells/mL in complete RPMI, then labeled with CFSE (Invitrogen). $2X10^5$ cells were seeded into 96-well plates, incubated with 30 μL 100 μg/mL GFP, and allowed to proliferate at 37 °C for 4 days. FACS was used to assess loss of CFSE in proliferating cells. Additional *in vivo* inflammation response analysis was done using subdermal injections in BALB/c mice ears (n=4), on which histopathology was conducted 30 h post-injection of the OMV samples.

**4.2.5: In vitro analysis of immune cell stimulation by EcN OMVs.** Bone marrow-derived macrophages were harvested from BALB/c femur bone marrow, column purified, and cultured in complete RPMI for 7 days. Following this, they were plated in 6-well plates, incubated with ClyA-GFP(+) OMVs, and assessed for phagocytosis-induced fluorescence and IL-12/4/10 expression via FACS analysis. T-cell activation via OMV-pulsed dendritic cells was assessed using DCs incubated for 2 days with OMVs; coculture was conducted with CFSE-labeled T-cells in 24-well plates and proliferative analysis was done 7 days following initial seeding. CFSE-labeled B-cells were assessed identically to antigen-restimulated T-cells, as described previously.

**4.2.6: ELISA.** Polystyrene microtiter 96-well plates (Maxisorp; Nunc Nalgene) were coated with GFP (5 μg/ml in carbonate buffer, pH 9.6) and incubated overnight at 4 °C. Plates were blocked with 3% BSA in PBS containing 0.05% Tween-20 (PBST). Samples were serially diluted 2-fold in blocking buffer in a range of 1:200–204,800, added to the wells, and incubated for 2 hours at 37 °C. Plates were washed six times with PBST, and biotinilated goat anti-mouse IgG, IgM (Sigma), or monoclonal IgG1 or IgG2 (BD Pharmingen) were added to the wells (1 μg/ml) for 1 hour at 37 °C. Avidin-horseradish peroxidase (1:1000; Sigma) was then added and incubation continued for 30 min at 37 °C. After six additional

washes with PBST, 3,3',5,5' tetramethylbenzidine substrate (1-Step TMB; Pierce) was added, and the enzyme reaction proceeded for 20 min. The reaction was stopped with 2 M $H_2SO_4$. The absorbance was quantified in a microplate spectrophotometer at a wavelength of 450 nm. Serum antibody titers were determined by measuring the last dilution that resulted in three standard deviations above background. For the determination of cytokines, cells were resuspended at a concentration of $2\times10^6$ cells/well in medium RPMI 1640 (supplemented with FCS and antibiotics), seeded into 96-well plates and incubated for 48 h with 5 µg GFP. Cytokine levels were measured in the supernatants by using standard ELISA kits (eBioscience).

**4.2.7: Hemagglutination Inhibition Assays.** Samples of A/PR8/34 and X31 influenza virus were inactivated in 0.02% formalin for 18h at 37°C, and then dialyzed against PBS at room temperature overnight. Each virus sample was titered for stock hemagglutination units (HAs) as described elsewhere (42) using serial two-fold dilutions of virus into freshly-drawn 1% MRBCs in PBS. Subsequently, serial two-fold dilutions of serum from appropriately vaccinated mice were incubated as described elsewhere (42) with 4 HA diluted virus samples and then exposed to 1% MRBCs in PBS. Both assays were read using the teardrop method to determine the cut-off between hemagglutination and hemagglutination absence/inhibition.

**4.2.8: T-cell Activation Analyses.** T-cell activation by stimulated DCs was assayed as described previously (46,47). Briefly, 96-well plates were incubated overnight with 10 µg/mL anti-mouse CD3 (clone 145-2C11; BD Biosciences) at 4 °C, after which plates were washed 3 times with complete RPMI. T cells were then labeled with CFSE as described and seeded into wells from at $2X10^5$ cell/well. T-cells were co-incubated with $4X10^4$ cell/well DCs, 5 µg/mL anti-mouse CD28 (clone 37.51, Biolegend), and 1-100 µg/mL EcJ or EcN OMVs. Samples prepared for flow cytometry analysis incubated for 48 h at 37 °C, incubated for 4-6 h with 25 ng/mL PMA, 1 µg/mL ionomycin, and 10 µg/mL brefeldin A, and then were

collected and stained with IFN-γ and IL-10 (eBiosciences). Samples prepared for ELISA analysis of culture supernatants were also incubated for 48h at 37 ˚C. Samples prepared for proliferation analysis were incubated at 37 ˚C for 7 days, then trypsinized and analyzed by flow cytometry for loss of CFSE staining.

**4.3: Results and Discussion**

Using a ClyA-H1N1 hemagglutinin fusion (expressed from a codon-optimized sequence derived from CA0409HA), we engineered EcN OMVs that surface displayed hemagglutinin as a recombinant antigen. A similar BABL/c mouse trial and subsequent humoral and cellular immune analysis were used as in **Chapter 2**, and the results were as expected: despite being a non-bacterial protein, humoral (**Fig. 4.1**) and cellular (**Fig. 4.2**) immunity specific to H1N1 hemagglutinin (derived from A/PR8/34 H1N1 viral capsids) was similar to that found previously. More impressive, however, were the results of the hemagglutination-inhibiton (HI) assay (**Fig. 4.3**). First, HI antibody titers against formalin-inactivated A/PR8/34 were comparable between serum from BALB/c mice vaccinated with H1N1 HA(+) EcN OMVs and an alum control, demonstrating that the OMV platform not only generates antigen-specific humoral immunostimulation comparable to traditional adjuvants, but additionally creates functional humoral immunity in the form of sufficient opsonizing/neutralizing antibody populations. The more interesting observation, however, came when we probed the same sera for cross-protection against H3N2 influenza hemagglutination (using H3N2 strain X31). While the alum control's HI titer plummeted, as expected, the EcN OMVs' HI titer remained fairly high and well above statistically significant functional range compared to the PBS negative control. While not conclusive, this strongly suggests EcN OMVs have the

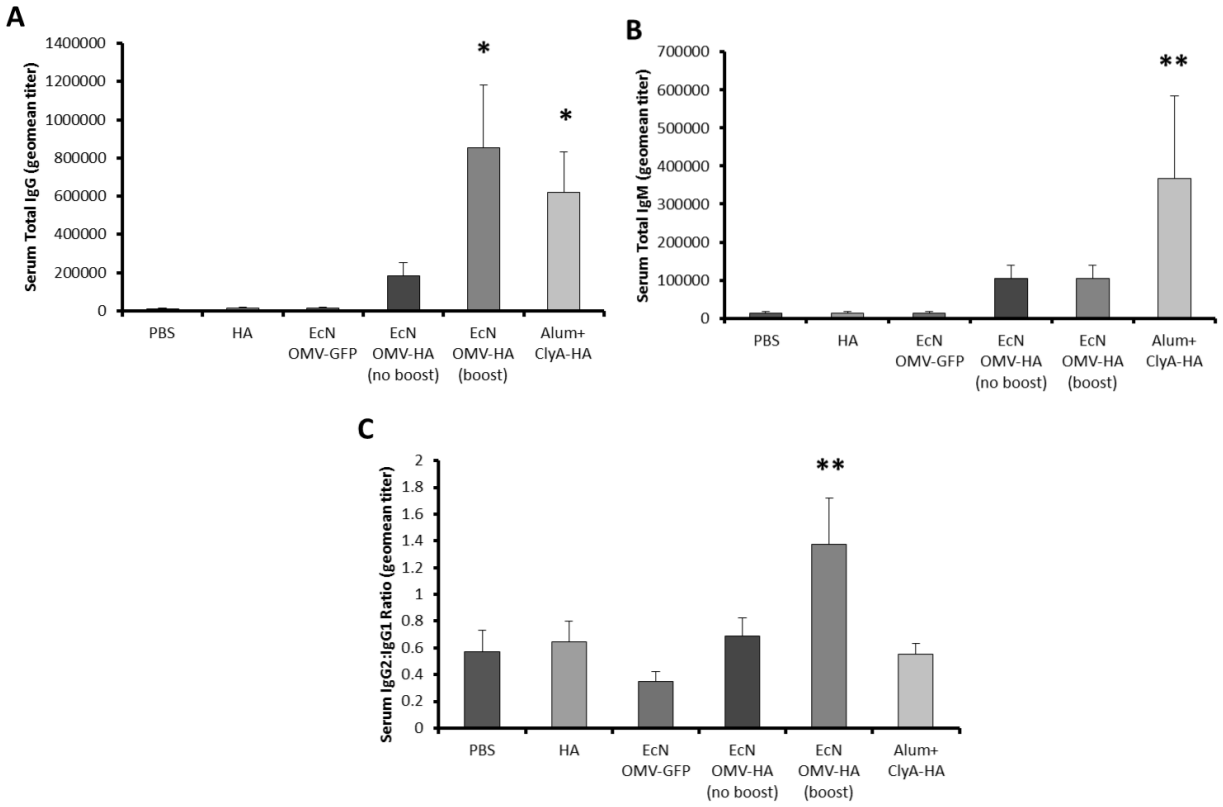


**Figure 4.1: EcN OMV carriers generate strong anti-H1N1 HA humoral immunity.** (**A-C**) Terminal data points from BALB/c mice vaccinated and boosted once (or not boosted, as noted) with antigen-normalized (or protein normalized, as appropriate) with EcN OMVs and controls (n=5). (**A-B**) Class-specific anti-H1N1 HA antibody serum titers. (**C**) Ratio of serum titers of IgG1 to IgG2. (**A-C**) Alum = Alhydrogel®. *****P<0.005, ******P<0.05 determined by Tukey's HSD post-hoc test. All values are given as mean + s.d.

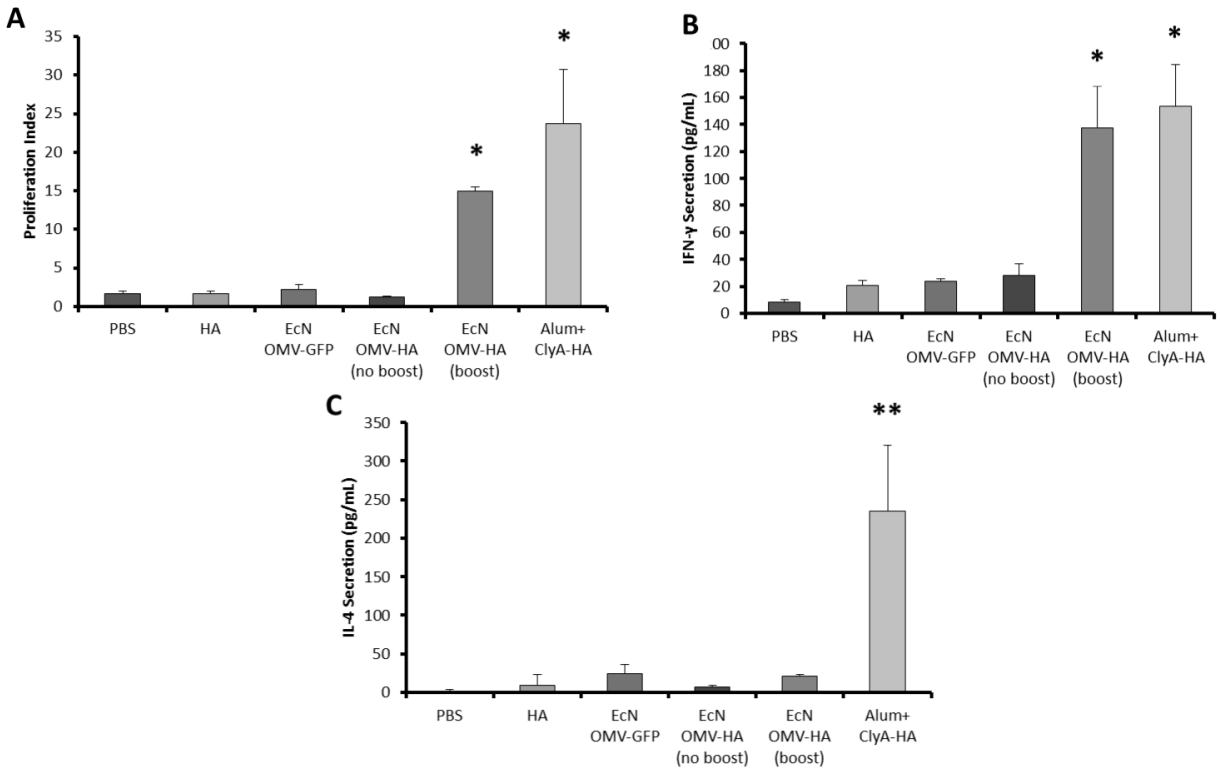


**Figure 4.2: EcN OMV carriers generate strong anti-H1N1 HA cellular immunity.** (**A-C**) Terminal data points from BALB/c mice vaccinated and boosted once (or not boosted, as noted) with antigen-normalized (or protein normalized, as appropriate) with EcN OMVs and controls (n=5). (**A**) Proliferation index of antigen-restimulated spleen-derived T-cells harvested from end-point subjects, measured via CFSE stain. (**B-C**) Cytokine secretion levels from cultured, antigen-restimulated spleen-derived T-cells harvested from end-point subjects. (**A-C**) Alum = Alhydrogel®. ***P<0.005, ****P<0.05 determined by Tukey's HSD post-hoc test. All values are given as mean + s.d.

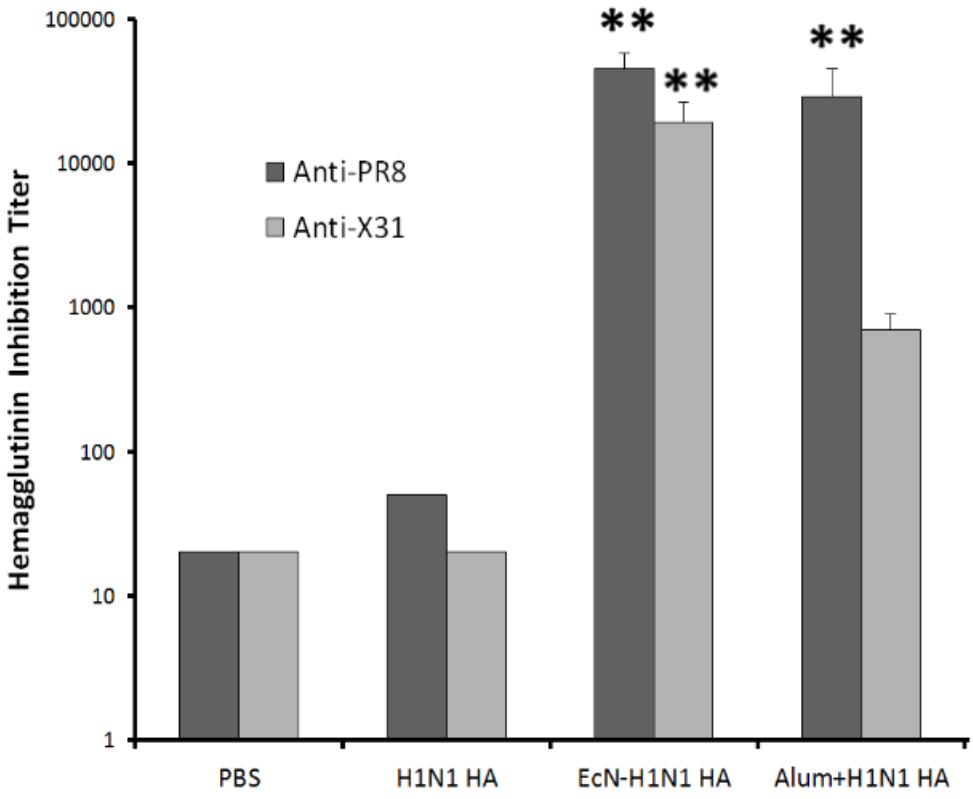


**Figure 4.3: Cross-strain protection is enhanced by recombinant hemagglutinin delivery via EcN OMVs.** Data was gathered from serum antibodies collected exclusively from terminal cardiac punctures assessed via hemagglutinin inhibition assays run on inactivated viral capsids. Alum = Alhydrogel®. **P<0.05 determined by Tukey's HSD post-hoc test. All values are given as mean + s.d.

capacity as antigen carriers to facilitate influenza cross-strain protection, something vaccinologists have struggled to achieve with classical adjuvants.

Considering the fact that this level of cross-strain reactivity is comparable to the discrepancy[78] found between individuals who have actually been infected with H1N1 (and have cross-strain immunity), and those who have only been vaccinated against H1N1 (and do not have cross-strain immunity), our findings also lend additional insight into the function of our platform as a PLP. In **2.3.2**, we noted a strong capacity for T-cell independent B-cell activation via our EcN OMVs, indicating they had the potential for presenting surface displayed antigens to B-cell receptors in an immunostimulatory fashion. The presence of enriched quantities of PAMP-rich biomolecules with an expanded range of TLR targets further supports a capacity for surface antigen presentation in tandem with self-adjuvanting co-stimulation. We also found in **2.3.4** that surface presentation in particular appeared to be important for EcN OMV antigen delivery, meaning it was somehow inherently involved in the stimulated antigen-specific response. Coupled with our observation of ClyA-GFP fusions resulting in surface displayed, functionally folded GFP[34], one could hypothesize that this B-cell presentation has the fairly unique capacity among non-whole pathogen vaccine formulation to present a full range of antigen linear and conformational epitopes in a relevantly immunogenic fashion. This hypothesis is well-supported by the results of this HI assay. While sequence mutations between strains result in modified linear epitopes and thus non-convergent immunity (should reactivity to such epitopes dominate the antibody population), divergent strain hemagglutinins are still functionally similar and thus often contain similar conformational epitopes. The ability to present an H1N1 HA to the immune system in a way that preserves its folded structure, as an intact virus obviously would and we hypothesize our EcN OMVs can, could therefore result in an expanded antibody population that targets conformational epitopes and can result in cross-protection. As this hypothesis correlates well with our data, we can at least tentatively

conclude that our EcN OMV is indeed functioning as a true PLP: delivering its antigen in a way that is functionally mimetic of an actual viral pathogen.

**4.4: Conclusions**

In this report, two key findings drive a continued interest in the adaptation of the EcN OMV platform for use as a recombinant vaccine carrier for vaccination against viral pathogens. First, vaccination in a mouse model demonstrated the stimulation of protective immunity against a bacterially-expressed recombinant subunit antigen of a viral protein. Second, the humoral response was quantified as being not only inhibitive on the level of a standardly adjuvanted control, but more importantly that this inhibition transferred to another strain containing a different form of hemagglutinin. The latter result bears the most attention in further testing, as it may be evidence of the realization an elusive promise of PLP vaccines, and therefore requires more rigorous challenge in an infectious protection mouse model. Finally, the observation that a lack of boosting resulted in a lack of protection serves as important inspiration for adaptation of microsphere controlled release from **Chapter 3** as a general facet of OMV vaccination, as for a new influenza vaccine to be competitive in the current market single-dose vaccination is likely a necessary feature. Regardless, the results presented herein are encouraging and demonstrate the robust applicability of EcN OMVs as vaccine carrier PLPs to non-bacterial antigen targets.

# CHAPTER 5

# ADAPTATION OF THE ECN OMW VACCINE PLATFORM FOR THE TREATMENT OF PEANUT ALLERGIES: GENERATION OF A PROPHYLACTIC PEANUT ALLERGY VACCINE AND CONTROLLED RELEASE OMV-MEDIATED IMMUNOTHERAPY

## 5.1 Introduction

While pathogen vaccine targets are certainly the most obvious application of a recombinant subunit antigen carrier platform such as the EcN OMV, they are not the only ones. Indeed, setting aside the classic medical definition of a vaccine as a prophylactic immunological treatment of pathogenic organism infection, at its core a vaccine delivery platform is much more simply a targeted immunomodulator. That is, its purpose is to alter the immune response in a favorable way to an exogenous moiety of interest. This consideration has certainly not been lost on the field of vaccine engineering. Vaccinologists, and even some more specialized molecular engineers working on PLPs, have pursued vaccines against everything from cancer[24,80], to Alzheimer's disease, to nicotine[8,21]. While such uses of vaccines are not currently on the market (though a vaccine for leukemia therapy[81] could become the first FDA approved example shortly), their development speaks to a broader potential of vaccine engineering – using the immune system to alter non-pathogenic disease via relevant molecular targeting. While we are indeed quite interested in the prospect of a cancer vaccine (see **4.3.2**), our first target for non-pathogen vaccination is allergy. This target represents an understandable middle ground: allergy is a non-pathogenic disease that the immune system is obviously highly involved with on a fundamental level, and immunomodulation therapy for the treatment of allergy is common.

Our model for allergy vaccination will be allergies to *Arachis hypogaea*, or peanuts. Food allergies are common among children three years and younger, with 6-8% of children having hypersenstive allergic reactions to products such as cow milk, eggs, and peanuts[82]. While 80-85% of

children eventually outgrow these allergies, approximately 1.5 million people in the US remain anaphylactically hypersensitive to peanut allergens throughout adulthood[82,83]. Current forms of management and rescue from severe peanut-induced anaphylaxis are limited[83,84]. While sensitization and other immunotherapies have been used to treat a variety of food allergies, exposure to even minute amounts of peanut allergen is prohibitively risky for hypersensitive individuals. This situation has prompted investigation into prophylactic vaccination as a potential means to prevent hypersensitive allergy altogether[85]. With such an approach, the immune system's propensity for quantal memory responses is harnessed to artificially simulate the $T_H1$-polarizing requirements of the 'hygiene hypothesis'[86,87]. While promising in theory, this approach requires strongly biased cellular immunity against the allergen beyond the capacity of currently available adjuvants[77].

The systematic modulation of immunity required for protection against type I hypersensitivity allergy, as found in cases of peanut allergy, is challenging to achieve using conventional adjuvants[1,2]. However, building on the success of the EcN OMV vaccine carrier reported in **Section 2**, there is ample evidence to hypothesize that the immunomodulation harnessed via this vaccine delivery approach could be beneficially applied to this medical challenge. Herein, we report the success of two adaptations of the EcN OMV system's PLP properties as a therapeutic prevention of symptoms related to hypersensitivity allergy in a mouse model for food allergy-triggered anaphylaxis. First, we demonstrate the efficacy of a prophylactic formulation using the standard prime/boost administration of EcN OMVs displaying Arah2 peanut allergen subunits, with vaccination occurring prior to sensitization. This administration resulted in 100% protection against lethal anaphylactic challenge and a protection against all detrimental symptoms in 60% of mice during challenge. Second, we report the adaptation of the EcN OMV's PLP capacity to a controlled release therapy using low-dose administration through the zero-order release scheme discussed in **Chapter 3**. The goal with this adaptation is to use the potent self-adjuvancy of the EcN OMV platform (combined with its capacity for immunity-direction at low

doses, as described in **2.3.4**) to serve as a replacement for traditional immunotherapy, which suffers from low patient compliance and efficacy concerns. This unconventional use of PLPs was also successful, resulting in protection from anaphylaxis in line with a standard weekly sublingual immunotherapy from a single injection of microparticles.

## 5.2: Materials and Methods

**5.2.1: Mouse Immunizations.** BALB/c mice (Charles River Laboratories) were primed and boosted s.c. with PBS containing purified protein or OMV preparations as described. The treatment groups were immunized with 100 µL of, respectively: PBS, raw peanut protein (RPP), ClyA, RPP and ClyA mixture, ClyA-RPP fusion, alum and ClyA-RPP mixture, and recombinant equivalents of EcJ OMVs + ClyA-RPP, EcJ OMVs (with no recombinant antigen, or "empty"), EcN OMVs + ClyA-Arah2, and EcN OMVs (empty). Blood was collected from the mandibular sinus and terminal splenectomies were performed.

**5.2.2: Adaptive Immunity Analysis.** ELISAs were conducted using 96-well plates that were coated with RPP, blocked, coated with serum samples, and incubated/washed prior to reading as reported previously[12]. In the proliferation and cytokine assays, cultured T-cells were trypsinized, centrifuged, and diluted in complete RPMI, then labeled with CFSE (Invitrogen). The cells were seeded into 96-well plates, incubated with RPP, and allowed to proliferate at 37 °C for 4 days. FACS was used to assess loss of CFSE in proliferating cells, while standard ELISA kits (eBioscience) were used to assess cytokines. T-cell activation by stimulated DCs was assayed similarly, allowing 2 days prior to DC coculture.

**5.2.3: Peanut protein sensitization and peanut allergy challenge of mice with corresponding analysis of serum and T-cells.** Mice were sensitized over a period of 3 weeks following the 8-week vaccination

protocol described above. All mice went through 3 rounds of sensitization (once per week). Each round involved oral administration of 1 mg RPP mixed with 10 µg cholera toxin per mouse via gavage, followed by intraperitoneal injection of 0.5 µg RPP mixed with Alhydrogel® on the next day. Mice were challenged with RPP following the completion of sensitization. Anaphylaxis was scored over a 30 minute interval immediately following the challenge, using a scoring system between 0 and 5, 0 having no observable reaction and 5 being death.

Histamine ELISAs are performed as described above. Splenocytes were isolated as described above, incubated with anti-CD3, anti-CD4, anti-CD8, anti-CD44, and anti-CD25 according to manufacturer recommendations (eBioscience), then run on a BD Biosciences LSR II Flow Cytometer. All analyses were done in FlowJo®.

**5.2.4: OMV encapsulation in PLGA microspheres.** OMVs were emulsified in a dichloromethane solution of poly(lactic-co-glycolic-acid) (PLGA) for 20 seconds using a handheld homogenizer at 18000 rpm (VWR Disperser VDI12, Dispersing Tool S12N-5S). Subsequently, this solution was emulsified in 10% or 1% polyvinyl alcohol (PVA) in aqueous solution, generating 2-5 µm and 15-20 µm microspheres respectively. Particles were harvested via centrifugation (5000g, 5 min, 4°C) following evaporative stirring in 0.3% PVA for 3 hours. Microspheres were then washed with deionized water and lyophilized following resuspension in an aqueous glucose buffer.

**5.2.5: Sublingual immunotherapy dosing.** 100 µL of RPP (10 µg – 1 mg) mixed with 50 U of vitamin D3 and 500 µg dexamethasone (Sigma Aldrich) was administered orally under the tongue of sensitized BALB/c mice for 12 weeks leading up to challenge. Dosing was given on a weekly ramp of RPP administration as follows: 10, 15, 30, 150, 300, 400, 500 µg. Mice were observed for 20 minutes

following this administration to ensure a lack of reaction, with continued observation occurring for the next 24 hours.

**5.2.6: ELISA for Serum Antibody Response.** Polystyrene microtiter 96-well plates (Maxisorp; Nunc Nalgene) were coated with RPP (5 µg/ml in carbonate buffer, pH 9.6) and incubated overnight at 4 °C. Plates were blocked with 3% BSA in PBS containing 0.05% Tween-20 (PBST). Samples were serially diluted 2-fold in blocking buffer in a range of 1:200-1:3,276,800, added to the wells, and incubated for 2 hours at 37 °C. Plates were washed six times with PBST, and biotinylated goat anti-mouse IgG, IgM (Sigma), or monoclonal IgG1 or IgG2 (BD Pharmingen) were added to the wells (1 µg/ml) for 1 hour at 37 °C. Avidin-HRP (1:1000; Sigma) was then added and incubation continued for 30 min at 37 °C. After six additional washes with PBST, 3,3',5,5' tetramethylbenzidine substrate (1-Step TMB; Pierce) was added, and the enzyme reaction proceeded for 20 min. The reaction was stopped with 2 M $H_2SO_4$. The absorbance was quantified in a microplate spectrophotometer at a wavelength of 450 nm. Serum antibody titers were determined by measuring the last dilution that resulted in three standard deviations above background.

**5.2.7: Cytokine Secretion Analyses.** Splenic T-cells were resuspended at a concentration of $2\times10^6$ cells/well in medium RPMI 1640 (supplemented with FCS and antibiotics), seeded into 96-well plates and incubated for 48 h with 5 µg GFP or RPP. Cytokine levels of IFN-γ, IL-4, and IL-10 were measured in the supernatants using standard ELISA kits (eBioscience).

**5.2.8: Peanut Allergy Challenge.** Mice were challenged with 200 ug RPP following the completion of the 3 rounds of sensitization. Anaphylaxis was scored over a 30 minute interval immediately following the challenge, using the following scoring system: 0, no observable reaction; 1, mild general agitation, scratching at nose and/or head; 2, intermittent lethargy, elevated respiratory rate, and/or ocular

redness; 3, visibly labored respiration, decreased response to stimuli, and/or consistent lethargy; 4, insufficient respiration, lack of response to stimuli, and/or convulsions; 5, death. Mice that entered a 4 or higher for longer than 10 minutes, and any mice that remained at a 3 or higher after 30 minutes, were euthanized according to recommendation from the IACUC.

## 5.3: Results

### 5.3.1: EcN OMVs direct $T_H1$-biased immunity against Arah2 allergens in BALB/c mice

We began as in **Chapter 2** with an assay of antigen-specific immunogenicity in BALB/c mice. This was an essential first step due to the nature of the antigen subunit target, which was selected to be the peanut protein Arah2[88]. Arah2, being a eukaryotic plant protein, posed the risk of not being sufficiently expressible in bacteria, or, if expressible, ran the risk of not folding in a fashion appropriate to generate meaningful anti-antigen specific immunity. To help ensure success, we began by codon-harmonizing the Arah2 sequence through Invitrogen's GeneArt® GeneOptimizer® algorithm. The resulting sequence was expressed as a ClyA-fusion and vaccinated as done previously against a positive control of alum and raw peanut protein (RPP). The immune response was then assayed as before against RPP, not purified recombinant Arah2, to ensure the desired retention of anti-antigen immunity. EcN OMV-induced humoral (**Fig. 5.1**) and cellular (**Fig. 5.2**) immunity was, as expected, equivalent to initial observations using GFP as a model antigen in **2.3.1**, demonstrating that at least in certain cases codon harmonization is sufficient to preserve eukaryotic protein antigenicity when delivered by the EcN OMV, though further studies would be required to make conclusive statements concerning whether or not this explicitly stems from retained tertiary antigen structure. Additionally, the Arah2-specific immune response in this study was clearly sufficient to warrant a more meaningful trial in a murine hypersensitivity model.

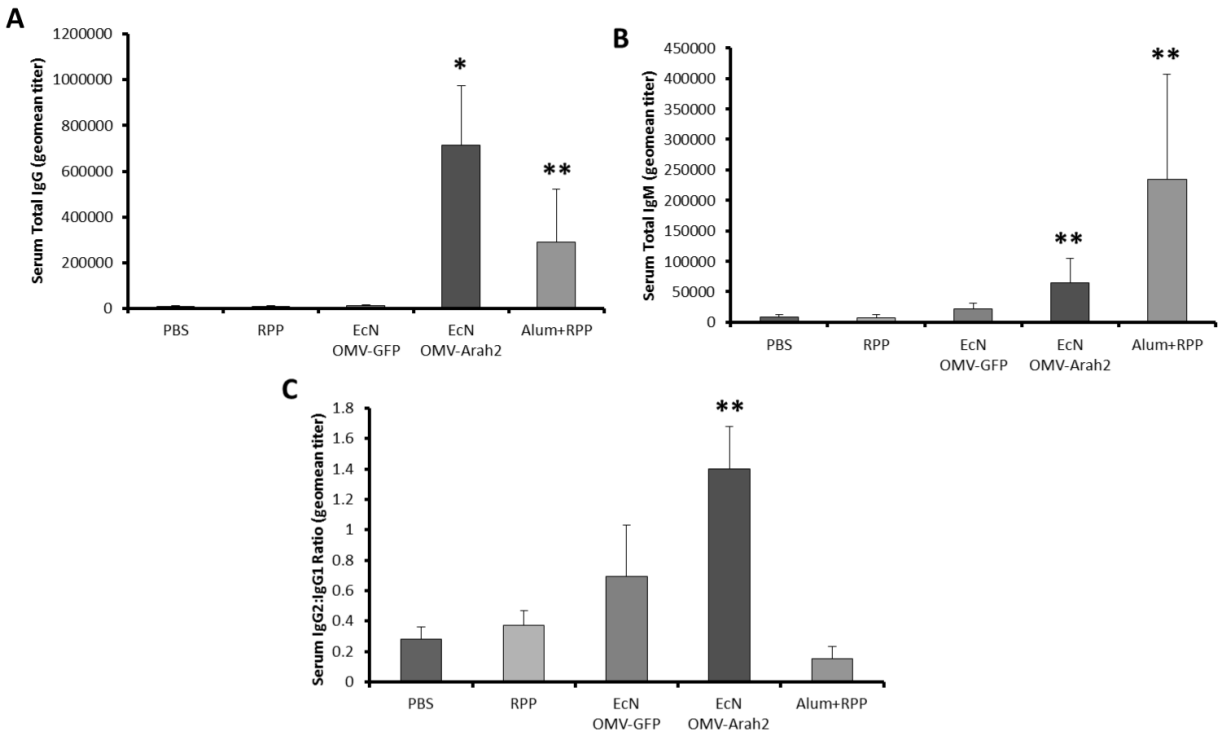


**Figure 5.1: EcN OMV carriers generate strong anti-Arah2 humoral immunity.** (**A-C**) Terminal data points from BALB/c mice vaccinated and boosted once with antigen-normalized (or protein normalized, as appropriate) with EcN OMVs and controls (n=5). (**A-B**) Class-specific anti-Arah2 antibody serum titers. (**C**) Ratio of serum titers of IgG1 to IgG2. (**A-C**) Alum = Alhydrogel®. ***P<0.005, ****P<0.05 determined by Tukey's HSD post-hoc test. All values are given as mean + s.d.

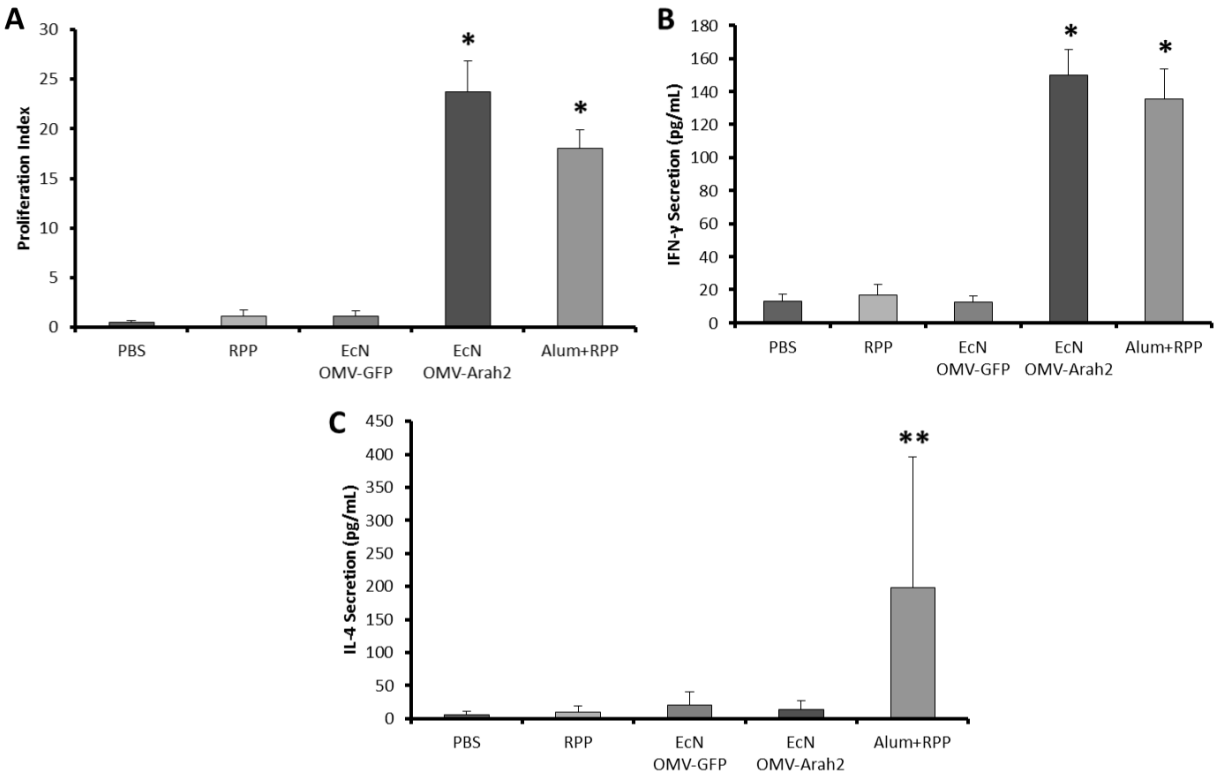


**Figure 5.2: EcN OMV carriers generate strong anti-Arah2 cellular immunity.** (**A-C**) Terminal data points from BALB/c mice vaccinated and boosted once with antigen-normalized (or protein normalized, as appropriate) with EcN OMVs and controls (n=5). (**A**) Proliferation index of antigen-restimulated spleen-derived T-cells harvested from end-point subjects, measured via CFSE stain. (**B-C**) Cytokine secretion levels from cultured, antigen-restimulated spleen-derived T-cells harvested from end-point subjects. (**A-C**) Alum = Alhydrogel®. ***P<0.005, ****P<0.05 determined by Tukey's HSD post-hoc test. All values are given as mean + s.d.

### 5.3.2: Prophylactic vaccination with EcN OMVs protects against anaphylactic challenge in sensitized BALB/c mice

With the mechanistic interface between EcN OMVs and innate and adaptive immunity thoroughly characterized in **Chapter 2**, and with the data presented in **5.3.1** strongly indicating a preservation of this mechanism for delivered Arah2 antigenic subunits, we focused on their potential to protect against induction of peanut allergen hypersensitivity. Mice were vaccinated with EcN OMVs carrying the peanut allergen Arah2 prior to sensitization and challenge (**Fig. 5.3**), and, following subsequent sensitization, reduced serum titers of IgA and IgE reactive to raw peanut protein (RPP) revealed modulation of the immune response by the EcN OMVs indicative of protection, unlike the negligible effects of a control $T_H2$-biasing alum adjuvanted vaccine (**Fig. 5.4**). Challenge with a large RPP dose confirmed protection by the EcN OMV vaccine, leading to 100% protection for challenged mice rather than terminal anaphylaxis (**Fig. 5.5**).

To explore the link between EcN OMV antigen delivery and protective tolerance, we further probed the specific immune response to sensitization and challenge. Competitive histamine ELISA on post-challenge serum samples confirmed the prevention of cytokine-driven anaphylaxis via vaccine-induced immunomodulation that successfully neutralized the effects of sensitization (**Fig. 5.6**). Analysis of splenic T-cells following sensitization and challenge helped to clarify the cellular component of this response. While both OMV-delivered and alum-adjuvanted vaccinations resulted in an engagement of some activated and regulatory cellular immunity post-sensitization (**Fig. 5.7a**,**Fig. 5.8a-d**), EcN OMV antigen delivery more successfully controlled an overactive cellular response in the form of decreased active $CD4^+$ and $CD8^+$ effector T-cells (**Fig. 7b**, **Fig. 8e-l**), likely facilitated by stronger engagement of immunological memory[3] (**Fig. 7c, Fig. 8m-p**). This finding could be a crucial discrepancy, as it highlights the fact that simply engaging a cellular response does not necessarily prevent type I hypersensitivity,

| Condition | t = 0 wk | t = 4 wk | t = 8 wk | t = 9 wk | t = 10 wk | t = 11 wk |
|---|---|---|---|---|---|---|
| PBS | **Vaccinated**: PBS (sc) | **Vaccinated**: PBS (sc) | N/A | N/A | N/A | **Challenged**: RPP+Alum (ip) |
| PBS, Sensitized | **Vaccinated**: PBS (sc) | **Vaccinated**: PBS (sc) | **Sensitized**: RPP+CT (o); RPP+Alum (ip) | **Sensitized**: RPP+CT (o); RPP+Alum (ip) | **Sensitized**: RPP+CT (o); RPP+Alum (ip) | **Challenged**: RPP+Alum (ip) |
| Alum+RPP, Sensitized | **Vaccinated**: Alum+RPP (sc) | **Vaccinated**: Alum+RPP (sc) | **Sensitized**: RPP+CT (o); RPP+Alum (ip) | **Sensitized**: RPP+CT (o); RPP+Alum (ip) | **Sensitized**: RPP+CT (o); RPP+Alum (ip) | **Challenged**: RPP+Alum (ip) |
| EcN(Arah2), Sensitized | **Vaccinated**: EcN(Arah2) (sc) | **Vaccinated**: EcN(Arah2) (sc) | **Sensitized**: RPP+CT (o); RPP+Alum (ip) | **Sensitized**: RPP+CT (o); RPP+Alum (ip) | **Sensitized**: RPP+CT (o); RPP+Alum (ip) | **Challenged**: RPP+Alum (ip) |

**Figure 5.3: Schedule for prophylactic EcN OMV vaccine trial – vaccination, sensitization, and challenge.** Vaccination, sensitization, and challenge schedule for mice used in the experiment. Abbreviations: RPP = raw peanut protein, CT = cholera toxin, sc = subcutaneous injection, o = oral administration, ip = intraperitoneal injection.

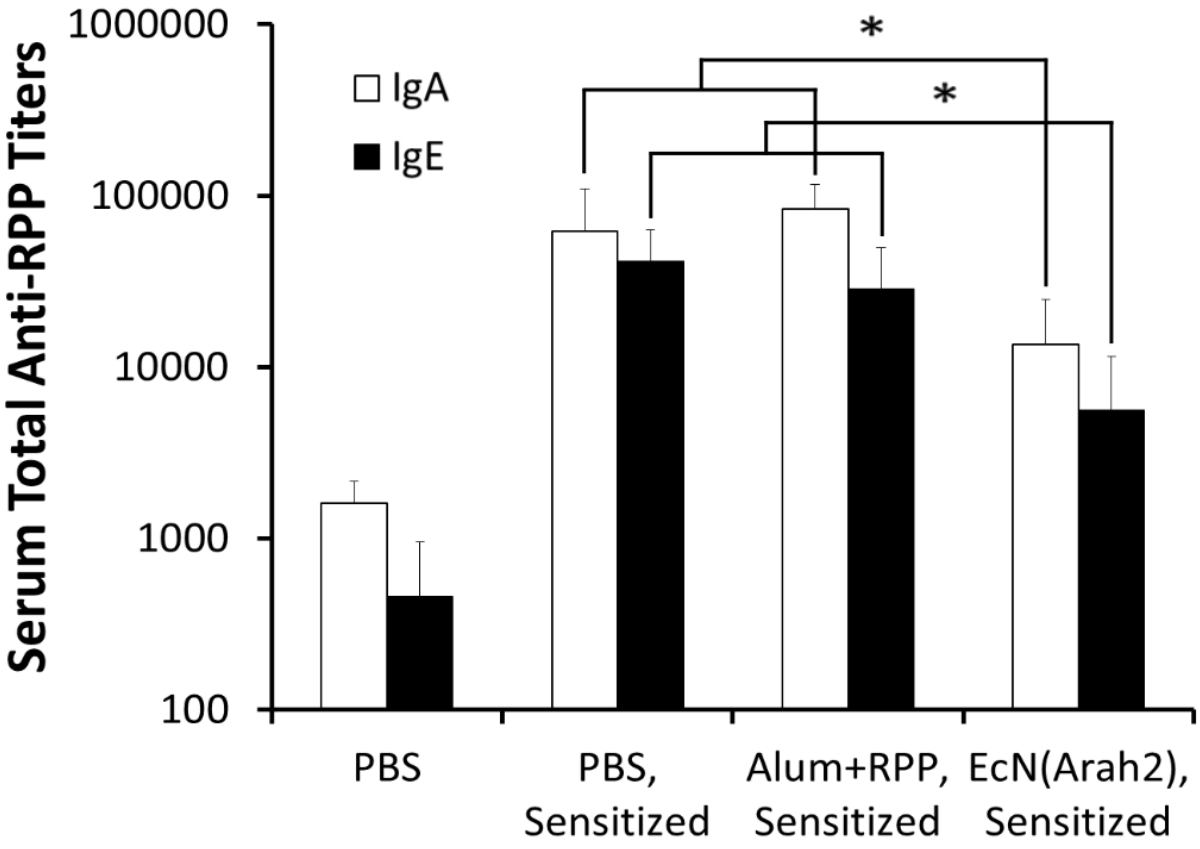


**Figure 5.4: EcN OMV vaccination results in significant decrease in humoral mediators of allergy following attempted sensitization.** Serum titers of anti-RPP IgA and IgE following sensitization show reduced allergy induction in EcN OMV-vaccinated mice. *P<0.05, as determined by Tukey's post-hoc test. All values given are mean + SD.

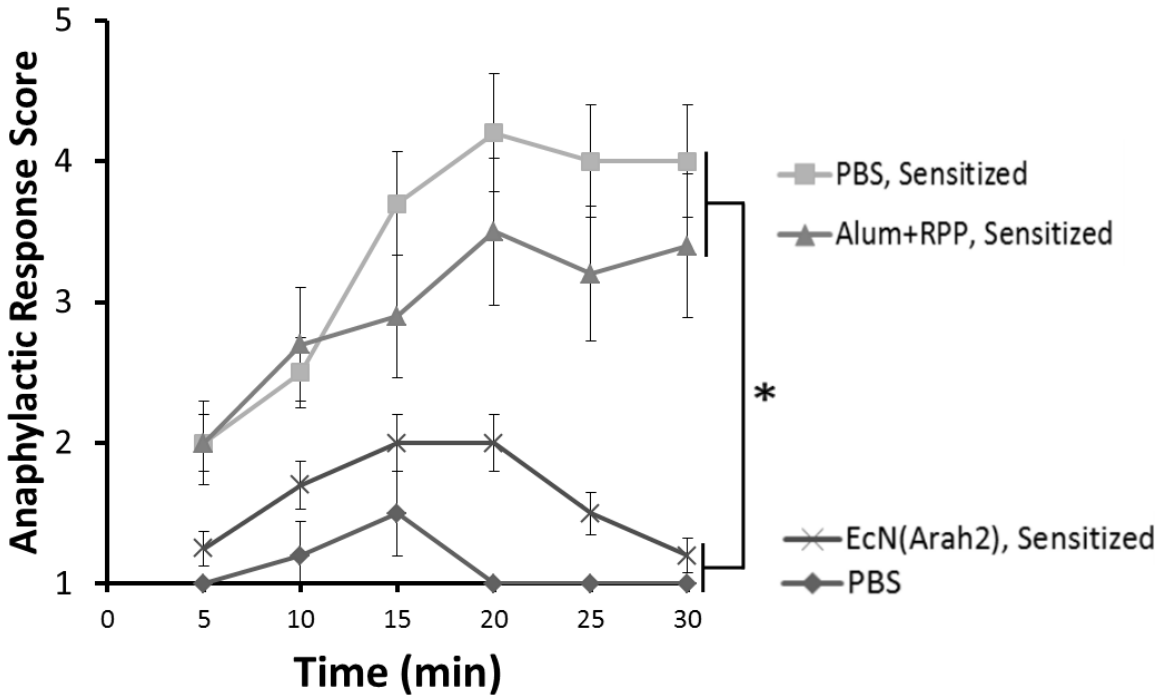


**Figure 5.5: EcN OMV carriers protect against peanut allergy induction, anaphylaxis.** Anaphylactic responses (scored 1-5) of vaccinated mice (n=5, all groups) post-sensitization and challenge with raw peanut protein (RPP). All mice with a score above 3 were euthanized after 30 min, while all other mice fully recovered, including 100% protected by the EcN OMV vaccine. *P<0.05, as determined by Tukey's post-hoc test. All values given are mean +/- SD.

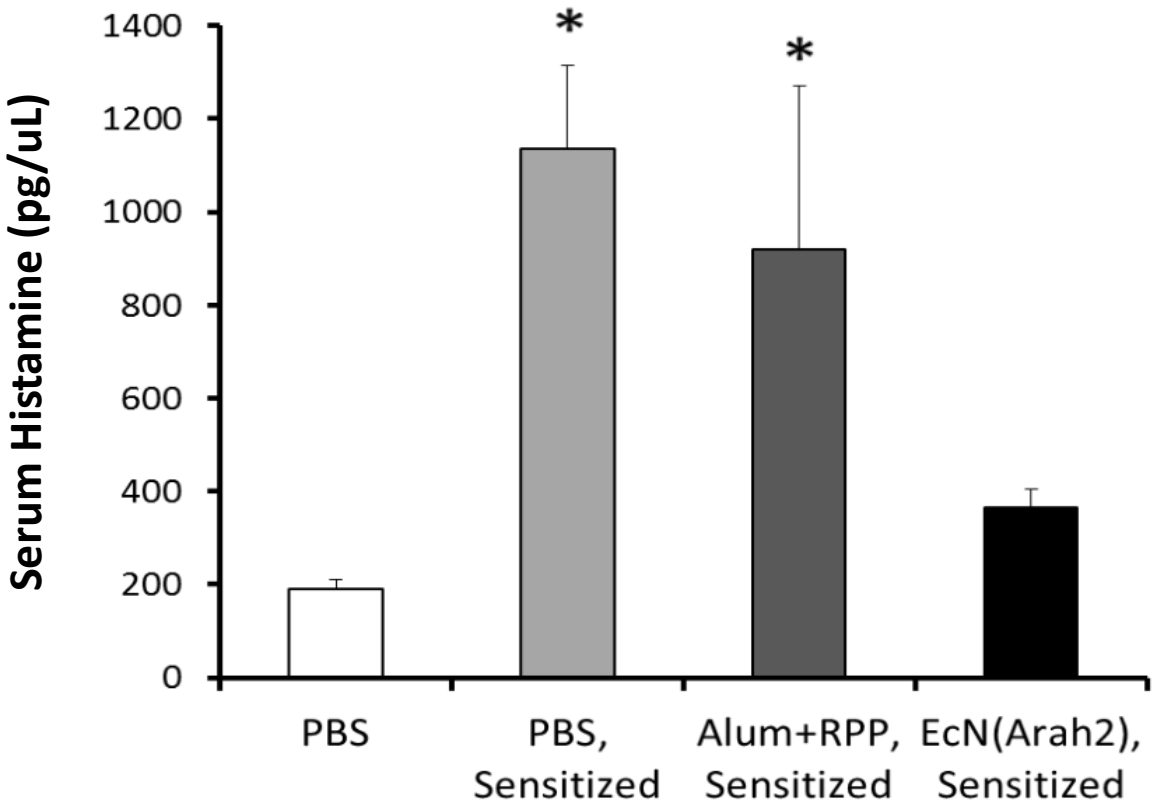


**Figure 5.6: Serum histamine levels immediately post-challenge were significantly less elevated in mice protected by prophylactic EcN OMV carrier vaccination.** *P<0.05, as determined by Tukey's post-hoc test. All values given are mean + SD.

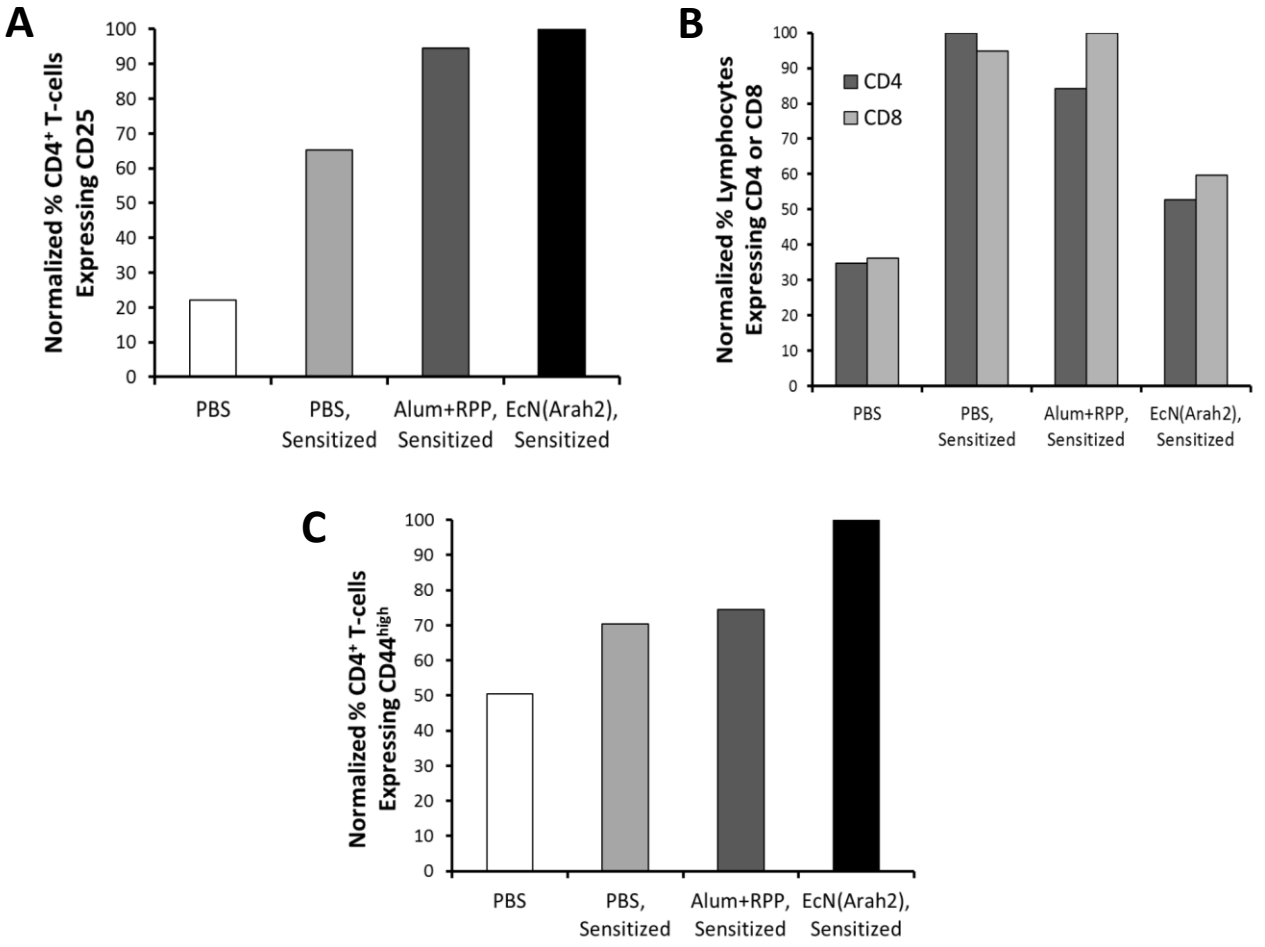


**Figure 5.7: Protection conferred by EcN OMV carrier vaccination resulted in splenic T-cell population shifts.** (**A-C)** Flow cytometry data of isolated primary splenocytes, normalized to the highest value in the data set, on pooled splenic T-cells isolated from mice in **c**, probing for regulatory T-cells (**A**), CD4/CD8 T-cells (**B**), and memory T-cells (**C**).

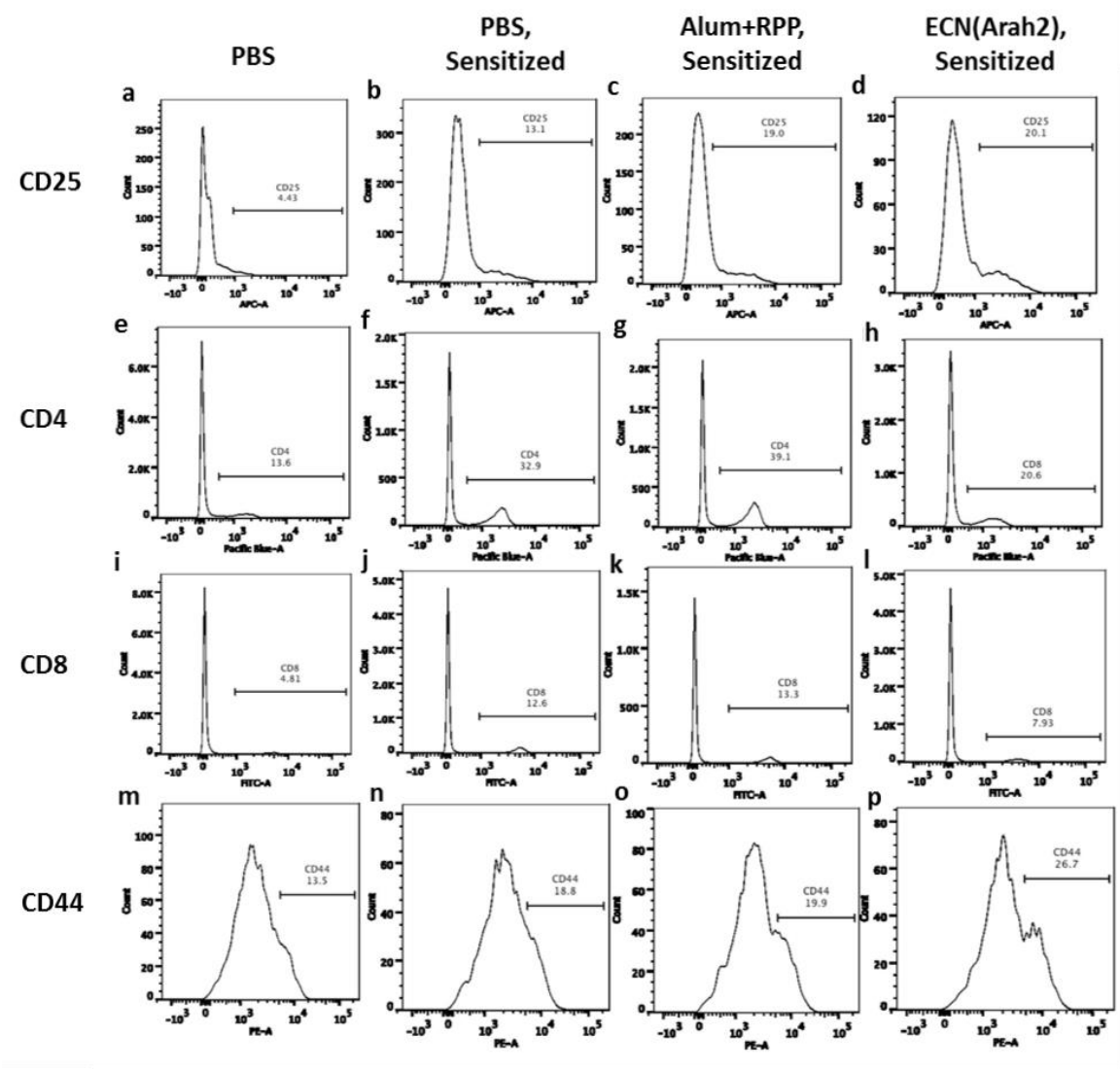


**Figure 5.8: Flow cytometry analysis of splenic T-cells from sensitized mice, expanded data set.** $CD4^+$ T-cells (**a-d, m-p**) or non-purified splenocytes (**e-l**) isolated from sensitized mice were tagged with fluorescent antibodies for CD25 (**a-d**), CD4 (**e-h**), CD8 (**i-l**), or CD44 (**m-p**) and analyzed using flow cytometry. Cell sources: PBS (**a,e,i,m**); PBS, sensitized (**b,f,j,n**), Alum+RPP, sensitized (**c,g,k,o**); and EcN(Arah2), sensitized (**d,h,l,p**). Samples represent pooled splenocyte populations (n=5).

but more sophisticated cellular analysis will likely be required to fully understand the underlying mechanism of protection.

### 5.3.3: Immunotherapy for peanut allergy possible via controlled release of EcN OMV vaccine carriers

Following successful demonstration of protective effects generated by EcN OMV vaccine PLPs administered prophylactically prior to sensitization, we next attempted to elucidate the effect the vaccine particles might have as immunomodulators if instead of being carriers for the allergens as a vaccine, they were instead carriers for the allergens as inducers of a competing immune response. Specifically, given how current immunotherapy is hypothesized to work by creating competing suppressive immunity by exposure to an allergen in tandem with immunosuppressing compounds, we rationalized that we could achieve similar effects with low doses of allergen delivered via EcN OMVs. Moreover, since the adjuvancy would be directly tied to the allergens via PLP delivery, we were able to take advantage of the microsphere-mediated controlled release described in **Chapter 3** to both slow the administration even more (thereby preventing side effects from an overexposure to the allergen) while not requiring the weekly administration current immunotherapies are limited by.

As in **5.3.2**, mice were sensitized, this time being treated with OMVs therapeutically rather than prophylactically. Following challenge, we observed encouraging protection by all OMV formulations: smaller zero-order release microparticles, larger multi-boost microparticles, and even free OMVs given similar to a vaccine (**Fig. 5.9**). Specifically, protection was conferred in a similar fashion as the dexamethasone-mediated immunotherapy. Importantly, histopathology of lung and intestinal sections revealed that controlled release schemes were capable of eliminating immunologically-mediated side effects from simply administering the OMVs in full vaccine doses (**Fig. 5.10**), which, while required under

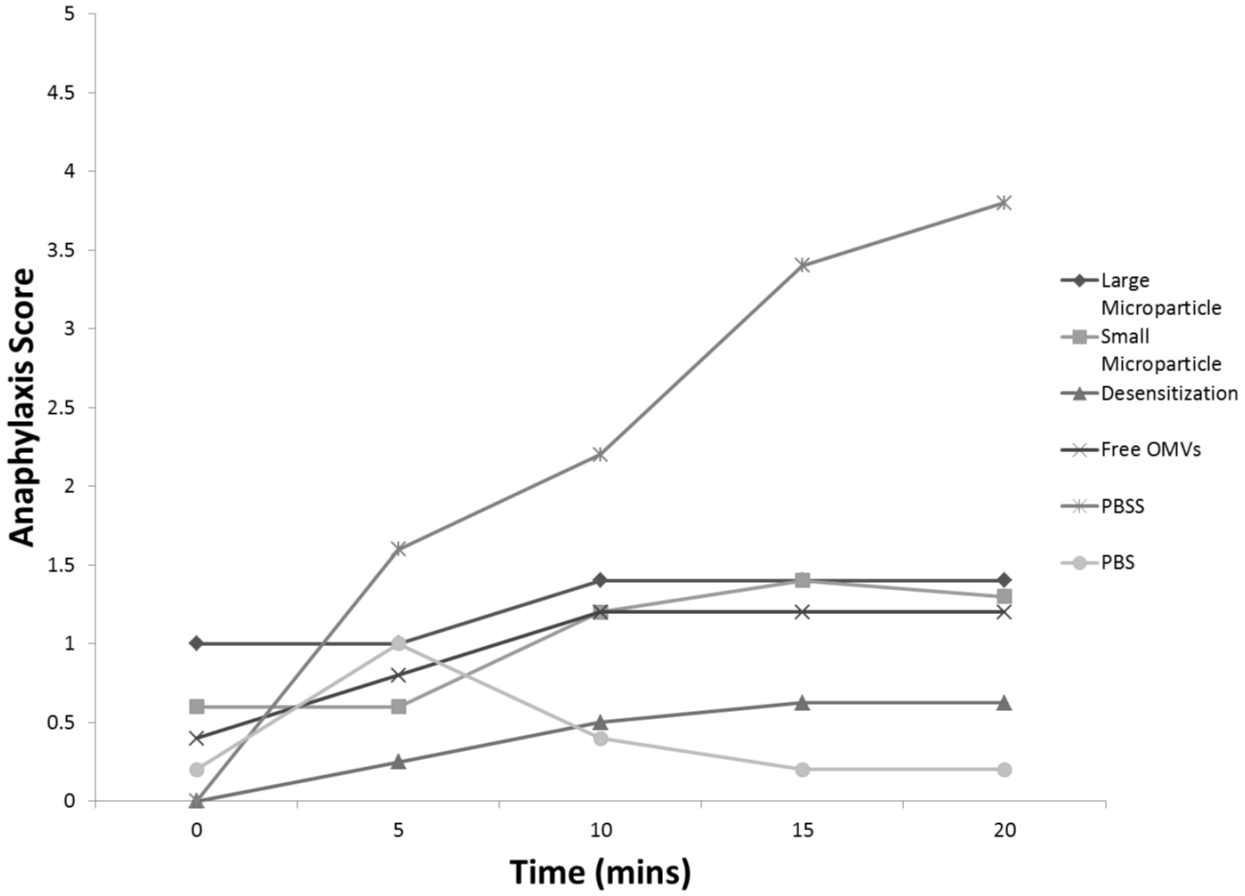


**Figure 5.9: Protection against anaphylactic challenge is conferred by controlled release immunotherapy doses of EcN OMVs displaying Arah2 antigen subunits**. Anaphylactic responses (scored 1-5) of treated mice (n=5, all groups) post-sensitization and challenge with raw peanut protein (RPP). All mice with a score above 3 were euthanized after 30 min, while all other mice fully recovered.

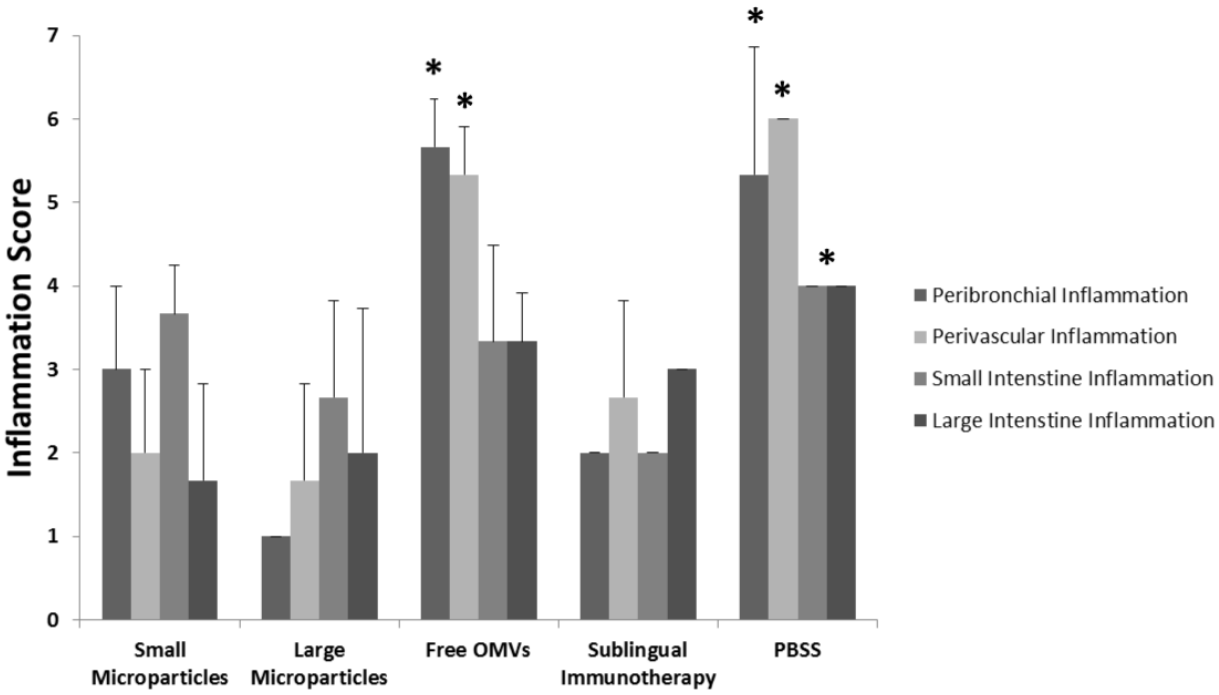


**Figure 5.10: Lung and intestinal inflammation caused by normal administration of freely injected OMVs is prevented by controlled release.** Tissue infiltration of inflammatory immune cells and associated tissue damage (scored 0-7) of treated mice (n=3, all groups) post-sensitization and challenge with RPP.

normal circumstances to induce the necessary immunity, unsurprisingly caused hypersensitivity when the mouse was exposed to that much allergen at once in immunostimulating circumstances.

Noting the success of the OMV-mediated therapy, we hypothesized two possible mechanisms: 1) the EcN OMVs had achieved a parallel response in accordance with normal immunotherapy methods that had competed with the hypersensitivity response upon anaphylactic challenge, or 2) the EcN OMVs had been such potent immunomodulators that they had achieved a quantal shift in immunity to their traditional $T_H1$ bias. In assaying the time-evolution of a humoral response post-treatment, we did indeed observe a dramatic response in line with a vaccine-like IgG response from both therapies (**Fig. 5.11**), supporting that one of the above hypotheses concerning mechanism of action was likely accurate – that is, the observed protection was conferred either by a change in the immune response once the elevated allergen-specific immunity had returned to a baseline value, or alternatively by the creation of a parallel immune response. Assaying for $T_H1$ bias in the serum IgG2a vs. IgG1 titers (**Fig. 5.12**) partially ruled out the admittedly less likely hypothesis of a quantal shift in immunity, however, as the overall composition of the anti-Arah2 humoral immunity remained essentially unchanged following the surge in total IgG titers following any treatment regimen. Further characterization of this immune response, such as via T-cell restimulation assays coupled with flow cytometry, may be beneficial to better elucidate just how the competing reaction generated by the EcN OMVs works, and what insights it might shed towards further harnessing the probiotic advantage via PLPs.

**5.4: Conclusions**

EcN OMVs displaying Arah2 antigen subunits were demonstrated to be effective therapies for peanut allergy in a mouse model. Interestingly, application of controlled release microsphere encapsulation allowed these OMVs to either be used as a prophylactic vaccine, which relied on a quantal establishment of non-hypersensitivity immunity, or as a more standard immunotherapy following

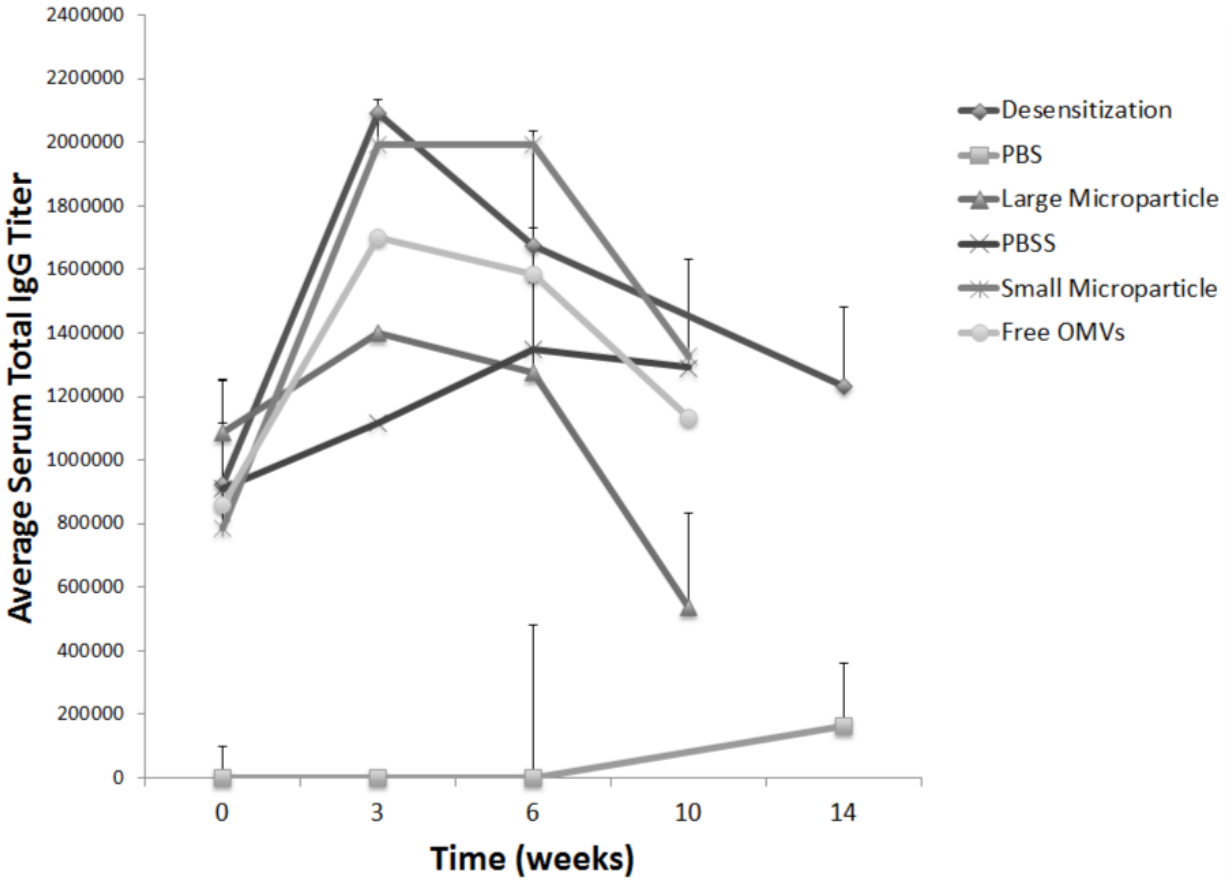


**Figure 5.11: EcN OMV Immunotherapy results in sharp increase in anti-Arah2 IgG titers following administration in sensitized mice.** Serum IgG titers derived from ELISAs run on pre-challenge mice jaw bleed samples (n=5, all groups).

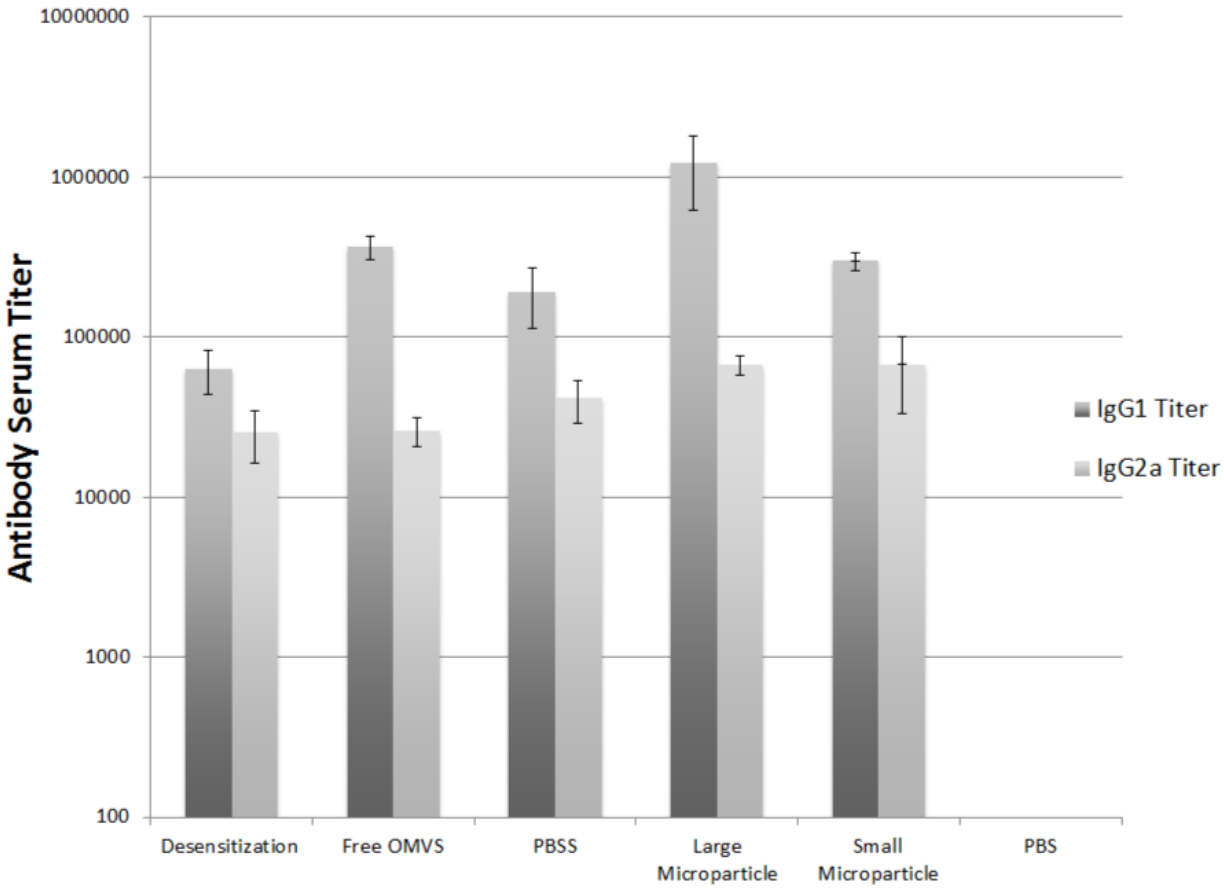


**Figure 5.12: EcN OMV immunotherapy did not succeed in creating a $T_H1$ bias in overwriting sensitization hypersensitivity immunity, despite protecting against it.** Serum IgG titers derived from ELISAs run on pre-challenge mice jaw bleed samples (n=5, all groups) taken immediately prior to anaphylactic challenge.

sensitization, which did not seem to rely on $T_H1$ biased immunity to protect against anaphylaxis. While prophylactic vaccination seemed to result in a greater control of symptoms in the mouse model, and required less modification to achieve acceptable results in minimizing both injection number and associated side effects, the concept of a universal prophylactic vaccine for allergies is still a fairly novel and controversial concept. On the other hand, enhanced immunotherapy modalities for control of allergy remains the widely accepted standard of care, and the general improvement of such modalities is an important goal of allergy study. As a result, both adaptations of the EcN OMV platform described here are of interest and bear further investigation for clinical development as improved treatment and prevention of the growing food allergy epidemic.

# CHAPTER 6

## CONCLUSIONS AND RECOMMENDATIONS

Engineering pathogen-like particle (PLP) vaccines can be a complicated science, whether it requires building a nanoparticle one component at a time or deriving biomimicry from a complicated biomaterial. But the benefits of using a PLP-guided approach to vaccination have clear advantages. It has been a long-accepted fact in the vaccine engineering community that the molecular and functional complexity of intact pathogens, while presenting its own list of complications, can direct the most potent immune responses. The immune system itself, having evolved to develop strong responses to aggregations of molecular and cellular interactions with pathogens, clearly benefits from an adjuvanting effect that goes beyond chemical disruption of native tissue or the engagement of a single immunostimulatory co-receptor per antigen. As a result, PLP-directed vaccine responses will likely continue to be a focus of vaccine engineering for some time. In this work, we contribute to the expanding field of OMV vaccines by uniting two disparate facets of bacterial contributions to medicine and bioengineering – probiotic bacteria and recombinant protein engineering – to create a promising vaccine delivery platform. Characterization of these vaccine carriers supported the driving intention to harness the unique immunogenicity of probiotic bacteria as the basis for potent PLP self-adjuvancy, and further immunogenicity enhancement via controlled release delivery helped eliminate one of the primary disadvantages that plague all acellular vaccines.

Immunological and biomolecular characterization of the EcN OMV, both as a self-adjuvanting particle alone and as a vaccine carrier, revealed intriguing lessons concerning immunogenicity while raising additional questions. Initially, we proposed using EcN as a source strain due to its unique and potent immunostimulation; we hypothesized an OMV from EcN would be able to harness enough of this

potential to achieve both self-adjuvancy and immunity bias in a favorable fashion. EcN's biomolecular identity did seem to be captured by the OMVs, and all evidence does support a capacity for vaccinating with a $T_H1$ bias. Additionally, two-photon microscopy and cellular interaction studies both highlight an finding: the EcN OMVs are not functioning simply as a convenient way to administer bacterial biomolecules as a natural adjuvant, but rather are functioning as delivery vehicles that can, like pathogens, diffuse or be themselves delivered to immune cells and link co-stimulation with antigen presentation. While the driving phenomenon behind why this is important is explored briefly in **Appendix III**, it should be noted that the phenomenon of using bacterial TLR agonists on the scale of a viral particle remains a insufficiently characterized phenomenon, and likely requires additional study to better understand just how EcN OMVs, and other OMVs, act as PLPs.

OMV vaccines are inherently a bacterial biotechnology, which comes with inherent advantages and disadvantages that were only initially explored in this work. The immunostimulatory advantages have been covered in some detail; that is, bacteria are themselves adjuvants due to the nature of TLR-directed innate immunity, which allows them to be capable of single-particle directed self-adjuvancy without any additional modification. This advantage is readily coupled with the general advantage of working with bacteria as a common source of recombinantly engineered protein products: bacteria are cheap to maintain, simple to manipulate, and scale well as a biological "factory". But these advantages are balanced by some notable inconveniences of working with bacteria, primarily their use as a vector for non-bacterial pathogens. While we address bacterial pathogen targets briefly in **Appendix II**, the bulk of this work used EcN OMVs as vaccines for non-bacterial targets. This is not a straightforward adaptation, as whole eukaryotic antigens are rarely easily expressed in bacteria without specific modification, and even once optimized for such expression the lack of glycosylation and similar folding conditions can still result in an end product for a vaccine that is ultimately unlike the eukaryotic source. This is problematic for PLP vaccines in particular, as pathogen-mimetic antigen presentation assumes

that the antigen is itself somewhat mimetic of the pathogen's own molecular identity. We addressed this with sufficient success for our purposes by careful subunit component selection and codon harmonization techniques, but it is unlikely that this approach will be sufficient for all applications. For this platform to truly be broadly applicable, a more straightforward platform for epitope display needs to be engineered to bridge the gap between bacterial expression and non-bacterial pathogen mimicry.

Regardless of the challenges inherent to OMV PLPs, their advantages were clearly demonstrated. Cross-strain immunity against influenza is rare, and protective quantal immunity for allergy traditionally has required more complex delivery vectors than a simple subcutaneous injection. In this way, EcN OMVs as PLPs demonstrated unique capacity as a vaccine platform to do what other vaccines cannot. Importantly, this success was achieved without sacrificing the inherent advantages discussed above purely for the sake of proving some proof-of-concept potency. Moreover, the utility of the EcN OMV in achieving prophylactic allergy prevention in the peanut allergy challenge model supports an ambitious precedent wherein PLP vaccines are not restricted simply to improving upon existing modalities of vaccination, but can open up entirely new avenues of utility for vaccine technology for the treatment of non-pathogenic, but immunologically intricate, diseases.

Future work with EcN OMVs, and recombinant subunit antigen carriers derived from bacterial OMVs in general, should focus primarily on two avenues: addressing inherent challenges to OMV utility and expanding on preclinical justification for OMVs as vaccine carriers. For the former, one unaddressed challenge with the EcN OMV is the stigma associated with bacterially-derived vaccines in general. With public opinion overwhelmingly focused on the potential toxicity of vaccine compounds and adjuvant components, the likelihood of mainstream acceptance of OMV vaccines laden with biomolecules such as LPS is unlikely. This work opened the door to the possibility of retaining OMV self-adjuvancy while removing some portion of LPS cytotoxicity, and future work to better understand and control the

negative effects of LPS would likely be necessary for a general OMV vaccine, likely to be classified more as an adjuvant than anything else, to be accepted both by the FDA and the public. Further validation of OMVs as capable of inducing protective immune responses translatable to humans is also a necessary continuation. For example, work already underway by our lab seeks to test the influenza EcN OMV vaccine in a murine and ferret influenza challenge model using species-adapted virus. Such steps are the obvious path towards getting a EcN OMV vaccine technology into the pipeline for pharmaceutical development, and it is logical to focus on similar viral and other non-bacterial diseases at this time to best expand a currently empty niche in OMV vaccine technology development.

Ultimately, the real promise of OMVs and similar PLPs lies in their flexibility to be further engineered to efficiently and flexibly mimic a variety of pathogens. The EcN source-strain in this work demonstrates the importance of strain selection, and a next logical step is to probe a library of similarly interesting bacterial immunomodulators (probiotic and otherwise) in a high-throughput fashion that can assess immune stimulation other than $T_H1$ bias. Of particular interest would be the identification of a bacterial source that could stimulate suppressive, regulatory immunity. While we were able to achieve some form of competitive suppression using an immunotherapy adaptation of the EcN OMVs, the potential for bacterial diversity to provide some engineerable platform for counteracting autoimmunity on a larger scale remains a promising and impactful direction to expand similar efforts. Additionally, further investigation into controlled release modalities on the microscale and epitope presentation on the molecular scale are necessary to harness the full potential of OMVs as a vaccine carrier. Self-adjuvancy on the nanoscale is only one piece of the complete picture of a pathogen-mimetic vaccine, and while arguably the one facet most capable of existing as a standalone technology, it would be a mistake not to find improved ways to control and apply such a potent immunomodulator.

In summary, we engineered pathogen-like recombinant vaccine carriers from OMVs derived from probiotic EcN bacteria and used a host of tools, from heterologous antigen codon harmonization to microparticle controlled release, to apply this bacterial system to non-bacterial disease vaccination. EcN OMVs were thoroughly assessed as potent self-adjuvanting immunomodulators for vaccine delivery applications, and could serve as the starting point for a platform technology uniting the molecular simplicity of recombinant vaccines with the molecular complexity of pathogen-mimetic immunity.

## APPENDIX I

## ADDITIONAL AND EXPANDED MATERIALS AND METHODS

**AI.1: Preparation of OMVs.** OMVs were purified in accordance with previously established procedure[89]. Briefly, plasmid pBAD-ClyA-GFP, containing an arabinose promoter, was transformed into *E. coli* vesicle-overproducing strains JC8031[63], JH1, and JH1-*LpxM*, and selected in LB-chloramphenicol or LB-kanamycin medium, respectively. Flasks containing 250 mL of medium were inoculated with overnight culture and allowed to grow until the $OD_{600}$ reached ~0.5. Protein expression was induced at this point by addition of L-arabinose to a final concentration of 0.2%. Cell-free culture supernatants were collected 12 hours after induction and filtered through a 0.45 µm filter. Vesicles were isolated by ultracentrifugation (Beckman-Coulter; Ti SW28 rotor, 26000xg, 3h, 4 °C) and resuspended in PBS.

**AI.2: Microscopy.** Scanning electron microscopy was conducted on purified vesicles flash-frozen on copper wafers in nitrogen slush and viewed in a LEO 1550 FESEM. Transmission electron microscopy was conducted on purified vesicles negatively stained with 2% uranyl acetate on 400-mesh Formvar carbon-coated copper grids and viewed in a FEI Tecnai F20 TEM. Fluorescence microscopy was conducted on purified vesicles suspended in PBS that were placed on a glass slide, sealed with a coverslip, and examined using an Olympus BX41 microscope with GFP filter set.

**AI.3: Protein Analyses.** Protein concentrations in OMV and purified recombinant protein preparations (used as controls in the vaccine study) were quantified by the bicinchoninic-acid assay (BCA Protein Assay; Pierce) using BSA as the protein standard. Fluorescence of GFP in protein and OMV samples was measured in a microplate spectrofluorometer (Gemini EM; Molecular Devices) using excitation and emission wavelengths of 481 nm and 507 nm, respectively[64]. For SDS/PAGE, samples were prepared in sample-loading buffer containing β-mercaptoethanol and heated at 90 °C for 10 min before electrophoresis on 10% polyacrylamide gels. Proteins were transferred to polyvinylidine difluoride

membranes for Western blot analysis and probed with monoclonal mouse anti-GFP IgG (Invitrogen; 1:2000) primary antibody, and horseradish peroxidase conjugated goat anti-mouse IgG (Jackson Immunoresearch; 1:10000) secondary antibody. Membranes were developed by autoradiography with ECL detection reagents (GE Healthcare).

**AI.4: LPS Analyses.** Bacterial LPS concentrations were determined by measuring the presence of KDO according to a previously described colorimetric assay[90,91]. Briefly, OMV samples (50 µL) in PBS were combined with 0.2 M $H_2SO_4$ (5 µL) and heated at 100 °C for 20 min. The samples were cooled to room temperature for 5 min, and then 25 µL of 0.04 M $NaIO_4$ was added to the mixture. After 20 min of incubation at room temperature, 2% $NaAsO_2$ (65 µL) was added to the sample tubes, and they were vortexed until the characteristic yellow color disappeared. Thiobarbituric acid (0.3%, 250 µL) was added, and the samples were returned to 100 C° for 10 min, followed by the immediate addition of dimethyl sulfoxide (125 µL). The samples were cooled to room temperature for 5 min, and the absorbance was read at 550 nm in a microplate spectrophotometer (Molecular Devices). Calibration standards were prepared from KDO ammonium salt (Sigma-Aldrich).

**AI.5: Dynamic Light Scattering.** Dynamic light scattering measurements were performed with the Nanosizer Nano ZS (Malvern Instruments) using Dispersion Technology Software version 4.20 for data acquisition and analysis. OMV samples contained 100 µg/mL total protein in 1 mL of PBS. The refractive index and viscosity of water were used as parameter inputs.

**AI.6: Recombinant Protein Purification.** Cultures of *E. coli* DH5α transformed with pBAD-ClyA-GFP-His, pBAD-ClyA-His, or pBAD-GFP-His were grown in 100 mL of LB medium containing chloramphenicol. Protein expression was induced by the addition of L-arabinose to a final concentration of 0.2% after the $OD_{600}$ reached ~0.5. Bacterial cultures were harvested 4 hours after induction and lysed by treatment with lysozyme (1 mg/mL) and Triton X-100 (1% vol/vol). The polyhistidine-tagged proteins in the soluble

fraction were purified by immobilized-metal affinity chromatography (Ni-NTA Agarose; Qiagen) according to the manufacturer's instructions. The proteins were eluted with 200 mM imidazole in a buffer containing 50 mM $NaH_2PO_4$ and 300 mM NaCl (pH 8.0), and they were subsequently desalted into PBS using PD-10 size exclusion chromatography columns (Amersham Biosciences).

**AI.7: Cell isolation and culture.** Mouse red blood cells (MRBCs) were extracted via post-euthanasia cardiac puncture into EDTA, then washed in PBS and stored at 4 °C as a 10% solution. For bone marrow-derived macrophages and dendritic cells (DCs), bone marrow was obtained from mouse femurs and grown for 6 to 8 days in RPMI 1640 in the presence of 10% L929 conditioned medium[92] and collected 7 days later. Bone marrow-derived DCs were cultured in the presence of 20 ng/ml GM-CSF and collected 6–8 days after culture[93]. For the splenic T-cells and B-cells, spleens were harvested, mechanically homogenized, and filtered through a 100 μm cell strainer (Falcon). Erythrocytes were lysed with cold ACK lysing buffer (Cellgro) for 5 min, and the cell suspension was washed with complete medium. T cells were purified with enrichment columns (R& D Systems) following the manufacturer's recommendations. B cells were enriched by negative selection using magnetic isolation kits, as per manufacturer's instructions (Miltenyi Biotec). This resulted in cell purities of >97% as determined by flow cytometry.

**AI.8: ELISA.** Polystyrene microtiter 96-well plates (Maxisorp; Nunc Nalgene) were coated with GFP (5 μg/ml in carbonate buffer, pH 9.6) and incubated overnight at 4 °C. Plates were blocked with 3% BSA in PBS containing 0.05% Tween-20 (PBST). Samples were serially diluted 2-fold in blocking buffer in a range of 1:200–204,800, added to the wells, and incubated for 2 hours at 37 °C. Plates were washed six times with PBST, and biotinylated goat anti-mouse IgG, IgM (Sigma), or monoclonal IgG1 or IgG2 (BD Pharmingen) were added to the wells (1 μg/ml) for 1 hour at 37 °C. Avidin-horseradish peroxidase (1:1000; Sigma) was then added and incubation continued for 30 min at 37 °C. After six additional washes with PBST, 3,3',5,5' tetramethylbenzidine substrate (1-Step TMB; Pierce) was added, and the

enzyme reaction proceeded for 20 min. The reaction was stopped with 2 M $H_2SO_4$. The absorbance was quantified in a microplate spectrophotometer at a wavelength of 450 nm. Serum antibody titers were determined by measuring the last dilution that resulted in three standard deviations above background. For the determination of cytokines, cells were resuspended at a concentration of $2\times10^6$ cells/well in medium RPMI 1640 (supplemented with FCS and antibiotics), seeded into 96-well plates and incubated for 48 h with 5 µg GFP. Cytokine levels were measured in the supernatants by using standard ELISA kits (eBioscience).

**AI.9: Hemagglutination Inhibition Assays.** Samples of A/PR8/34 and X31 influenza virus were inactivated in 0.02% formalin for 18h at 37°C, and then dialyzed against PBS at room temperature overnight. Each virus sample was titered for stock hemagglutination units (HAs) as described elsewhere[94] using serial two-fold dilutions of virus into freshly-drawn 1% MRBCs in PBS. Subsequently, serial two-fold dilutions of serum from appropriately vaccinated mice were incubated as described elsewhere[94] with 4 HA diluted virus samples and then exposed to 1% MRBCs in PBS. Both assays were read using the teardrop method to determine the cut-off between hemagglutination and hemagglutination absence/inhibition.

**AI.10: Cytokine Expression Analyses.** For splenic lymphocytes, cells were stimulated overnight with 5 µg/ml GFP, 5 ng/ml IL-2 and 10 µg/ml anti-CD28, and then cultured with brefeldin A. Cells were stained with fluorescent antibodies against the surface markers CD3 (clone 17A2) and CD4 (clone RM4-5), permeabilized, fixed and incubated with antibodies against the cytokines IFN-ɣ (clone XMG1.2) or IL-10. All incubations were carried out on ice for 30 min. All antibodies were purchased from BD Bioscience or eBioscience. For each sample, at least 50,000 cells were analyzed. The data were collected and analyzed using CELLQuest or FlowJo software and a FACScalibur flow cytometer (Becton Dickinson, San Jose, CA). For macrophages, cells were plated as above and also incubated with increasing concentrations of

OMVs. Sixteen hours later, brefeldin A (10 μg/ml) was added and cells were incubated for 6 additional hours. DCs were then collected to be stained and analyzed by flow cytometry. Prior to staining, cells were incubated with an anti-Fcγ III/II receptor (BD Biosciences) and 10% normal mouse serum (NMS) in PBS containing 0.1% BSA, 0.01% $NaN_3$. Cells were stained with antibodies against the surface marker CD11c (clone 223H7), fixed in 2% paraformaldehyde, permeabilized with saponin and then incubated with fluorescent antibodies against the cytokines IL-12p40/p70 (clone C17.8), IL-10 (clone JES5-16E3) or IL-4 (clone 11B11). Incubations were carried out for 30 min on ice. All antibodies were purchased from BD Biosciences or eBioscience. Data was collected and analyzed as described above.

**AI.11: Inflammopathology.** Four groups of three 8-week old BALB/c mice (Charles River Laboratories) each were injected s.d. in each ear with 10% of the vaccine dosage described previously for PBS, EcJ OMVs, EcN OMVs, and EcN-*LpxM* OMVs. Mice were euthanized 30 hours after injection, and their ears were resected and immediately fixed in 10% formalin. Tissue samples were processed routinely for histopathology and stained with hematoxylin and eosin for light microscopic evaluation. Slides were read and graded in a blinded fashion by a licensed pathologist. Changes were given an overall score based on the grade of inflammation, edema, and tissue damage/remodeling as well as the presence or absence of vasculitis or vascular thrombi.

**AI.12: Phagocytosis assay.** Bone marrow-derived macrophages were plated in 6-well plates ($10^6$/well) for 16 hours and incubated with increasing concentrations of ClyA-GFP(+) EcN or EcJ OMVs. Two hours after the addition of the OMVs, plates were washed vigorously; cells were collected and analyzed by flow cytometry to detect internalized GFP. The data were collected using a FACScalibur flow cytometer and analyzed in CELLQuest software (Becton Dickinson, San Jose, CA). For each sample, at least 30,000 cells were analyzed.

**AI.13: T-cell Activation Analyses.** T-cell activation by stimulated DCs was assayed as described previously[44,95]. Briefly, 96-well plates were incubated overnight with 10 μg/mL anti-mouse CD3 (clone 145-2C11; BD Biosciences) at 4 °C, after which plates were washed 3 times with complete RPMI. T cells were then labeled with CFSE as described and seeded into wells from at $2X10^5$ cell/well. T-cells were co-incubated with $4X10^4$ cell/well DCs, 5 μg/mL anti-mouse CD28 (clone 37.51, Biolegend), and 1-100 μg/mL EcJ or EcN OMVs. Samples prepared for flow cytometry analysis incubated for 48 h at 37 °C, incubated for 4-6 h with 25 ng/mL PMA, 1 μg/mL ionomycin, and 10 μg/mL brefeldin A, and then were collected and stained with IFN-γ and IL-10 (eBiosciences). Samples prepared for ELISA analysis of culture supernatants were also incubated for 48h at 37 °C. Samples prepared for proliferation analysis were incubated at 37 °C for 7 days, then trypsinized and analyzed by flow cytometry for loss of CFSE staining.

**AI.14: Two-photon imaging of lymph node tissue**. BALB/c mice (n=3) were injected s.c. with 100 μg EcN OMVs and/or $1x10^6$ splenic DCs, stained with DiO and DiD respectively (Invitrogen), then euthanized after 4 days. After euthanasia, intact draining cervical lymph nodes were resected, placed in PBS, and immediately imaged via two-photon excited fluorescence microscopy on a custom setup.

## APPENDIX II

## APPLICATION OF THE ECN OMV PLATFORM TO HETEROLOGOUS BACTERIAL ANTIGEN DELIVERY, A TEST CASE: *MYCOBACTERIUM AVIUM SUBSPECIES PARATUBERCULOSIS*

### AII.1: Introduction

One of the great frontiers of current vaccine research is designing vaccines against complicated intracellular pathogens that the mammalian immune system normally has great difficulty clearing. Some pathogens, like the *Plasmodium* family of protozoan parasites, use intracellular evasion to dodge the immune system for fairly short amounts of time as they go through their life cycle within a mammalian host and cause great, often fatal, destruction in resident tissues[18]. Others, like the *Mycobacterium* family (best known for causing tuberculosis in humans), use intracellular evasion inside macrophages themselves to lie dormant for decades before re-emerging as pathogenic[19,44,96]. Regardless of the timescale of infection, intracellular evasion is best combatted by a $T_H1$ –biased immune response, and it has been theorized that a leading factor in the consistent failure of vaccines against pathogens such as *Plasmodium* and *Mycobacterium* is a lack of sufficient antigen-specific $T_H1$ immunity induction. Therefore, we hypothesized that our EcN OMV platform may be an ideal candidate for vaccines against such non-viral intracellular pathogens.

As our preliminary model pathogen to test this application, we chose *Mycobacterium avium subs. paratuberculosis* (MAP), which causes Johne's disease in cattle[96]. Johne's disease is essentially the bovine analogue of human tuberculosis (TB), thus making it a compelling and highly relevant animal model to study given the billions of people currently infected globally with TB and the millions of new chronic active cases occurring each year. We began similarly to our approach in **Chapter 3** by testing basic anti-antigen immune response in BALB/c mice. For our antigen of choice, however, we took a slightly different approach. Instead of simply choosing a native antigen of MAP (as we did with H1N1

HA), we decided to broaden the test of our platform's recombinant subunit antigen carrier applicability and instead use the fusion polyprotein antigen MAP 74F[96]. 74F contains a segmented fusion of MAP3527 and MAP1519, and its inclusion in this study represents an attempt to demonstrate that the ClyA-antigen expression pathway can be used to enhance vaccine antigen multivalency through multiple-antigen inclusion. Secondly, its choice pushes the boundaries of ClyA's ability to externalize a C-terminally fused moiety – 74F is 803 amino acids long, substantially larger than the original model antigen GFP's 242 amino acids. It is highly likely that there is some upper limit to ClyA's ability to act as an externalizing transporter; a larger polyprotein such as 74F may serve as a useful probing of the upper limit.

**AII.2: Materials and Methods**

**AII.2.1: Construction of pBAD-ClyA-MAP74F.** The MAP74F construct was acquired from Dr. Yung-fu Chang and modified via site-directed mutation to insert a HindIII site at the 5' end and an XbaI site at the 3' end of the MAP74 gene contained within the pMAP74F plasmid. The plasmid was subsequently digested via restriction enzymes as described in **AI.1** and inserted in the place of GFP in pBAD-ClyA-GFP.

**AII.2.2: Generation of EcN OMVs displaying MAP74F. AI.1** was followed using pBAD-ClyA-MAP74F.

**AII.2.3: Vaccine studies of EcN OMVs displaying MAP74F. 2.2.2** was followed using the product of **AII.2.2.**

**AII.2.4: Assessing OMV vaccine immune response. 2.2.3-2.2.4** was followed to analyze the samples generated by **AII.2.3.**

**AIII.3: Results and Discussion**

Currently, we have not moved beyond the BALB/c trial, but the initial immunological data from that trial is promising. The humoral (**Fig. AII.1**) and cellular (**Fig. AII.2**) data clearly indicate that despite the larger size and complexity of the 74F polyprotein antigen, the EcN OMV was still able to deliver it as an antigen and facilitate the development of antigen-specific immunity. Of note is that by comparison to the data in **2.3**, there was indeed a slightly diminished response relative to alum that was not seen using H1N1 HA in **3.3**. At this stage it is hard to determine whether that was the result of the nature of the 74F antigen itself, a diminished capacity of the EcN mutants to surface display the antigen via ClyA due to its size or some other antigen-related factor, or whether some additional factor of the trial itself played a role. Perhaps most importantly, the data still indicates a strong enough response to the 74F antigen to be worth further investigation in a relevant animal challenge model, though future EcN OMV applications involving even larger antigens may require additional attention nonetheless.

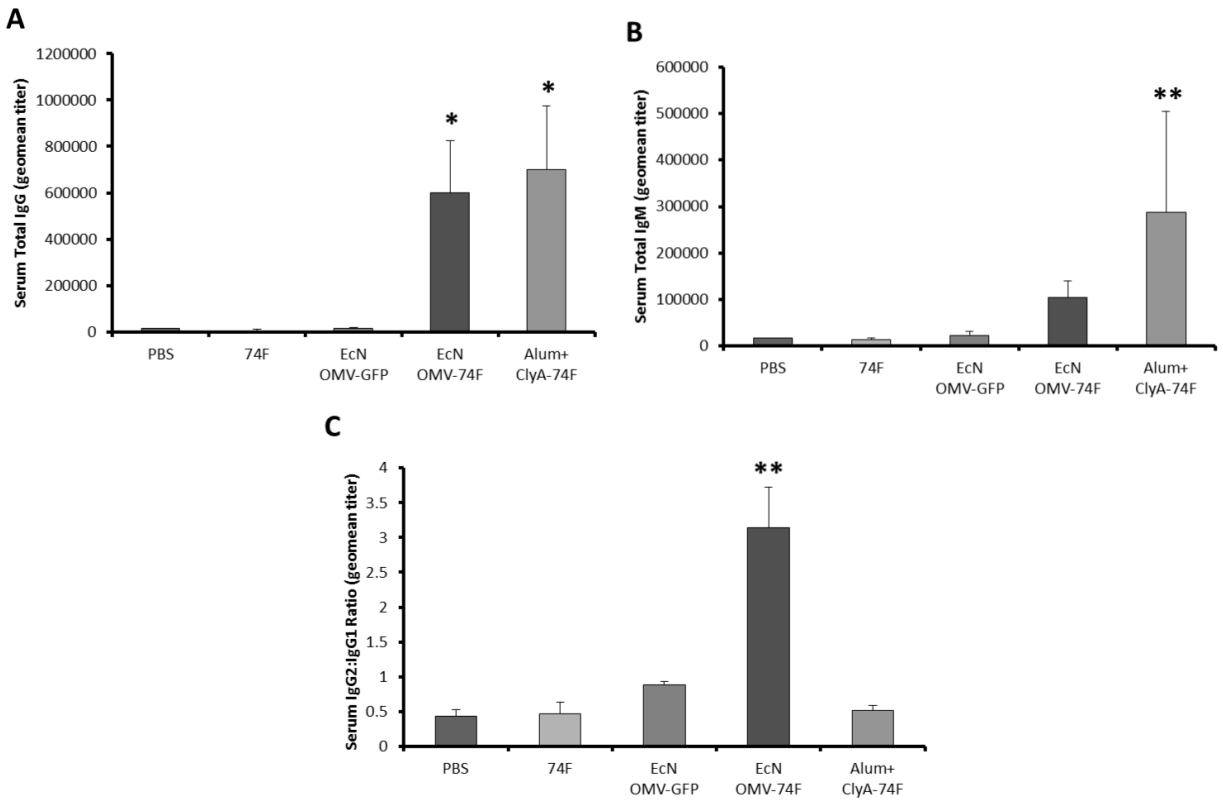


**Figure AII.1: EcN OMV carriers generate strong anti-MAP 74F humoral immunity.** (**A-C**) Terminal data points from BALB/c mice vaccinated and boosted once with antigen-normalized (or protein normalized, as appropriate) with EcN OMVs and controls (n=5). (**A-B**) Class-specific anti-74F antibody serum titers. (**C**) Ratio of serum titers of IgG1 to IgG2. (**A-C**) Alum = Alhydrogel®. ***P<0.005, ****P<0.05 determined by Tukey's HSD post-hoc test. All values are given as mean + s.d.

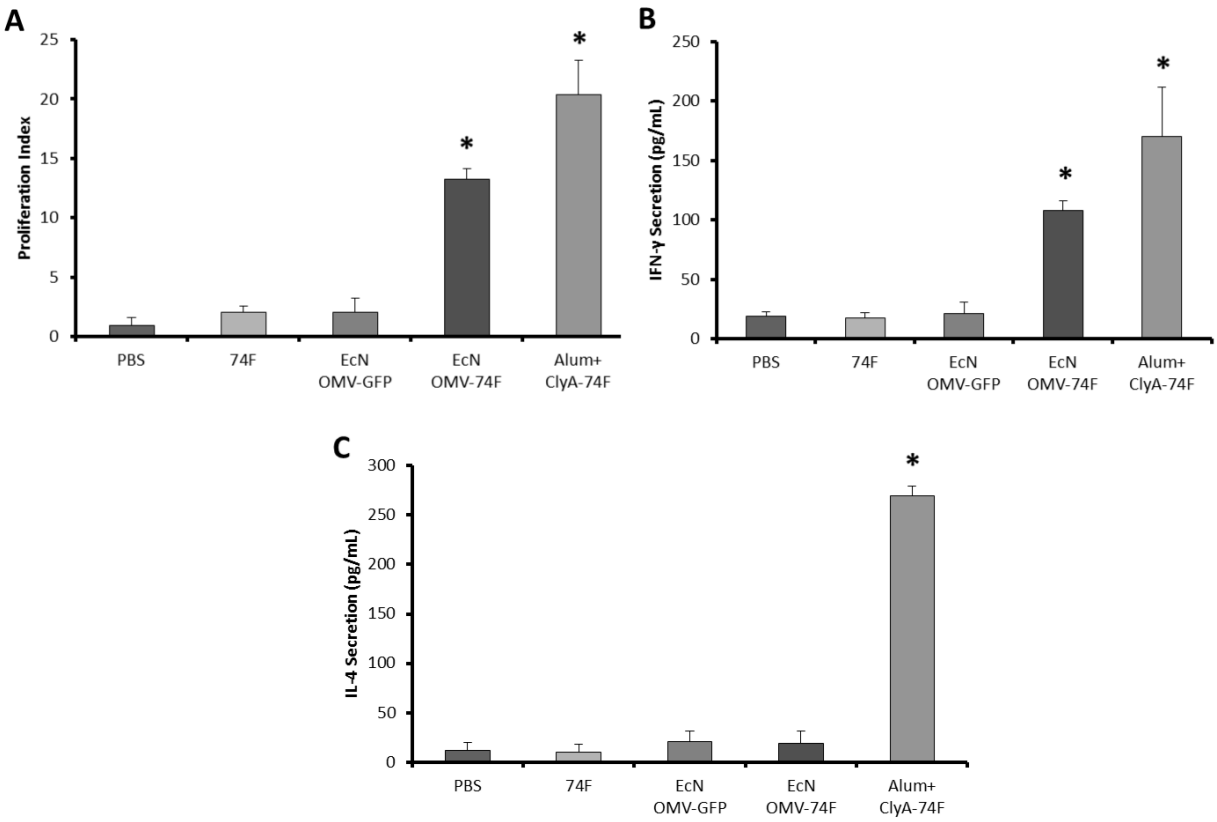


**Figure AII.2: EcN OMV carriers generate strong anti-MAP 74F cellular immunity.** (**A-C**) Terminal data points from BALB/c mice vaccinated and boosted once with antigen-normalized (or protein normalized, as appropriate) with EcN OMVs and controls (n=5). (**A**) Proliferation index of antigen-restimulated spleen-derived T-cells harvested from end-point subjects, measured via CFSE stain. (**B-C**) Cytokine secretion levels from cultured, antigen-restimulated spleen-derived T-cells harvested from end-point subjects. (**A-C**) Alum = Alhydrogel®. *****P<0.005. All values are given as mean + s.d.

## APPENDIX III

## MODELING INTACT PATHOGEN IMMUNE CELL PRESENTATION AND POLYREACTIVE ANTIBODY GENERATION (USING HIV AS A MODEL)

### AIII.1: Introduction

Up to this point, we have demonstrated how the EcN OMV platform is an engineered vaccine carrier that has the demonstrated advantages of 1) $T_H1$-biasing antigen-specific responses, and 2) surface displaying functionally folded exogenous antigens. While this certainly represents a substantial step towards engineering a true PLP, and hopefully will provide enough advancement to spur the creation of several vaccines against previously out-of-reach vaccine targets, the truth is that simple immune modulation may not be enough for many pathogens. Indeed, certain pathogens (and other non-pathogen targets) have aspects of a required immune response that defy the traditional application of even the ideally immunostimulatory recombinant subunit vaccine.

An unfortunately good example is the human immunodeficiency virus (HIV). Despite monumental efforts on the part of virologists, immunologists, and epidemiologists to find a cure for the human immunodeficiency virus (HIV), there remains a startling absence of an effective vaccine[97]. Unsurprisingly, the very reasons that make HIV a difficult target for the immune system to handle make it equivalently difficult to design a vaccine against it. HIV has a high mutagenic rate for its capsid proteins and, once stably integrated within T-cells, has effective mechanisms for avoiding extracellular contact with the immune system[98]. Both of these aspects make developing a good immune response with neutralizing antibody populations very difficult, and this difficulty reflects back on a vaccine's ability to make meaningful contributions to adaptive immunity. Certain viral moieties, such as capsid protein gp120 and gp140, are decent vaccine targets due to their low mutagenicity; unfortunately, their low

expression level on the HIV surface membrane has led to gp120/gp140 vaccines only providing minimally enhanced defense[99].

Recent work by Mouquet et al.[100] may finally have given vaccine engineering the direction it needs, however, and in turn given us inspiration on how to further enhance our EcN OMV platform. Working with serum samples from HIV "controllers" with high titers of neutralizing antibodies, they found that polyreactive antibodies, a rare form of antibody demonstrating bispecificity for two specific antigens on a pathogen surface, dominated the immunoglobulin population. These antibodies showed moderate affinity for gp120 as well as lower affinity for gp41, a mutagenic surface protein. While it is easy to postulate that this combination of affinities would allow the antibody to superiorly neutralize HIV in the serum, comprehending how such an antibody, whose associated B-cells would be greatly disadvantaged under normal developmental conditions with the lower affinities required to generate polyreactivity (particularly when it is partially targeted towards a mutagenic antigen), could actually come to dominate polyclonal expression is an entirely different matter altogether. That being said, the answer to that question may prove to be incredibly important. If we understand how in this specific case certain individuals' adaptive immunity can skew towards the dominance of polyreactive antibodies, we might be able to engineer a similar ability into our own vaccine carrier platform (especially given its strong PLP capacity). Consequently, we used computational immunology to tackle this challenge. Specifically, we applied an affinity-dependent kinetic proofreading model to the unique antigen presentation of HIV by dendritic cells (DCs) to naïve B-cells. We then employed kinetic Monte Carlo (KMC) to simulate B-cell receptor (BCR) –antigen interactions and their effect on downstream signaling of B-cell activation pathways.

**AIII.2: Modeling Methods**

Our model of choice is based on a similar attempt at simplifying and quantifying the B-cell/DC interface and its effect on naïve B-cell molecular activation pathways used by Tsourkas et al.[101] Briefly, a 1.5x1.5x0.01 μm section of both cells is brought within 20 nm of each other and discretized into 10 nm blocks (representing the exclusion radius of an average cellular protein)[102]. BCRs and antigen are randomly distributed throughout the two membranes at the beginning of the trial. Two B-cell downstream signaling proteins are also included: Lyn, which is bound to the inside of the B-cell membrane; and Syk, which diffuses freely throughout the B-cell interior. When BCRs come within binding range of opposite antigen, a reversible attachment can occur. Should this attachment last for a minimum time μ, the BCR undergoes a conformational change and becomes capable of binding Lyn – hence the aforementioned affinity dependence. Lyn can then phosphorylate the BCR, which can then in turn phosphorylate Syk. The amount of phosphorylated Syk at the end of a B-cell/DC interaction, usually lasting around 100 s, is directly correlated with the extent of naïve B-cell activation, which itself directly determines which B-cells go on to become dominant clones in the antibody production process.

Our first modification to the Tsourkas et al. kinetic proofreading model involves allowing for heteroligation of more than one antibody per BCR, a likely requirement to demonstrate any advantage the polyreactive BCRs (correlating to the cell's potential polyreactive antibody production) might have in promoting naïve B-cell selection[100]. The full schematic of the model can be found in **Figure AIII.1**. Initially, BCRs and presented antigen diffuse freely (with event probability $P_{diffF}$) in their respective membranes (**Fig. AIII.1a**). If the antigen is within one 10 nm exclusion radius of the BCR (whose arms are assumed to extend up to one additional exclusion radius in any direction beyond its core), it can bind the BCR ($P_{onBA1}$) (**Fig. AIII.1b**). This complex can diffuse around the B-cell surface ($P_{diffC}$), where it might encounter additional diffusing antigen or Lyn (**Fig. AIII.1c**). If the BCR has been in *any* current or previous BCR-Ag complex for longer than μ, then it is conformationally capable of binding the Lyn and

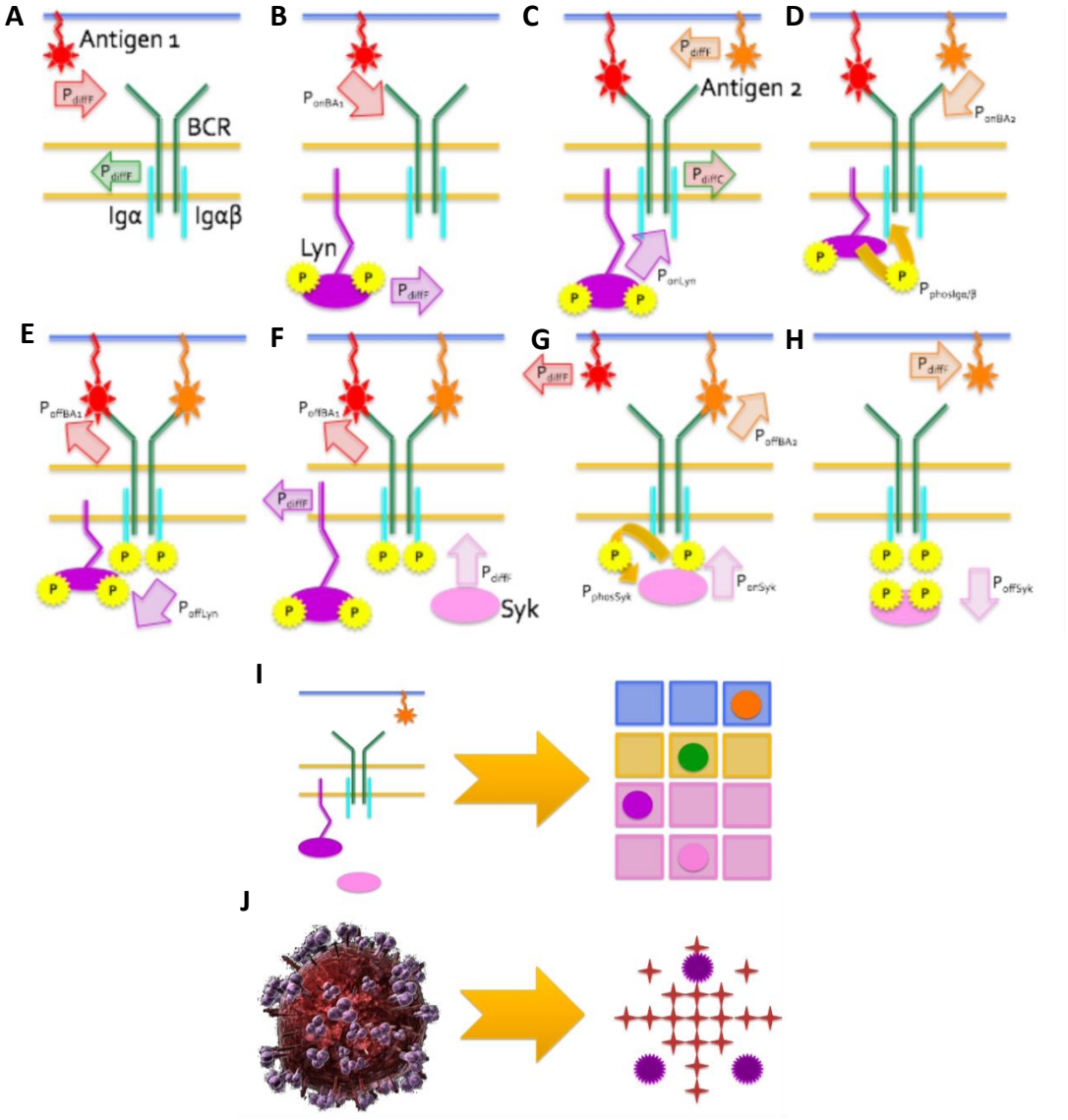


**Figure AIII.1: Kinetic proofreading model for B-cell activation via BCR-antigen interactions between naïve B-cells and DCs.** Initially, diffusing BCRs and antigen (**A**) can bind if appropriately opposite each other (**B**), conformationally activating the BCR's intracellular domain to bind Lyn (**C**) and be phosphorylated (**D**). (**E**) Each iteration may (in the displayed case of Lyn) or may not (in the displayed case of Antigen 1) result in disengagement of a complex. Finally, Syk can diffuse to (**F**), become phosphorylated by (**G**), and diffuse away from a phosphorylated BCR, triggering downstream signaling. (**I**) A z-axis view of the lattice set-up for the extracellular and intracellular model components. (**J**) An x-y plane view of the pattern of gp41 (red) and gp120 (purple) HIV antigens on a simulated DC-displayed intact virion.

being subsequently phosphorylated on either its α or β chain ($P_{phosIg\alpha/\beta}$) (**Fig. AIII.1d**). Additional antigen might also bind - in the polyreactive case, this may be a similar or different antigen ($P_{onBA2}$). Regardless of whether or not these additional binding events occur, both bound Lyn and antigen are capable of detaching ($P_{offBA1/Lyn}$) (**Fig. AIII.1e**). Finally, diffusing intracellular Syk can bind phosphorylated BCRs ($P_{onSyk}$), be phosphorylated ($P_{phosSyk}$), and then detach ($P_{offSyk}$) (**Fig. AIII.1f-h**).

This model was fully coded in MATLAB and was initially run on a 150x150x8 node lattice representing the two membranes and a 60 nm-deep portion of the intracellular compartment (**Fig. AIII.1i**). Due to computational constraints, however, data ultimately had to be supplemented by down-sized, representative runs on a 15x15x8 node lattice. In the model, parameters are mapped from cellular concentrations and kinetic rate constants to local populations and event probabilities, respectively, as previously described[101–103] and currently detailed in **AIII.3**. The crucial parameter of μ is additionally dependent on the oligomerization time of the BCRs, which is affinity-dependent and experimentally found to be equivalent to the amount of time needed for half the total BCR population becoming dimerized. Thus μ is calculated for each BCR individually by averaging the amount of time required to reach 50% dimerization over 10 trials[101]. Additional details are provided in **AIII.3**.

The second modification stems from the unique way we hypothesize HIV is presented by mature DCs to B-cells. Via a recently-discovered mechanism[104], HIV avoids the processing pathway of the DC's phagosome and instead hijacks its parallel antigen presentation pathway to get itself externalized in an intact and functional form on the surface of the DCs, where it lies in wait for T-cells scanning the DC surface for antigen. While this is a definite advantage for the HIV virion's infectious capacity, it should also dramatically alter the way HIV antigen is presented to a B-cell. Normally, antigen from a phagosome-digested pathogen would be randomly mounted on the DC surface; in this case, all HIV antigens would be displayed exactly as it would be encountered by the B-cells and their antibodies in the blood and lymph. Concerning the model, this would mean all antigens would be essentially linked in

specific patterns representative of the viral surface and distributed in nodes across the DC surface (**Fig. AIII.1j**). These patterned nodes will be modeled as arrangements of 18 gp41 and 3 gp120 each[105,106]. The details concerning this set-up are further discussed in **AIII.3**. It should be noted that this primarily only affects the way parameters are inputted into the model; the model still remains fully capable of running simulations on distributed free antigen.

Finally, we decided to approach the model using a truer application of KMC. We hypothesized from the outset that while the affinity-dependent nature of the model would be essential in fully probing the effects of BCR heteroligation (due to the enhancement of BCR oligomerization by linked antigen valency), this phenomenon would likely not be a substantial enough increase in favorability to overcome the noise of the unbiased coin tosses used to determine events that Tsourkas et al. noted as problematic in differentiating between the upper end of apparent BCR-Ag affinities. To help refine event tracking, we implemented the Gillespie approach to tracking transition probabilities across the model[107,108]. It should be noted, however, that we kept the coarse-graining approach used by Tsourkas et al. to define the time step. Based on empirical observation, M surface molecules involved in an immunological synapse are capable of M independent, random diffusive or reactive events over the course of 1 μs[102]. Therefore, we use a time step of 1 μs to loop across M free and complexed molecules for the experimental duration of 100 s, only updating the transition probabilities at the beginning of each time step. This coarse-graining was kept both so as to take advantage of the simplistic parameter mapping developed by Tsourkas et al., as well as to reduce computational time.

### AIII.3: Model Parameters

**AIII.3.1: Basic Model Parameters Table.** The following is a table compiled from Tsourkas et al.[101] and represents the core parameters of the model, with key exceptions noted below:

| Experimental parameter | Measured or estimated value | Simulation parameter | Mapped value |
|---|---|---|---|
| $k_{on}$ BCR-antigen | $10^6$ $M^{-1}s^{-1}$ | $P_{onBA1}$, $P_{onBA2}$ | 0.1 |
| $K_{off}$ BCR-antigen | 1-$10^{-3}$ $s^{-1}$ | $P_{offBA1}$, $P_{offBA2}$ | $10^{-3}$-$10^{-6}$* |
| BCR molecules/cell | $10^5$ | $B_0$ | 400 |
| Antigen concentration | ~100 molecules/μm | $A_0$ ($A1_0$+$A2_0$) | ~200** |
| $k_{on}$ Igαβ-Lyn | ~$10^7$ $M^{-1}s^{-1}$ | $P_{onLyn}$ | 1.0 |
| $k_{off}$ Igαβ-Lyn | ~10 $s^{-1}$ | $P_{offLyn}$ | 0.01 |
| $k_{on}$ Igαβ-Syk | ~$10^7$ $M^{-1}s^{-1}$ | $P_{onSyk}$ | 1.0 |
| $k_{off}$ Igαβ-Syk | ~10 $s^{-1}$ | $P_{offLyn}$ | 0.01 |
| Lyn molecules/cell | 2x$10^4$ | $L_0$ | 100 |
| Syk molecules/cell | 4x$10^5$ | $S_0$ | 400 |
| $k_{phosIgaB}$ | ~100 $s^{-1}$ | $P_{phosIgα/β}$ | 0.1 |
| $k_{phosSyk}$ | ~100 $s^{-1}$ | $P_{phosSyk}$ | 0.1 |
| $D_{freemolecules}$ | 0.1 $μm^2/s$ | $P_{diffF}$ | 1.0 |
| $D_{complexes}$ | ~0.01 $μm^2/s$ | $P_{diffC}$ | 0.1*** |

*For the nodal HIV antigen case, this is considered *effective* kinetic off rate and is increased by a factor of 10 for the gp41 antigen. This is derived from Tsourkas et al.'s BCR-antigen model, which views the bond as a simple spring:

$$p_{\mathrm{off(i)}}(z) = p_{\mathrm{off(i)}}^{\min} \exp\left(\frac{(\kappa_{\mathrm{i}} - \kappa_{\mathrm{i}}')(z - z_{\mathrm{eq(i)}})^2}{2k_{\mathrm{B}}T}\right)$$

where $p_{off}$ is the probability for a dissociative event, κ is the bond "stiffness", and z is the intramembrane distance. Assuming shedding of gp120 through the exosome navigation line with empirical observations[105,106], we observe gp41 being "shielded" by the close proximity to unshed gp120, increasing the intramembrane distance and thus increasing stress on the bond (see below).

**For the nodal HIV antigen case, $A_0$ = 210, $A1_0$ (gp41) = 180, $A2_0$ (gp120)= 30. These numbers are based on HIV virion density observations on mature dendritic cells[102], coupled with a desire to normalize the results as close as possible to the previous $A_0$ = 200 standard used by Tsourkas et al.[101] ~10 virions per 1.5x1.5μm was deemed reasonably accurate, and a section of the surface was selected based on the curvature guidelines of the original Tsourkas et al. paper[76]. Within the 30x30nm surface, a total of 21

gp41/120 complexes would normally exist[79,80]; given gp120's shedding response to environmental factors such as pH, we assume a 6:1 free gp41:gp120 ratio, additionally assuming that the existing gp120 are evenly distributed relative to the patterned distributions empirically observed of sectioned membranes.

***For the nodal HIV antigen case, this is assumed to be ~0.01 due to the difference between the diffusion of a two-molecule complex and a single molecule multiplex with a nanoparticle (HIV diameter = ~120 nm, vs. a 10 nm protein); $\Delta D \sim 1/\Delta r$.

**AIII.3.2: Parameter mapping**. A detailed discussion of the Tsourkas et al. parameter mapping can be found elsewhere[76]. As no additional mapping calculations are done in this paper, a brief explanation is provided. Three forms of mapping are required: mapping kinetic rates to probabilities, mapping cell concentrations to model populations, and mapping the diffusive terms to real time. For the first, a set of maximum event probabilities $P_{max}$ are arbitrarily chosen and used to obtain the relationship between $P_{max}$ and $K_A$ based on the number density definition of $K_A$ for a pseudo-chemical reaction. This is then adjusted from 2D to 3D simply by assuming the average protein exclusion radius to be 10 nm. For the second, cell concentrations are adjusted for the 1.5x1.5x0.01μm lattice using a B-cell radius of 7 nm and assuming the cell to be spherical. Finally, all probabilities are normalized to the free diffusion term, which is set to 1.0 based on empirical observations of relative diffusion across cell surfaces within the time step of 1 μs.

**AIII.3.3: Affinity-variable BCR oligomerization time μ.** A key finding by Tsourkas et al.[75] was that kinetic proofreading was best represented by including the well-known phenomenon of BCR microclustering in the model. Surface protein microclustering in the immunological synapse is well-known means by which naïve B- and T-cells are selected to clonally expand, and there is ample evidence tying this event molecularly to downstream phosphorylation event enhancement. Tsourkas et al. found that on the

timescale of B-cell/DC interactions, merely modeling dimerization was sufficiently accurate to model the more complex event of BCR microclustering of larger valencies. While this assumption remains a good candidate for model improvement, we chose to keep the approximation due to the evidence on hand of its applicability and the simplicity it brought to a complicated molecular event. As described in the main body of the text, μ was taken to be the amount of time required for 50% of the BCRs to become dimerized. The dimerization event is assumed to occur whenever two conformationally active BCRs are adjacent to each other in the lattice. μ was calculated for each $K_A$ of each BCR as an average of 10 simulation trials, the results of which are tabulated here:

| BCR | $K_A$ ($M^{-1}$) | μ (s) |
|---|---|---|
| Generic monospecific BCR | $10^5$ | 15.5 |
| | $10^6$ | 7.3 |
| | $10^7$ | 5.8 |
| | $10^8$ | 4.4 |
| | $10^9$ | 3.7 |
| Anti-gp41 BCR, free antigen case | $10^5$ | 17.8 |
| | $10^9$ | 4.5 |
| Anti-gp120 BCR, free antigen case | $10^5$ | 39.6 |
| | $10^9$ | 23.5 |
| Polyreactive BCR, free antigen case | $10^5/10^7$ | 10.1 |
| Anti-gp41 BCR, linked antigen case | $10^5$ | 13.5 |
| | $10^9$ | 5.2 |
| Anti-gp120 BCR, linked antigen case | $10^5$ | 12.7 |
| | $10^9$ | 15.8 |
| Polyreactive BCR, linked antigen case | $10^5/10^7$ | 3.4 |

**AIII.4: Results and Discussion**

To ensure that the modifications to the model did not in some way cause it to behave differently than the Tsourkas et al. model under similar circumstances, we first ran the model using parameters reflective of a normal B-cell/DC immunological interaction. 200 non-linked antigens (designated A1) were distributed randomly across the simulated DC membrane surface, and allowed to interact with 400

BCRs over 100 s. The downstream effects on 100 Lyn and 400 Syk molecules were also observed. BCRs of varied anti-antigen $K_A$ were probed across a physiologically relevant interval ($K_A$=$10^5$-$10^9$ $M^{-1}$), and data was collected over 100 independent trials concerning final number of BCR-Ag complexes (to assess general BCR-Ag activity) as well as the time-evolution of phosphorylated BCR and Syk populations (pBCR and pSyk, respectively). Resulting data matched well with the trends reported by Tsourkas et al.[101] BCR-Ag complex number increased regularly with $K_A$, as would be expected (**Fig. AIII.2**). Pseudo-exponential growth was seen in pBCR (**Fig. AIII.3a**) and pSyk (**Fig. AIII.3b**) populations, with an expected time delay between the two, at rates that increased with $K_A$. Overall, we can conclude that our model behaves normally relative to its foundation despite the fairly major modifications of heteroligation capacity incorporation and KMC transition probability application, which allows us to proceed to the more complicated circumstances of interest.

Though we hypothesized the importance of intact HIV presentation to naïve B-cells by DCs during the T-cell independent activation interaction, it was important to first ascertain whether or not the capacity for increased heteroligation alone was enough to confer a crucial advantage to our bispecific BCR of interest. Specifically, we were interested in a BCR representative of the antibody populations reported by Mouquet et al.[100], where a BCR with $K_A = 10^5$ against gp41 (designated A1) and $K_A = 10^7$ against gp120 (designated A2) would be sufficient to compete in B-cell activation with a significantly stronger monospecific antigen. Looking at a similar range of $K_A$ as described previously, we found that in the free-antigen case both monospecific antigens against the rarer gp120 as well as the polyreactive BCR (designated αPR) were significantly disadvantaged in BCR-Ag complex formation (**Fig. AIII.4a**). Thus this particular circumstance did not produce results reflective of those observed in HIV controllers.

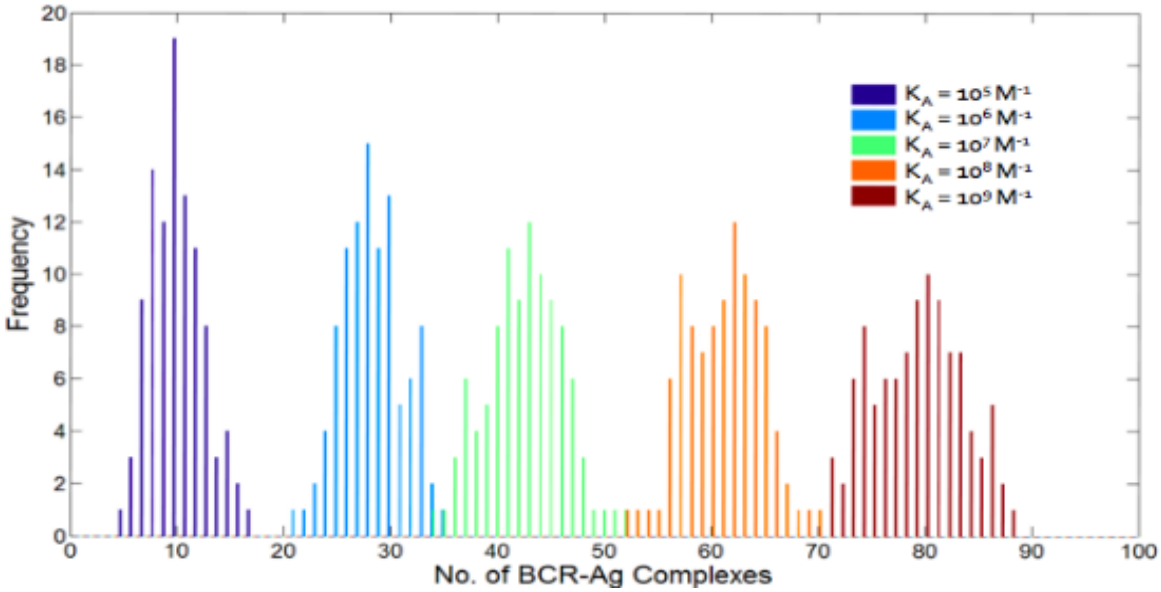


**Figure AIII.2: Modeled interactions between naïve B-cell BCRs and free dendritic cell presented antigen.** Terminal BCR-Ag complex histograms are displayed. Each A1 = 200, T=100s run was repeated 100 times. (**B,C**) data given as mean +/- s.d.

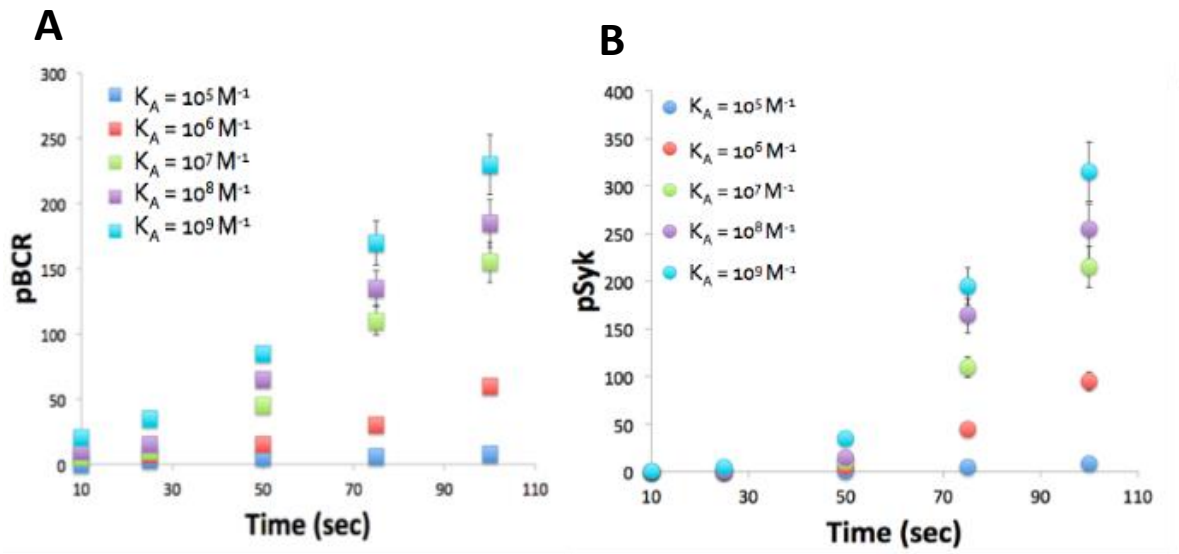


**Figure AIII.3: Modeled interactions between naïve B-cell BCRs and free dendritic cell presented antigen.** Terminal pBCR/pSyk time-evolutions (**A,B** ) are displayed. Each A1 = 200, T=100s run was repeated 100 times. Data given as mean +/- s.d.

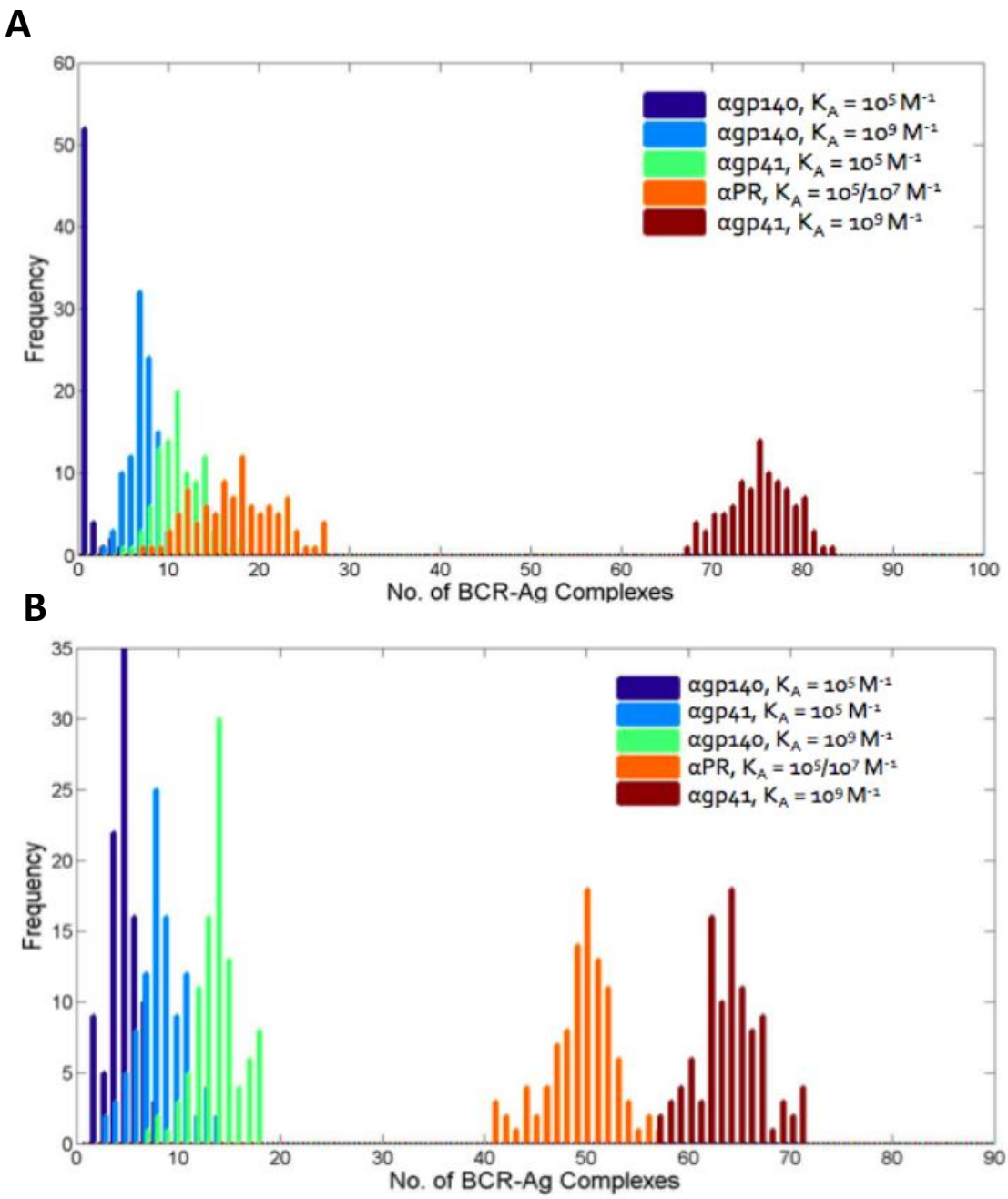


**Figure AIII.4: Modeled interactions between naïve B-cell BCRs and HIV antigens presented on intact capsid predicts polyreactive antibody (αPR) competitive advantage via enhanced BCR-complexing.** HIV antigen presentation to naïve B-cells using dispersed (**A**) and intact-virion linked (**B**) simulated antigen is shown. Terminal BCR-Ag complex histogram distributions are given for dispersed (**A**) and linked (**B**) antigen. As g p140 is equivalent to gp120 immunologically[106], gp140 is used here for comparison to data from Mouquet et al.[100]

We finally assessed the effect nodal assembly of HIV antigens had on BCR activity. Unlike the free antigen case, we noted marked enhancement of BCR-Ag complex formation that increased apparent $K_A$ of the polyreactive BCR by several orders of magnitude, similar to Mouquet et al.'s findings[100] (**Fig. AIII.4b**). Moreover, initial determination of an enhanced μ ($\mu_{PR}$ = 3.4 s) predicted a BCR microcomplex-enhanced increase in downstream phosphorylation reflected by the polyreactive BCR's pBCR (**Fig. AIII.5a**) and pSyk (**Fig. AIII.5b**) populations eventually overtaking those of a much higher affinity BCR monospecific for gp41, suggesting that the true advantage of heteroligation is derived from enhanced BCR oligomerization.

**AIII.4: Conclusion**

Herein, we successfully demonstrated the enhancement of an existing model for BCR antigen screening via affinity-dependent kinetic proofreading. Collected data compared to the Tsourkas et al. model not only demonstrated preserved trends, but also better separation between data sets at the higher end of the affinity spectrum[101]. This could be due to the more precise pseudo-KMC application, though a larger trial number would be required to fully support such a conclusion. More importantly, we confirmed our hypothesis that the unique presentation of the HIV virion via mature DCs could be used to explain the development of polyreactive antibodies, noting the apparent importance of an immunoactive surface that can enhance BCR oligomerization and thus decrease the threshold BCR activation time μ. This insight in particular, combined with appropriate model parameter input and mapping, not only helps clarify a unique component of the HIV immune response, but additionally promises the ability to predict and guide engineered vaccine approaches capable of triggering the same phenomenon.

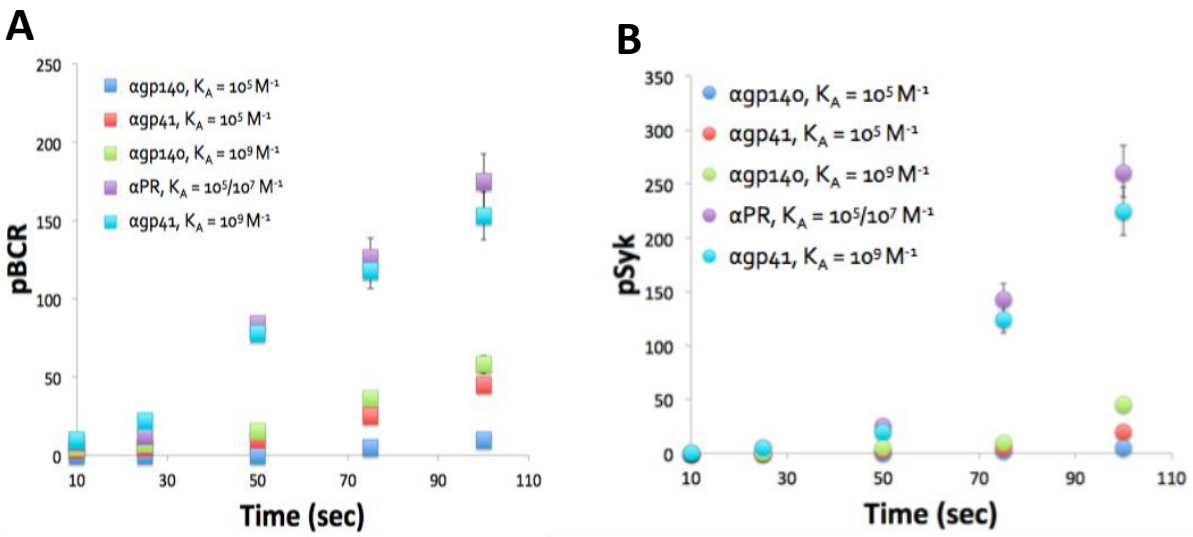


**Figure AIII.5: Modeled interactions between naïve B-cell BCRs and HIV antigens presented on intact capsid predicts polyreactive antibody (αPR) competitive advantage dependent on enhanced pBCR and pSyk time evolution.** HIV antigen presentation to naïve B-cells using only intact-virion linked simulated antigen is shown. Data given as mean +/- s.d.

## REFERENCES


1. Murphy, Kenneth PT, Walport. M. *Janeway's Immunobiology*. 8th ed. Taylor & Francis; 2011.

2. Bevan MJ. Understand memory, design better vaccines. *Nat Immunol*. 2011;12(6):463–465. doi:10.1038/ni.2041.

3. Beverley PCL. Immunology of vaccination. *Br Med Bull*. 2002;62:15–28. Available at: http://www.ncbi.nlm.nih.gov/pubmed/12176847.

4. Schijns VEJC, Degen WGJ. Vaccine immunopotentiators of the future. *Clin Pharmacol Ther*. 2007;82(6):750–5. doi:10.1038/sj.clpt.6100394.

5. Poland G a, Jacobson RM, Ovsyannikova IG. Trends affecting the future of vaccine development and delivery: the role of demographics, regulatory science, the anti-vaccine movement, and vaccinomics. *Vaccine*. 2009;27(25-26):3240–4. doi:10.1016/j.vaccine.2009.01.069.

6. Petrovsky N, Aguilar JC. Vaccine adjuvants : Current state and future trends. *Immunol Cell Biol*. 2004:488–496. doi:10.1111/j.1440-1711.2004.01272.x.

7. Calabro S, Tortoli M, Baudner BC, et al. Vaccine adjuvants alum and MF59 induce rapid recruitment of neutrophils and monocytes that participate in antigen transport to draining lymph nodes. *Vaccine*. 2011;29(9):1812–23. doi:10.1016/j.vaccine.2010.12.090.

8. O'Hagan DT, Valiante NM. Recent advances in the discovery and delivery of vaccine adjuvants. *Nat Rev Drug Discov*. 2003;2(9):727–35. doi:10.1038/nrd1176.

9. Huang C-J, Lowe AJ, Batt C a. Recombinant immunotherapeutics: current state and perspectives regarding the feasibility and market. *Appl Microbiol Biotechnol*. 2010;87(2):401–10. doi:10.1007/s00253-010-2590-7.

10. Ellis TN, Kuehn MJ. Virulence and immunomodulatory roles of bacterial outer membrane vesicles. *Microbiol Mol Biol Rev*. 2010;74(1):81–94. doi:10.1128/MMBR.00031-09.

11. Blasius AL, Beutler B. Intracellular toll-like receptors. *Immunity*. 2010;32(3):305–15. doi:10.1016/j.immuni.2010.03.012.

12. Kissner TL, Ruthel G, Alam S, Ulrich RG, Fernandez S, Saikh KU. Activation of MyD88 signaling upon staphylococcal enterotoxin binding to MHC class II molecules. *PLoS One*. 2011;6(1):e15985. doi:10.1371/journal.pone.0015985.

13. Holst J, Martin D, Arnold R, et al. Properties and clinical performance of vaccines containing outer membrane vesicles from Neisseria meningitidis. *Vaccine*. 2009;27 Suppl 2:B3–12. doi:10.1016/j.vaccine.2009.04.071.

14. Feldman MF, Wacker M, Hernandez M, et al. Engineering N-linked protein glycosylation with diverse O antigen lipopolysaccharide structures in Escherichia coli. *Proc Natl Acad Sci U S A*. 2005;102(8):3016–21. doi:10.1073/pnas.0500044102.

15. O'Hagan DT. MF59 is a safe and potent vaccine adjuvant that enhances protection against influenza virus infection. *Expert Rev Vaccines*. 2007;6(5):699–710. doi:10.1586/14760584.6.5.699.

16. Steeghs L, Tommassen J, Leusen JHW, van de Winkel JGJ, van der Ley P. Teasing apart structural determinants of “toxicity” and “adjuvanticity”: implications for meningococcal vaccine development. *J Endotoxin Res*. 2004;10(2):113–9. doi:10.1179/096805104225004059.

17. Gupta R. Aluminum compounds as vaccine adjuvants. *Adv Drug Deliv Rev*. 1998;32(3):155–172. Available at: http://www.ncbi.nlm.nih.gov/pubmed/10837642.

18. Girard MP, Reed ZH, Friede M, Kieny MP. A review of human vaccine research and development: malaria. *Vaccine*. 2007;25(9):1567–80. doi:10.1016/j.vaccine.2006.09.074.

19. Baldwin SL, Bertholet S, Reese V a, Ching LK, Reed SG, Coler RN. The importance of adjuvant formulation in the development of a tuberculosis vaccine. *J Immunol*. 2012;188(5):2189–97. doi:10.4049/jimmunol.1102696.

20. Niwa T, Takeuchi H, Hino T, Nohara M, Kawashima Y. Biodegradable submicron carriers for peptide drugs : Preparation of DL-lactide / glycolide copolymer ( PLGA ) nanospheres with nafarelin acetate by a novel emulsion-phase separation method in an oil system. *Construction*. 1995;121:45–54.

21. Singh M, Chakrapani A, O’Hagan D. Nanoparticles and microparticles as vaccine-delivery systems. *Expert Rev Vaccines*. 2007;6(5):797–808. doi:10.1586/14760584.6.5.797.

22. Swartz M a, Hirosue S, Hubbell J a. Engineering approaches to immunotherapy. *Sci Transl Med*. 2012;4(148):148rv9. doi:10.1126/scitranslmed.3003763.

23. Barr IG, Mitchell GF. ISCOMs (immunostimulating complexes): the first decade. *Immunol Cell Biol*. 1996;74(1):8–25. doi:10.1038/icb.1996.2.

24. Bryan JT. Developing an HPV vaccine to prevent cervical cancer and genital warts. *Vaccine*. 2007;25(16):3001–6. doi:10.1016/j.vaccine.2007.01.013.

25. Azad N, Rojanasakul Y. Vaccine delivery--current trends and future. *Curr Drug Deliv*. 2006;3(2):137–46. Available at: http://www.ncbi.nlm.nih.gov/pubmed/16611000.

26. Kulp A, Kuehn MJ. Biological functions and biogenesis of secreted bacterial outer membrane vesicles. *Annu Rev Microbiol*. 2010;64:163–84. doi:10.1146/annurev.micro.091208.073413.

27. Kuehn MJ, Kesty NC. Bacterial outer membrane vesicles and the host-pathogen interaction. *Genes Dev*. 2005;19(22):2645–55. doi:10.1101/gad.1299905.

28. McBroom AJ, Kuehn MJ. Release of outer membrane vesicles by Gram-negative bacteria is a novel envelope stress response. *Mol Microbiol*. 2007;63(2):545–58. doi:10.1111/j.1365-2958.2006.05522.x.

29. Sander LE, Davis MJ, Boekschoten M V, et al. Detection of prokaryotic mRNA signifies microbial viability and promotes immunity. *Nature*. 2011:0–7. doi:10.1038/nature10072.

30. Granoff DM. Review of meningococcal group B vaccines. *Clin Infect Dis*. 2010;50 Suppl 2(Suppl 2):S54–65. doi:10.1086/648966.

31. Sandbu S, Feiring B, Oster P, et al. Immunogenicity and safety of a combination of two serogroup B meningococcal outer membrane vesicle vaccines. *Clin Vaccine Immunol*. 2007;14(9):1062–9. doi:10.1128/CVI.00094-07.

32. Arigita C. Stability of mono- and trivalent meningococcal outer membrane vesicle vaccines. *Vaccine*. 2004;22(5-6):630–643. doi:10.1016/j.vaccine.2003.08.027.

33. Zollinger WD, Donets M a, Schmiel DH, et al. Design and evaluation in mice of a broadly protective meningococcal group B native outer membrane vesicle vaccine. *Vaccine*. 2010;28(31):5057–5067. doi:10.1016/j.vaccine.2010.05.006.

34. Kim J-Y, Doody AM, Chen DJ, et al. Engineered bacterial outer membrane vesicles with enhanced functionality. *J Mol Biol*. 2008;380(1):51–66. doi:10.1016/j.jmb.2008.03.076.

35. Chen DJ, Osterrieder N, Metzger SM, et al. Delivery of foreign antigens by engineered outer membrane vesicle vaccines. *Proc Natl Acad Sci U S A*. 2010;107(7):3099–104. doi:10.1073/pnas.0805532107.

36. Muralinath M, Kuehn MJ, Roland KL, Curtiss R. Immunization with Salmonella enterica serovar Typhimurium-derived outer membrane vesicles delivering the pneumococcal protein PspA confers protection against challenge with Streptococcus pneumoniae. *Infect Immun*. 2011;79(2):887–94. doi:10.1128/IAI.00950-10.

37. Cvd S, Galen JE, Zhao L, et al. Adaptation of the Endogenous Salmonella enterica Serovar Typhi clyA-Encoded Hemolysin for Antigen Export Enhances the Immunogenicity of Anthrax Protective Antigen Domain 4 Expressed by the Attenuated Live-Vector Vaccine. *Society*. 2004;72(12):7096–7106. doi:10.1128/IAI.72.12.7096.

38. Kouokam JC, Wai SN. Outer Membrane Vesicle-Mediated Export of a Pore-Forming Cytotoxin From Escherichia Coli. *Toxin Rev*. 2006;25(1):31–46. doi:10.1080/15569540500320888.

39. Feiring B, Fuglesang J, Oster P, et al. Persisting immune responses indicating long-term protection after booster dose with meningococcal group B outer membrane vesicle vaccine. *Clin Vaccine Immunol*. 2006;13(7):790–6. doi:10.1128/CVI.00047-06.

40. Holst J, Oster P, Arnold R, Tatley M. Vaccines against meningococcal serogroup B disease containing outer membrane vesicles (OMV). *Hum Vaccin Immunother*. 2013;9(June):1241–1253. Available at: http://www.landesbioscience.com/journals/vaccines/2012HV0393R.pdf. Accessed March 19, 2014.

41. Tamargo B, Márquez Y, Ramírez W, Cedré B, Fresno M, Sierra G. New proteoliposome vaccine formulation from N. meningitidis serogroup B, without aluminum hydroxide, retains its antimeningococcal protectogenic potential as well as Th-1 adjuvant capacity. *BMC Immunol*. 2013;14 Suppl 1(Suppl 1):S12. doi:10.1186/1471-2172-14-S1-S12.

42. Williams JN, Weynants V, Poolman JT, Heckels JE, Christodoulides M. Immuno-proteomic analysis of human immune responses to experimental Neisseria meningitidis outer membrane vesicle vaccines identifies potential cross-reactive antigens. *Vaccine*. 2014;32(11):1280–6. doi:10.1016/j.vaccine.2013.12.070.

43. Vidakovics ML a P, Jendholm J, Mörgelin M, et al. B cell activation by outer membrane vesicles--a novel virulence mechanism. *PLoS Pathog*. 2010;6(1):e1000724. doi:10.1371/journal.ppat.1000724.

44. Noss E, Pai R, Sellati T, Radolf J. Toll-like receptor 2-dependent inhibition of macrophage class II MHC expression and antigen processing by 19-kDa lipoprotein of Mycobacterium tuberculosis. *J*. 2001;167(2):910–8. Available at: http://www.ncbi.nlm.nih.gov/pubmed/11441098. Accessed April 26, 2012.

45. Kim OY, Hong BS, Park K-S, et al. Immunization with Escherichia coli outer membrane vesicles protects bacteria-induced lethality via Th1 and Th17 cell responses. *J Immunol*. 2013;190(8):4092–102. doi:10.4049/jimmunol.1200742.

46. Fox CB, Baldwin SL, Vedvick TS, Angov E, Reed SG. Effects on immunogenicity by formulations of emulsion-based adjuvants for malaria vaccines. *Clin Vaccine Immunol*. 2012;19(10):1633–40. doi:10.1128/CVI.00235-12.

47. Ellis TN, Leiman S a, Kuehn MJ. Naturally produced outer membrane vesicles from Pseudomonas aeruginosa elicit a potent innate immune response via combined sensing of both lipopolysaccharide and protein components. *Infect Immun*. 2010;78(9):3822–31. doi:10.1128/IAI.00433-10.

48. Trebichavsky I, Splichal I, Rada V, Splichalova A. Modulation of natural immunity in the gut by Escherichia coli strain Nissle 1917. *Nutr Rev*. 2010;68(8):459–64. doi:10.1111/j.1753-4887.2010.00305.x.

49. Arribas B, Rodríguez-Cabezas ME, Camuesco D, et al. A probiotic strain of Escherichia coli, Nissle 1917, given orally exerts local and systemic anti-inflammatory effects in lipopolysaccharide-induced sepsis in mice. *Br J Pharmacol*. 2009;157(6):1024–33. doi:10.1111/j.1476-5381.2009.00270.x.

50. Bickert T, Trujillo-Vargas CM, Duechs M, et al. Probiotic Escherichia coli Nissle 1917 suppresses allergen-induced Th2 responses in the airways. *Int Arch Allergy Immunol*. 2009;149(3):219–30. doi:10.1159/000199717.

51. Grabig A, Paclik D, Guzy C, et al. Escherichia coli strain Nissle 1917 ameliorates experimental colitis via toll-like receptor 2- and toll-like receptor 4-dependent pathways. *Infect Immun*. 2006;74(7):4075–82. doi:10.1128/IAI.01449-05.

52. Schultz M. Clinical use of E. coli Nissle 1917 in inflammatory bowel disease. *Inflamm Bowel Dis*. 2008;14(7):1012–8. doi:10.1002/ibd.20377.

53. Ukena SN, Singh A, Dringenberg U, et al. Probiotic Escherichia coli Nissle 1917 inhibits leaky gut by enhancing mucosal integrity. *PLoS One*. 2007;2(12):e1308. doi:10.1371/journal.pone.0001308.

54. Do VT, Baird BG, Kockler DR. Probiotics for maintaining remission of ulcerative colitis in adults. *Ann Pharmacother*. 2010;44(3):565–71. doi:10.1345/aph.1M498.

55. Sturm A, Rilling K, Baumgart DC, et al. Escherichia coli Nissle 1917 distinctively modulates T-cell cycling and expansion via toll-like receptor 2 signaling. *Infect Immun*. 2005;73(3):1452. doi:10.1128/IAI.73.3.1452.

56. Hafez M, Hayes K, Goldrick M, Grencis RK, Roberts IS. The K5 capsule of Escherichia coli strain Nissle 1917 is important in stimulating expression of Toll-like receptor 5, CD14, MyD88, and TRIF together with the induction of interleukin-8 expression via the mitogen-activated protein kinase pathway in epithel. *Infect Immun*. 2010;78(5):2153–62. doi:10.1128/IAI.01406-09.

57. Guzy C, Paclik D, Schirbel A, Sonnenborn U, Wiedenmann B, Sturm A. The probiotic Escherichia coli strain Nissle 1917 induces gammadelta T cell apoptosis via caspase- and FasL-dependent pathways. *Int Immunol*. 2008;20(7):829–40. doi:10.1093/intimm/dxn041.

58. Zídek Z, Kmonícková E, Kostecká P, Tlaskalová-Hogenová H. Decisive role of lipopolysaccharide in activating nitric oxide and cytokine production by the probiotic Escherichia coli strain Nissle 1917. *Folia Microbiol (Praha)*. 2010;55(2):181–9. doi:10.1007/s12223-010-0027-4.

59. Vejborg RM, Friis C, Hancock V, Schembri M a, Klemm P. A virulent parent with probiotic progeny: comparative genomics of Escherichia coli strains CFT073, Nissle 1917 and ABU 83972. *Mol Genet Genomics*. 2010;283(5):469–84. doi:10.1007/s00438-010-0532-9.

60. Hancock V, Vejborg RM, Klemm P. Functional genomics of probiotic Escherichia coli Nissle 1917 and 83972, and UPEC strain CFT073: comparison of transcriptomes, growth and biofilm formation. *Mol Genet Genomics*. 2010;284(6):437–54. doi:10.1007/s00438-010-0578-8.

61. Kruis W, Fric P, Pokrotnieks J, et al. Maintaining remission of ulcerative colitis with the probiotic Escherichia coli Nissle 1917 is as effective as with standard mesalazine. *Gut*. 2004;53(11):1617–23. doi:10.1136/gut.2003.037747.

62. Seegers JFML. Lactobacilli as live vaccine delivery vectors: progress and prospects. *Trends Biotechnol*. 2002;20(12):508–15. Available at: http://www.ncbi.nlm.nih.gov/pubmed/12443872.

63. Baba T, Ara T, Hasegawa M, et al. Construction of Escherichia coli K-12 in-frame, single-gene knockout mutants: the Keio collection. *Mol Syst Biol*. 2006;2:2006.0008. doi:10.1038/msb4100050.

64. Miller JH. *Experiments in Molecular Genetics*. U.S.: Cold Spring Harbor Laboratory Press; 1972.

65. Mbulaiteye SM, Gold BD, Pfeiffer RM, et al. H. pylori-infection and antibody immune response in a rural Tanzanian population. *Infect Agent Cancer*. 2006;1:3. doi:10.1186/1750-9378-1-3.

66. Klier J, May A, Fuchs S, et al. Immunostimulation of bronchoalveolar lavage cells from recurrent airway obstruction-affected horses by different CpG-classes bound to gelatin nanoparticles. *Vet Immunol Immunopathol*. 2011:1–9. doi:10.1016/j.vetimm.2011.07.009.

67. Weeratna RD, McCluskie MJ, Xu Y, Davis HL. CpG DNA induces stronger immune responses with less toxicity than other adjuvants. *Vaccine*. 2000;18(17):1755–62. Available at: http://www.ncbi.nlm.nih.gov/pubmed/10699323.

68. Mosmann TR, Coffman RL. TH1 and TH2 cells: different patterns of lymphokine secretion lead to different functional properties. *Annu Rev Immunol*. 1989;7:145–73. doi:10.1146/annurev.iy.07.040189.001045.

69. Kim S-H, Kim K-S, Lee S-R, et al. Structural modifications of outer membrane vesicles to refine them as vaccine delivery vehicles. *Biochim Biophys Acta*. 2009;1788(10):2150–9. doi:10.1016/j.bbamem.2009.08.001.

70. Hsieh C, Macatonia S, Tripp C, Wolf S, O'Garra a, Murphy K. Development of TH1 CD4+ T cells through IL-12 produced by Listeria-induced macrophages. *Science (80- )*. 1993;260(5107):547–549. doi:10.1126/science.8097338.

71. Zheng Y, Manzotti CN, Liu M, Burke F, Mead KI, Sansom DM. CD86 and CD80 differentially modulate the suppressive function of human regulatory T cells. *J Immunol*. 2004;172(5):2778–84. Available at: http://www.ncbi.nlm.nih.gov/pubmed/14978077.

72. Vos Q, Lees a, Wu ZQ, Snapper CM, Mond JJ. B-cell activation by T-cell-independent type 2 antigens as an integral part of the humoral immune response to pathogenic microorganisms. *Immunol Rev*. 2000;176:154–70. Available at: http://www.ncbi.nlm.nih.gov/pubmed/11043775.

73. Strauch E, Georgiou G. A bacterial two hybrid system based on the twin arginine transporter pathway of E. coli. *Protein Sci*. 2007:1001–1008. doi:10.1110/ps.062687207.Bork.

74. Yeo Y, Park K. Control of encapsulation efficiency and initial burst in polymeric microparticle systems. *Arch Pharm Res*. 2004;27(1):1–12. Available at: http://www.ncbi.nlm.nih.gov/pubmed/14969330.

75. Sales-Junior P a, Guzman F, Vargas MI, et al. Use of biodegradable PLGA microspheres as a slow release delivery system for the Boophilus microplus synthetic vaccine SBm7462. *Vet Immunol Immunopathol*. 2005;107(3-4):281–90. doi:10.1016/j.vetimm.2005.05.004.

76. Park JH, Ye M, Park K. Biodegradable polymers for microencapsulation of drugs. *Molecules*. 2005;10(1):146–61. Available at: http://www.ncbi.nlm.nih.gov/pubmed/18007283.

77. Wilson-Welder JH, Torres MP, Kipper MJ, Mallapragada SK, Wannemuehler MJ, Narasimhan B. Vaccine adjuvants: current challenges and future approaches. *J Pharm Sci*. 2009;98(4):1278–1316. doi:10.1002/jps.

78. Nguyen HH, Zemlin M, Ivanov II, et al. Heterosubtypic immunity to influenza A virus infection requires a properly diversified antibody repertoire. *J Virol*. 2007;81(17):9331–8. doi:10.1128/JVI.00751-07.

79. Grund S, Adams O, Wählisch S, Schweiger B. Comparison of hemagglutination inhibition assay, an ELISA-based micro-neutralization assay and colorimetric microneutralization assay to detect antibody responses to vaccination against influenza A H1N1 2009 virus. *J Virol Methods*. 2011;171(2):369–73. doi:10.1016/j.jviromet.2010.11.024.

80. Ko B, Kawano K, Murray J, Disis M. Clinical studies of vaccines targeting breast cancer. *Clin cancer …*. 2003;9:3222–3234. Available at: http://clincancerres.aacrjournals.org/content/9/9/3222.short. Accessed November 22, 2012.

81. Zhang W-G, Liu S-H, Cao X-M, et al. A phase-I clinical trial of active immunotherapy for acute leukemia using inactivated autologous leukemia cells mixed with IL-2, GM-CSF, and IL-6. *Leuk Res*. 2005;29(1):3–9. doi:10.1016/j.leukres.2004.04.015.

82. Skolnick HS, Conover-Walker MK, Koerner CB, Sampson H a, Burks W, Wood R a. The natural history of peanut allergy. *J Allergy Clin Immunol*. 2001;107(2):367–74. doi:10.1067/mai.2001.112129.

83. Oppenheimer J, Nelson H. Treatment of peanut allergy with rush immunotherapy. *J allergy …*. 1992:256–262. Available at: http://www.sciencedirect.com/science/article/pii/009167499290080L. Accessed July 31, 2013.

84. Burks a W. Peanut allergy. *Lancet*. 2008;371(9623):1538–46. doi:10.1016/S0140-6736(08)60659-5.

85. Miller DS, Brown MP, Howley PM, Hayball JD. Current and emerging immunotherapeutic approaches to treat and prevent peanut allergy. *Expert Rev Vaccines*. 2012;11(12):1471–81. doi:10.1586/erv.12.119.

86. Smith K a. The quantal theory of immunity. *Cell Res*. 2006;16(1):11–9. doi:10.1038/sj.cr.7310003.

87. Okada H, Kuhn C, Feillet H, Bach J-F. The “hygiene hypothesis” for autoimmune and allergic diseases: an update. *Clin Exp Immunol*. 2010;160(1):1–9. doi:10.1111/j.1365-2249.2010.04139.x.

88. Mcdermott RAÃ, Porterfield HSÃ, Ã REM, et al. Contribution of Ara h 2 to peanut-specific , immunoglobulin E-mediated , cell activation Clinical and Experimental Allergy. *Clin Exp Allergy*. 2007:752–763.

89. Valderrama-Rincon JD, Fisher AC, Merritt JH, et al. An engineered eukaryotic protein glycosylation pathway in Escherichia coli. *Nat Chem Biol*. 2012;8(5):434–436. doi:10.1038/nchembio.921.

90. Kolling GL, Matthews KR. Export of virulence genes and Shiga toxin by membrane vesicles of Escherichia coli O157:H7. *Appl Environ Microbiol*. 1999;65(5):1843–8. Available at: http://www.pubmedcentral.nih.gov/articlerender.fcgi?artid=91264&tool=pmcentrez&rendertype=abstract.

91. Bernadac a, Gavioli M, Lazzaroni JC, Raina S, Lloubès R. Escherichia coli tol-pal mutants form outer membrane vesicles. *J Bacteriol*. 1998;180(18):4872–8. Available at: http://www.pubmedcentral.nih.gov/articlerender.fcgi?artid=107512&tool=pmcentrez&rendertype=abstract.

92. Cormack BP, Valdivia RH, Falkow S. FACS-optimized mutants of the green fluorescent protein (GFP). *Gene*. 1996;173(1 Spec No):33–8. Available at: http://www.ncbi.nlm.nih.gov/pubmed/8707053.

93. Carlo DJ, Jackson JJ. A New and improved Microassay to Determine in Lipopolysaccharide of Gram-Negative Bacteria. 1978;601:595–601.

94. Robert Cottey, Cheryl A. Rowe BSB. Influenza Virus. *Curr Protoc Immunol*. 2001:1–32. doi:10.1002/0471142735.im1911s42.

95. Herlax V, de Alaniz MJT, Bakás L. Role of lipopolysaccharide on the structure and function of alpha-hemolysin from Escherichia coli. *Chem Phys Lipids*. 2005;135(2):107–15. doi:10.1016/j.chemphyslip.2005.02.009.

96. Chen L-H, Kathaperumal K, Huang C-J, et al. Immune responses in mice to Mycobacterium avium subsp. paratuberculosis following vaccination with a novel 74F recombinant polyprotein. *Vaccine*. 2008;26(9):1253–62. doi:10.1016/j.vaccine.2007.12.014.

97. Sekaly R-P. The failed HIV Merck vaccine study: a step back or a launching point for future vaccine development? *J Exp Med*. 2008;205(1):7–12. doi:10.1084/jem.20072681.

98. Letvin NL. Moving Forward in HIV Vaccine Development. *Science (80- )*. 2009;326(November):1196–1198.

99. Girard MP, Osmanov SK, Kieny MP. A review of vaccine research and development: the human immunodeficiency virus (HIV). *Vaccine*. 2006;24(19):4062–81. doi:10.1016/j.vaccine.2006.02.031.

100. Mouquet H, Scheid JF, Zoller MJ, et al. Polyreactivity increases the apparent affinity of anti-HIV antibodies by heteroligation. *Nature*. 2010;467(7315):591–5. doi:10.1038/nature09385.

101. Tsourkas PK, Liu W, Das SC, Pierce SK, Raychaudhuri S. Discrimination of membrane antigen affinity by B cells requires dominance of kinetic proofreading over serial engagement. *Cell Mol Immunol*. 2012;9(1):62–74. doi:10.1038/cmi.2011.29.

102. Tsourkas PK, Baumgarth N, Simon SI, Raychaudhuri S. Mechanisms of B-cell synapse formation predicted by Monte Carlo simulation. *Biophys J*. 2007;92(12):4196–208. doi:10.1529/biophysj.106.094995.

103. Tsourkas PK, Longo ML, Raychaudhuri S. Monte Carlo study of single molecule diffusion can elucidate the mechanism of B cell synapse formation. *Biophys J*. 2008;95(3):1118–25. doi:10.1529/biophysj.107.122564.

104. Izquierdo-Useros N, Naranjo-Gómez M, Archer J, et al. Capture and transfer of HIV-1 particles by mature dendritic cells converges with the exosome-dissemination pathway. *Blood*. 2009;113(12):2732–41. doi:10.1182/blood-2008-05-158642.

105. Gelderblom H, Hausmann E, Pauli G. Fine structure of human immunodeficiency virus (HIV) and immunolocalization of structural proteins. *Virology*. 1987;156:171–176. Available at: http://www.sciencedirect.com/science/article/pii/0042682287904491. Accessed May 8, 2012.

106. Weissenhorn W, Dessen A, Harrison S, Skehel J. Atomic structure of the ectodomain from HIV-1 gp41. *Nature*. 1997;387:426–430. Available at: http://www.nature.com/nature/journal/v387/n6631/abs/387426a0.html. Accessed May 8, 2012.

107. Gillespie D. Exact stochastic simulation of coupled chemical reactions. *J Phys Chem*. 1977;81(25):2340–2361. Available at: http://onlinelibrary.wiley.com/doi/10.1002/cbdv.200490137/abstract. Accessed May 8, 2012.

108. Yang J, Monine M, Faeder J, Hlavacek W. Kinetic Monte Carlo method for rule-based modeling of biochemical networks. *Phys Rev E*. 2008;78(3):1–7. doi:10.1103/PhysRevE.78.031910.